INFORMATION TO USERS

This manuscript has been reproduced from the microfilm master. UMI films the text directly from the original or copy submitted. Thus, some thesis and dissertation copies are in typewriter face, while others may be from any type of computer printer.

The quality of this reproduction is dependent upon the quality of the copy submitted. Broken or indistinct print, colored or poor quality illustrations and photographs, print bleedthrough, substandard margins, and improper alignment can adversely affect reproduction.

In the unlikely event that the author did not send UMI a complete manuscript and there are missing pages, these will be noted. Also, if unauthorized copyright material had to be removed, a note will indicate the deletion.

Oversize materials (e.g., maps, drawings, charts) are reproduced by sectioning the original, beginning at the upper left-hand corner and continuing from left to right in equal sections with small overlaps.

Photographs included in the original manuscript have been reproduced xerographically in this copy. Higher quality 6" x 9" black and white photographic prints are available for any photographs or illustrations appearing in this copy for an additional charge. Contact UMI directly to order.

ProQuest Information and Learning
300 North Zeeb Road, Ann Arbor, MI 48106-1346 USA
800-521-0600

UMI®

Université d'Ottawa • University of Ottawa

Effect of Transverse Convex Surface Curvature on Turbulent Fluid Flow and Heat Transfer in Concentric Annuli with Moving Cores

by

Sang Hun Lee

A thesis submitted to the Faculty of Graduate
and Postdoctoral Studies in partial fulfilment of
the requirements for the degree of

Master of Applied Science
in
Mechanical Engineering

The Ottawa-Carleton Institute for
Mechanical and Aeronautical Engineering

Department of Mechanical Engineering
Faculty of Engineering
University of Ottawa

ABSTRACT

This study investigates the effect of Transverse Convex Surface Curvature of the inner core (T.C.S.C) on the fully developed fluid flows in a concentric annulus with a moving core, by analytically predicting friction forces, velocity profiles, temperature profiles and heat transfer in terms of convex surface curvature, radius ratio, Prandtl number, Reynolds number and relative velocity.

The analytical predictions are produced by a mathematical model based on the variable von Kármán constant, κ_i, proposed by Kim and Lee [1] and the variable van Driest damping parameter, A_i^+, proposed in previous research by Suk [2]. The computer program developed for this study employs a numerical process to match velocity and temperature profiles with force and energy balances and calculates the desired momentum and thermal characteristics. The solutions are found in the case of the heat transfer where the inner core surface is uniformly heated and the outer insulated. It is assumed that the fluid flow is turbulent everywhere and the thermodynamic fluid properties are independent of temperature.

It is concluded that in the fully developed turbulent flow in a concentric annulus with a moving core, the effects of Transverse Convex Surface Curvature (T.C.S.C), core velocity and turbulent motion on the momentum and heat transfer characteristics of the flow seem significant.

ACKNOWLEDGEMENTS

The author wishes to express his sincere appreciation to Professor Yung Lee for the opportunity to work under his supervision and guidance. His help and patience with immeasurable love and his knowledge in this field helped bring this study to fruition.

Special thanks go to the author's father and mother for their love and support. The author is personally indebted to colleagues S. Rhi and B. Kim for their advice.

The author sincerely appreciates his good friends, Choong-Gi, Brian, Ted, and Qian gave continuous encouragement and love which made it possible to carry on this work.

Finally, the author specially appreciates to the author's wife, So-Youn, and his daughter, Elaine, whose continuous patience and encouragement with endless love made it possible to persevere during the years of work.

TABLE OF CONTENTS

Abstract i

Acknowledgement ii

Table of Contents iii

List of Figures vi

Nomenclature x

1. Introduction 1

    1.1 General Overview 1

    1.2 Literature Survey 3

2. Analytical Study 10

    2.1 Basic Equation 10

    2.2 Governing Equations: Turbulent Boundary Layer Flow in a Concentric Annulus 15

    2.3 Variable von Karman Constants: a New Modified Model 18

    2.4 Analysis: Fully Developed Turbulent Fluid Flow in a Concentric Annulus with a moving core 21

        2.4.1 Problem Definition and Assumptions 21

        2.4.2 Velocity Distribution 22

        2.4.3 Eddy Diffusivity for Momentum 22

        2.4.4 Friction Factor and Reynolds Number 26

2.5 Relative Velocity 28

2.6 Diabatic Turbulent Flow in the Fully Developed Regions of a Concentric Annulus with a moving core 29

2.6.1 Eddy Diffusivity for Heat 29

2.6.2 Temperature Distribution 32

2.6.3 Nusselt Number 33

2.7 Method of Solution 35

3. Computation 37

3.1 General Approach 37

3.2 Calculation Procedure 40

3.2.1 Methodology for Section 1 40

3.2.2 Methodology for Sections 2 and 3 41

3.3 Results of Computations 43

4. Results and Discussions 47

4.1 General Overview 47

4.2 Turbulent Flow in the Fully Developed Regions 49

4.2.1 Velocity Distribution 50

4.2.2 Friction Factor 53

4.3 Turbulent Flow and Heat Transfer in the Fully Developed Regions 55

4.3.1 Temperature Distribution 55

4.3.2 Nusselt Number 57

4.3.3 Relationship between Non-Dimensional Parameters and the Convex Curvature of the Inner Core 57

5. Conclusion 60

Appendices 62

Appendix 1 Distribution of Shear Stress and Radial Heat Flux in a Concentric Annulus with a moving core 62

Appendix 2 Non-Dimensionalized Forms of the Velocity and Temperature Equation for Concentric Annular Geometry 68

Appendix 3 Non-Dimensionalized Forms of the Turbulence Model for Concentric Annular Geometry 71

Appendix 4 Non-Dimensionalized Forms of Other Fluid Parameters for Concentric Annular Geometry 75

References 82

Figures 87

LIST OF FIGURES

Figure 2.1 Determination of the van Driest Damping Parameter, A_t^+; $R_t^* = 0.005$ 87

Figure 2.2 Determination of the van Driest Damping Parameter, A_t^+; $R_t^* = 0.01$ 88

Figure 2.3 Determination of the van Driest Damping Parameter, A_t^+; $R_t^* = 0.05$ 89

Figure 2.4 Determination of the van Driest Damping Parameter, A_t^+; $R_t^* = 0.1$ 90

Figure 2.5 Determination of the van Driest Damping Parameter, A_t^+; $R_t^* = 1.0$ 91

Figure 2.6 Effect of R_t^* on the variation of the van Driest Damping Parameter for Inner Region, A_t^+ 92

Figure 2.7 Effect of R_t^+ on the Reynolds Number, $\mathrm{Re} = u_b \cdot 2(R_o - R_t)/\nu$ 93

Figure 2.8 Velocity Distribution; U* = 0.5 94

Figure 2.9 Velocity Distribution; U* = 1.0 95

Figure 2.10 Dimensionless Velocity Profiles 96

Figure 2.11 Effect of R_t^* on Maximum Velocity; Re = 10^5 and U* = 0.4 97

Figure 2.12 Effect of R_t^* on Maximum Velocity; Re = 10^5 and U* = 0.4 98

Figure 2.13 Effect of R_i^* on Maximum Velocity; Re = 10^5 and U* = 0.8 99

Figure 2.14 Effect of R_i^* on Dimensionless Bulk Velocity; U* = 0.4 and Re = 10^5 100

Figure 2.15 Effect of R_i^* on Dimensionless Bulk Velocity; U* = 0.8 and Re = 10^5 101

Figure 2.16 Friction Factors; $R_i^* = 1.0$, $\alpha = 0.999$ and U*=0.0; $\mathrm{Re} = u_b \cdot 2(R_o - R_i)/\nu$ 102

Figure 2.17 Effect of R_i^* on Normalized Friction Factors ($f^* = f / f_{1.0m}$); $\alpha = 0.2$, U* = 0.5; $\mathrm{Re} = u_b \cdot 2(R_o - R_i)/\nu$ 103

Figure 2.18 Effect of R_i^* on Normalized Friction Factors ($f^* = f / f_{1.0m}$); $\alpha = 0.2$, U* = 1.0; $\mathrm{Re} = u_b \cdot 2(R_o - R_i)/\nu$ 104

Figure 2.19 Effect of R_i^* on Normalized Friction Factors ($f^* = f / f_{1.0m}$); $\alpha = 0.5$, U* = 0.5; $\mathrm{Re} = u_b \cdot 2(R_o - R_i)/\nu$ 105

Figure 2.20 Effect of R_i^* on Normalized Friction Factors ($f^* = f / f_{1.0m}$); $\alpha = 0.5$, U* = 1.0; $\mathrm{Re} = u_b \cdot 2(R_o - R_i)/\nu$ 106

Figure 2.21 Effect of R_i^* on Normalized Friction Factors ($f^* = f / f_{1.0m}$); $\alpha = 0.8$, U* = 0.5; $\mathrm{Re} = u_b \cdot 2(R_o - R_i)/\nu$ 107

Figure 2.22 Effect of R_i^* on Normalized Friction Factors ($f^* = f / f_{1.0m}$); $\alpha = 0.8$, U* = 1.0; $\mathrm{Re} = u_b \cdot 2(R_o - R_i)/\nu$ 108

Figure 2.23 Dimensionless Temperature Profile; U* = 1.0 and Pr = 0.72 109

Figure 2.24 Dimensionless Temperature Profile; U* = 1.0 and Pr = 5.0 110

Figure 2.25 Effect on R_i^* on Temperature Distribution; $\alpha = 0.5$ and U* = 1.0 111

Figure 2.26 Effect of U* on Dimensionless Temperature Distribution; $R_i^* = 1.0$, $\alpha = 0.5$, Pr = 0.72 and U* = 0.0, 0.5 & 1.0 112

Figure 2.27 Effect of U* on Dimensionless Temperature Distribution; $R_i^* = 1.0$, $\alpha = 0.5$, Pr = 5.0 and U* = 0.0, 0.5 & 1.0 113

Figure 2.28 Effect of R_i^* on Maximum Dimensionless Temperature; Effect of Radius Ratio, α; Pr = 0.72, Re = 10^5 and U* = 0.4 114

Figure 2.29 Effect of R_i^* on Maximum Dimensionless Temperature; Effect of Radius Ratio, α; Pr = 0.72, Re = 10^5 and U* = 0.8 115

Figure 2.30 Nusselt Number for Fully Developed Turbulent Flow between Parallel Plates and in a Concentric Annulus, $R_i^* = 1.0$, $\alpha = 0.999$; Constant Heat Flux; Pr = 0.7; Re = $u_b \cdot 2(R_o - R_i)/\nu$ 116

Figure 2.31 Nusselt Number for Fully Developed Turbulent Flow between Parallel Plates and in a Concentric Annulus, $R_i^* = 1.0$, $\alpha = 0.999$; Constant Heat Flux; Pr = 1.0; Re = $u_b \cdot 2(R_o - R_i)/\nu$ 117

Figure 2.32 Nusselt Number for Fully Developed Turbulent Flow between Parallel Plates and in a Concentric Annulus, $R_i^* = 1.0$, $\alpha = 0.999$; Constant Heat Flux; Pr = 10.0; Re = $u_b \cdot 2(R_o - R_i)/\nu$ 118

Figure 2.33 Nusselt Number; Effect of Relative Velocity, $\alpha = 0.5$, Re = 20,000 and Pr = 0.72 119

Figure 2.34 Nusselt Number; Effect of Relative Velocity, $\alpha = 0.5$, $Re = 10^5$ and $Pr = 0.72$ 120

Figure 2.35 Nusselt Number; Effect of Prandtl Numbers, $\alpha = 0.5$, $U^* = 0.5$ and $Re = 10^5$ 121

Figure 2.36 Nusselt Number; Effect of Prandtl Numbers, $\alpha = 0.5$, $U^* = 1.0$ and $Re = 10^5$ 122

Figure 2.37 Nusselt Number; Effect of Radius Ratio, $Pr = 0.72$, $U^* = 0.5$ and $Re = 10^5$ 123

Figure 2.38 Nusselt Number; Effect of Radius Ratio, $Pr = 0.72$, $U^* = 1.0$ and $Re = 10^5$ 124

Figure 2.39 Nusselt Number; Effect of Reynolds Numbers, $\alpha = 0.5$, $U^* = 0.5$ and $Pr = 0.72$ 125

Figure 2.40 Nusselt Number; Effect of Reynolds Numbers, $\alpha = 0.5$, $U^* = 1.0$ and $Pr = 0.72$ 126

Figure 2.41 Nusselt Number; Effect of Relative Velocity, $Pr = 0.72$, $\alpha = 0.5$ and $Re = 20{,}000$ 127

Figure 2.42 Nusselt Number; Effect of Relative Velocity, $Pr = 1.0$, $\alpha = 0.5$ and $Re = 20{,}000$ 128

Figure 2.43 Nusselt Number; Effect of Relative Velocity, $Pr = 10.0$, $\alpha = 0.5$ and $Re = 20{,}000$ 129

Figure A1.1 Shear Stress and Heat Flux Distribution in a Concentric Annular Flow 130

Figure A4.1 Idealized Model: Fully Developed Turbulent Flow in a Concentric Annulus 131

NOMENCLATURE

A	surface area of the hot junction [m^2], van Driest's damping constant
A^+	dimensionless van Driest's damping parameter
C or c	constant
c_p	specific heat at constant pressure $[{}^{kJ}/_{kg \cdot {}^\circ C}]$
d	distance
D	substantial derivatives defined by Eq. (2.2)
De	equivalent diameter of annulus, 2 (R_o - R_i), [m]
f_j	friction factor, concentric annulus, $\left({}^{2\tau_j}/_{\rho \cdot u_b^2}\right)$
F	force [N], function
h	convective heat transfer coefficient [$W/m^2\ {}^\circ C$]
k	thermal conductivity [$W/m\,{}^\circ C$], turbulent kinetic energy
k_t	eddy conductivity [$W/m\,{}^\circ C$]
l	Prandtl's mixing length [m]
l^+	dimensionless Prandtl mixing length parameter, circular cylinder, $\left({}^{l \cdot u_\tau}/_{\nu}\right)$
L	length [m]
Nu	Nusselt number; circular cylinder $\left({}^{h \cdot x}/_{k}\right)$, concentric annulus $\left({}^{h \cdot D_e}/_{k}\right)$
p	pressure [N/m^2]

Pr	Prandtl number, $\left(c_p \cdot \mu / k\right)$
Pr_t	turbulent Prandtl number, $\left(\varepsilon_M / \varepsilon_H\right)$
q	heat flux per unit area [W/m^2]
q'	heat generation per unit volume [J/m^3]
r	radial coordinate measured from cylinder axis [m]
r_j	radius of circular cylinder [m]
R_j	radius of concentric annuli [m]
R_j^+	dimensionless radius parameter, concentric annulus, $\left(R_j \cdot u_{\tau_j} / \nu\right)$
Re	Reynolds number
t	time [sec]
T	temperature [$°C$]
T^+	dimensionless temperature parameter, $[(T_w - T) \cdot \rho \cdot c_p \cdot u_{\tau_j} / q_t]$
u	velocity in x-direction [m/s]
u_j^+	dimensionless velocity parameter, $\left(u / u_{\tau_j}\right)$
U*	dimensionless relative velocity, U / u_b
u_{τ_j}	friction velocity, $\left(\tau_j / \rho\right)^{0.5}$ [m/s]
u_b	bulk velocity [m/s]
v	velocity in y-direction [m/s]

w	velocity in z-direction [m/s]
x, y, z	cartesian coordinates [m]
y	distance from the wall [m]
y_j^+	dimensionless distance parameter, $\left(y \cdot u_{\tau_j} / \nu \right)$

Greek Symbols:

α	radius ratio of annulus, (R_i/R_o); thermal diffusivity [m^2/s]
δ_j	$\lvert R_m - R_j \rvert$
δ_j^+	$\delta_j (\tau_w/\rho)_j^{0.5} / \nu$
Δ_j	δ_j^+ / R_j^+
ε	eddy diffusivity [m^2/s]
ζ_j	normalized distance, (y_j^+ / δ_j^+)
θ	azimuthal coordinate
κ_j	von Karman's constant
μ	dynamic viscosity [$kg/m \cdot s$]
μ_t	eddy viscosity [$kg/m \cdot s$]
ν	kinematic viscosity [m^2/s]
ρ	density [kg/m^3]

τ	shear stress [$kg/m \cdot s^2$].

Superscripts:

+	quantity non-dimensionalized
/	fluctuating component or specific value
–	mean
*	normalized by the value of R = 1.0 m, R^* (= $R / R_{1.0\,m}$)

Subscripts:

b	bulk
H	thermal
i	inner
i, j, k	inner or cartesian coordinate direction
j	designate number (i or o)
k	turbulent kinetic energy
l	laminar
m	corresponding to the maximum velocity point
M	momentum
o	outer

t	turbulent
w	wall
x	local or developing

CHAPTER 1
INTRODUCTION

1.1 General Overview

Fluid flow has been studied extensively because of its importance in engineering. Ducts with circular cross-sections are the most convenient geometry from an engineering point of view, but annular cross-sections are also important because of their use in a variety of heat transfer systems, such as nuclear reactors and heat exchangers. The class of problems concerning annulus flow with moving cores arises out of real engineering applications such as high-speed trains in long tunnels, heavy traffic in tunnels, etc. In certain manufacturing processes such as extrusion, hot rolling and drawing, a hot plate or cylindrical rod continuously exchanges heat with the surrounding environment. The inverted annular film boiling which takes place during the emergency core cooling of nuclear fuel channels [3] is another example which involves such fluid flow and heat transfer phenomena. For such cases, there seems to be no reliable prediction for momentum and heat transfer available in the literature. The study by Shigechi & Lee [4], which considered the effect of the moving inner core on turbulent flow in a concentric annulus, has further completed and provided accuracy to previous studies on fluid flow and heat transfer phenomena.

For the analytical work in this study, modified versions of previously accepted turbulence models were combined with integral momentum and energy equations to predict the effect of transverse convex surface curvature (T.C.S.C) on friction factors and

heat transfer rates in concentric annuli with moving inner core. The modified form of the turbulence models of van Driest [5] and Reichardt [6] were used for the developed turbulent flow and heat transfer. All the turbulence models were adapted to reflect the variable von Kármán constant, κ_t, proposed in the previous study [7] and the variable van Driest damping parameter, A_i^+, proposed in the previous study [2], which are required to identify the effect of the transverse convex surface curvature in concentric annuli with moving inner cores.

The aim of the present study is to apply the proposed variable von Kármán constant and the variable van Driest damping parameter that can successfully describe the effect of the transverse convex surface curvature and to obtain an analytical prediction based on the model for the fully developed turbulent fluid flow and heat transfer in the fully developed region of concentric annuli with moving cores.

The work is subdivided into several parts. First, a survey of relevant works in published literature is carried out, outlining past theoretical analyses of fully developed turbulent flows and heat transfer on the geometries in question. This is followed by a mathematical development of analyses, showing the integration of momentum and energy equations with the adapted turbulence models based on the variable von Kármán constants, κ_t, and the variable van Driest damping parameter, A_i^+, which must be obtained for a given condition individually from the boundary conditions. The governing equations of the systems were presented, then their numerical solutions were described, demonstrating the approximation of the governing equations. Finally, the analytical results were produced to evaluate the effects of the transverse convex surface curvatures.

Throughout the analysis, the fluid properties are considered constant to simulate an ideal situation. Conditions for the analysis were constant wall heat flux at the moving inner cores and the fluid flow is fully developed. The effects of natural convection and axial conduction on the temperature distributions were considered negligible.

1.2 Literature Survey

The study of turbulent fluid flow in smooth surface conduits has been the subject of intense research over the years, due to the numerous engineering applications in which turbulent fluid flow occurs. The research has been successful in establishing high degrees of correlation with the characteristics of flows in circular pipes, annuli and long ducts with large aspect ratios. The problems of fully developed turbulent flow in a concentric annulus have been studied experimentally and analytically by many workers [1 ~ 31]. Among these studies just listed, the studies by Suk [2] and Shigech & Lee [4] are particularly relevant to the present study.

A complete analytical solution of the modified Navier-Stokes equations for turbulent flows can not be obtained even for a simple flow in a circular duct. Consequently, the development of a mathematical model for the problem in question necessarily requires artificial modelling of the turbulent parameters such as $u'v', u'u', u'w'$, and so on. An early and highly successful attempt to model the turbulent terms was proposed by Prandtl. The mixing length theory provided excellent insight into the mechanisms involved in the transport of momentum in locally fluctuating regions of a flow. However, the mixing length theory had serious shortfalls [15]. Von Kármán [32] expanded on the Prandtl's hypothesis by adding the second derivative of the mean velocity into the equation. However, von Kármán's mixing length theory does not improve significantly upon the predictions of Prandtl.

Despite these shortcomings, Prandtl's mixing length theory has been successfully used in numerous calculation schemes to predict momentum and heat transfer characteristics. It has also been the subject of numerous improvements, particularly by

van Driest [5] and Reichardt [6]. The works of Lee et al. [3, 18, 19, 20, 21, 22], as well as those of Kays and Leung [33], Barrow et al. [13, 14], and Brighton & Jones [15] have demonstrated that the modified models can be able to predict, with high confidence flow, the parameters across most of annulus' cross-section.

Concurrent to the search for modelling the turbulent parameters have been the effort to derive expressions for predicting the velocity and temperature profiles across the annulus. One simple yet effective expression can be obtained from the Prandtl's mixing length theory: the *logarithmic law of the wall.* Workers previously have had equal success in matching experimental data to computer predictions. Data have shown that the law of wall works very well for circular cylinders [34]. The temperature profile can also be derived from Prandtl's mixing length theory [34], but workers have traditionally reverted to performing numerical integration to obtain these profiles. The technique, used notably by Kim & Lee [1], Kim [7], and Lee et al. [21], has correlated well with the experimental data.

Most of the analytical studies for the fully developed fluid flows and heat transfer in annular ducts were based on the eddy diffusivity concept for momentum and heat. They assumed that velocities and eddy diffusivities for the momentum of the two regions at the plane of zero-shear are the same.

Bailey [12] computed the heat transfer coefficients for the inner core wall having a constant heat flux for liquid metals. He used the fully developed modified velocity distribution of Prandtl's equation combined with the equation of von Kármán [34] by direct integration of the energy equation. The modification of Prandtl's equation for a fully turbulent layer was necessary because of the different friction coefficients for each

wall. However, he assumed that the overall friction coefficient in an annulus was equal to the friction coefficient for smooth tubes at the same Reynolds number. In his analysis, the radii of zero-shear and maximum velocity were assumed to be the same. The flow in each region divided by the radius of maximum velocity was divided into three zones, a laminar sublayer, a buffer layer, and a fully turbulent layer. The ratio of eddy diffusivities for heat and momentum was taken as unity.

Reynolds et al. [35] made a general formulation of the annulus problem and had a superposition approach to the solution of the governing equation. Their research considered four "fundamental" solutions from which the solution for any prescribed set of boundary conditions could be determined. In their study, the fundamental solution of "the second kind" considered the fluid flowing with a constant temperature in the annulus with both tube walls kept at the same temperature. The heat fluxes from either the core wall or the outer wall were increased stepwise, while the opposite wall was insulated.
Levy [16] reported an analysis for fully developed turbulent flows in concentric annular ducts. He derived equations based on Reichardt's expression [6] for the momentum eddy diffusivity. He predicted the location of the zero shear stress and the distributions of the eddy diffusivity, the velocity profile, and the friction coefficient. His predicted results were compared with available experimental data, and reported to be in good agreement with each other.

Wilson & Medwell [36] carried out analyses for fully developed turbulent flows in concentric annular ducts. They used the eddy diffusivity distribution expression proposed by Levy [16] with a constant universal mixing length for the fully developed

annular flow. However, their predicted results did not agree with the experimental data at low radius ratios, α.

Quarmby [9] also derived equations for the velocity distributions based on Deissler's expression [37] for the eddy diffusivity of momentum in the sublayer. The theoretical predictions for friction coefficients and radius of the maximum velocity as a function of the Reynolds numbers and radius ratios were in a reasonably good agreement with their experimental data.

Lee & Park [22] and Suk [2] carried out a study of the simultaneous developing turbulent flow and heat transfer in concentric annuli. They derived equations based on Reichardt's expression [6] for the eddy diffusivity of momentum for the sublayers and on Levy's expression [16] in the fully turbulent layers. Their analytical results were compared with their experimental data for the turbulent flow of air in four concentric annular ducts at a Reynolds number range from 20,000 to 110,000 and were in good agreement with the experimental results.

The latest development in annulus research has been the extension of the analysis to that of annuli with moving cores which was motivated by considerations of long tunnels used in train transportation and cooling of nuclear rods in a nuclear power reactor. Several workers have laid down the mathematical models for calculating the heat and momentum transfer parameters of such cases, in particular Lee et al. [3] and Shigechi et al. [4]. Their work has primarily been in modeling the problem for computer calculations, because it is very difficult to study the subject matter experimentally. Nevertheless, the results obtained were, by extension from the static core case, favorable and realistic. The study of Shigechi et al. [4] showed that a moving core would increase

in general the values of Nu but decrease the friction factor, f. The computer models developed by these workers all used the principles of Prandtl's mixing length theory, along with the improvements made by van Driest [5] and Reichardt [6].

The effect of transverse convex surface curvature on turbulent fluid flow and heat transfer in concentric annuli with smooth surfaces was empirically and analytically studied [2, 7].

Kim [7] made a mathematical formulation of the variable von Kármán constant, κ_t, for turbulence models of the circular concentric annular ducts through experimental and analytical studies. The experimental study of Kim [7] for the cases of circular cylinders and concentric annular ducts was conducted by changing several different radii of the inner cores, keeping the radius ratio constant.

Suk [2] carried out analyses for the effect of transverse convex surface curvature on developing turbulent fluid flow and heat transfer in concentric annuli with smooth surfaces. The modified variable van Driest damping parameter, A_i, was obtained through the analytical studies [2].

The computer program for the studies [2, 7] employs an iterative process to match the velocity and temperature profiles force and energy balances and calculates the desired momentum and thermal characteristics. It is assumed that thermodynamics fluid properties in the analyses were independent of temperature. These studies showed that the transverse convex curvature significantly affects the velocity distribution and temperature distribution of turbulent flow in concentric annuli with stationary cores. Both the friction factor and Nusselt number increase with a decreasing inner core radius value are always greater than those for the flows over a flat plate for the ranges of

parameter studied indicating that the effect of transverse convex surface curvature on heat transfer increases with an increasing Prandtl number.

It is apparent that the effect of transverse convex surface curvature on turbulent flow and heat transfer in the fully developed region of concentric annuli with moving cores has not been considered from the review of published literature of studies.

CHAPTER 2
ANALYTICAL STUDY

2.1 Basic Equations

Let x denote the axial direction along the wall, while r and θ represent the radial and azimuthal direction to the wall in cylindrical coordinates. The velocities corresponding to these coordinates are u, v, and w, respectively. For the case of incompressible fluid flow, the Navier-Stokes equations for the cylindrical coordinate system can be expressed in the following forms:

$$\rho\left(\frac{\partial u}{\partial t}+u\frac{\partial u}{\partial x}+v\frac{\partial u}{\partial r}+\frac{w}{r}\frac{\partial u}{\partial \theta}\right)=F_x-\frac{\partial p}{\partial x}+\mu\nabla^2 u \tag{2.1a}$$

$$\rho\left(\frac{\partial v}{\partial t}+u\frac{\partial v}{\partial x}+v\frac{\partial v}{\partial r}+\frac{w}{r}\frac{\partial v}{\partial \theta}-\frac{w^2}{r}\right)=F_r-\frac{\partial p}{\partial r}-\mu\left(\frac{v}{r^2}+\frac{2}{r^2}\frac{\partial w}{\partial \theta}\right)+\mu\nabla^2 v \tag{2.1b}$$

$$\rho\left(\frac{\partial w}{\partial t}+u\frac{\partial w}{\partial x}+v\frac{\partial w}{\partial r}+\frac{w}{r}\frac{\partial w}{\partial \theta}+\frac{vw}{r}\right)=F_\theta-\frac{1}{r}\frac{\partial p}{\partial r}-\mu\left(\frac{w}{r^2}-\frac{2}{r^2}\frac{\partial v}{\partial \theta}\right)+\mu\nabla^2 w \tag{2.1c}$$

For the constant thermodynamic properties of density, ρ, specific heat, C_p, and thermal conductivity, k, the corresponding energy equation has the following forms:

$$\rho c_p\frac{DT}{Dt}=k\nabla^2 T+v\frac{Dp}{Dt}+q'+\mu\left(\frac{\partial u}{\partial r}\right)^2 \tag{2.2}$$

where the Laplacian operator is

$$\nabla^2=\frac{1}{r}\frac{\partial}{\partial r}\left(r\frac{\partial}{\partial r}\right)+\frac{1}{r^2}\frac{\partial^2}{\partial \theta^2}+\frac{\partial^2}{\partial x^2}$$

$\frac{DT}{Dt}$ and $\frac{Dp}{Dt}$ are the substantial derivatives of temperature, T, and pressure, p. q' is specific heat generation.

The continuity equation for incompressible steady flow is:

$$\frac{\partial u}{\partial x}+\frac{\partial v}{\partial r}+\frac{1}{r}\frac{\partial w}{\partial \theta}+\frac{v}{r}=0 \tag{2.3}$$

The momentum and energy equations are applicable to turbulent flow if instantaneous values for the velocity, pressure, and temperature are used. Reynolds modified the momentum equation by introducing the mean fluctuation values of the flow quantities in place of instantaneous values. As the instantaneous velocity component is the sum of the mean component and fluctuating velocity component in the same direction, the transformation of the above Navier-Stokes equation due to Reynolds can be obtained by introducing:

$$u=\overline{u}+u', \quad v=\overline{v}+v', \quad w=\overline{w}+w', \quad \& \quad p=\overline{p}+p'$$

where

$\overline{u},\overline{v},\overline{w}$; mean velocity

u',v',w'; fluctuation from the mean velocity

The Navier-Stokes equations in cylindrical coordinates for incompressible steady flow in a straight uniform cross section in which the body force can be neglected have the following forms [34]:

$$\rho\left(\frac{\partial \overline{u}}{\partial t}+\overline{u}\frac{\partial \overline{u}}{\partial x}+\overline{v}\frac{\partial \overline{u}}{\partial r}+\frac{\overline{w}}{r}\frac{\partial \overline{u}}{\partial \theta}\right)=-\frac{\partial \overline{p}}{\partial x}+\mu\nabla^2\overline{u} - \left[\frac{\partial}{\partial x}\left(\rho\overline{u'^2}\right)+\frac{1}{r}\frac{\partial}{\partial r}\left(r\rho\overline{u'v'}\right)+\frac{1}{r}\frac{\partial}{\partial \theta}\left(\rho\overline{u'w'}\right)\right] \tag{2.4a}$$

$$\rho\left(\frac{\partial \bar{v}}{\partial t}+\bar{u}\frac{\partial \bar{v}}{\partial x}+\bar{v}\frac{\partial \bar{v}}{\partial r}+\frac{\bar{w}}{r}\frac{\partial \bar{v}}{\partial \theta}-\frac{\bar{w}^2}{r}\right)=-\frac{\partial \bar{p}}{\partial r}+\mu\left(\nabla^2\bar{v}-\frac{\bar{v}}{r^2}-\frac{2}{r^2}\frac{\partial \bar{w}}{\partial \theta}\right)$$
$$-\left[\frac{\partial}{\partial x}\left(\rho\overline{u'v'}\right)+\frac{\partial}{\partial r}\left(\rho\overline{v'^2}\right)+\frac{1}{r}\frac{\partial}{\partial \theta}\left(\rho\overline{v'w'}\right)-\frac{\rho\overline{w'^2}}{r}\right] \quad (2.4b)$$

$$\rho\left(\frac{\partial \bar{w}}{\partial t}+\bar{u}\frac{\partial \bar{w}}{\partial x}+\bar{v}\frac{\partial \bar{w}}{\partial r}+\frac{\bar{w}}{r}\frac{\partial \bar{w}}{\partial \theta}+\frac{\bar{v}\bar{w}}{r}\right)=-\frac{1}{r}\frac{\partial \bar{p}}{\partial \theta}+\mu\left(\nabla^2\bar{w}+\frac{2}{r^2}\frac{\partial \bar{w}}{\partial \theta}-\frac{\bar{w}}{r^2}\right)$$
$$-\left[\frac{\partial}{\partial x}\left(\rho\overline{u'w'}\right)+\frac{\partial}{\partial r}\left(\rho\overline{v'w'}\right)+\frac{1}{r}\frac{\partial}{\partial \theta}\left(\rho\overline{w'^2}\right)-\frac{2\left(\rho\overline{v'w'}\right)}{r}\right] \quad (2.4c)$$

The corresponding energy equation for heat transfer in turbulent flow is:

$$\frac{\partial \bar{T}}{\partial t}+\bar{u}\frac{\partial \bar{T}}{\partial x}+\bar{v}\frac{\partial \bar{T}}{\partial r}+\frac{\bar{w}}{r}\frac{\partial \bar{T}}{\partial \theta}=\alpha\nabla^2\bar{T}-\left[\frac{\partial}{\partial x}\left(\overline{u'T'}\right)+\frac{1}{r}\frac{\partial}{\partial r}\left(r\overline{v'T'}\right)+\frac{1}{r}\frac{\partial}{\partial \theta}\left(\overline{w'T'}\right)\right] \quad (2.5)$$

In Eq. (2.4), the three normal stresses $-\rho\overline{u'^2}, -\rho\overline{v'^2}$, and $-\rho\overline{w'^2}$ and three shear stresses $-\rho\overline{u'v'}, -\rho\overline{v'w'}$, and $-\rho\overline{u'w'}$ are known as Reynolds stresses or eddy stresses. The problem under consideration here is that of a steady, incompressible, and turbulent flow for straight uniform cross section. Therefore, all of the derivatives with respect to time, t, and the body force can also be neglected.

In turbulent flow through a non-circular cross-section, the shear stresses are nearly constant along the sides, dropping off sharply to zero in the corners of cross-section [2]. This is because of the phenomenon of turbulent secondary flow, in which there are non-zero mean velocities v and w in the plane of the cross-section. In a circular section, if there is no secondary flow, Eq. (2.4a) is sufficient for determining the axial velocity distribution. In most situations, axial thermal conduction and axial eddy diffusion are either zero or negligibly small, and terms $\frac{\partial^2 T}{\partial x^2}-\frac{\partial}{\partial x}(\overline{u'T'})$ can be ignored. For further

simplification of Eq. (2.4a), the boundary layer approximation is applied, so that terms $\frac{\partial^2 u}{\partial x^2}$, and $\frac{\partial \overline{u'^2}}{\partial x}$ are also ignored.

For axisymmetric and two-dimensional flow such as in a pipe or in a concentric annulus, the appropriate equation of momentum is [34]:

$$\bar{u}\frac{\partial \bar{u}}{\partial x} + \bar{v}\frac{\partial \bar{u}}{\partial r} + \frac{1}{\rho}\frac{\partial \bar{p}}{\partial x} = \frac{\nu}{r}\frac{\partial}{\partial r}\left(\frac{\partial \bar{u}}{\partial r}\right) - \frac{1}{r}\frac{\partial}{\partial r}\left(r\overline{u'v'}\right) \tag{2.6}$$

and the equation of energy is:

$$\bar{u}\frac{\partial \bar{T}}{\partial x} + \bar{v}\frac{\partial \bar{T}}{\partial r} = \frac{\alpha}{r}\frac{\partial}{\partial r}\left(r\frac{\partial \bar{T}}{\partial r}\right) - \frac{1}{r}\frac{\partial}{\partial r}\left(r\overline{v'T'}\right) \tag{2.7}$$

To solve Eqs. (2.6) and (2.7) using the concept of eddy diffusivity, ε, the turbulence terms $-\overline{u'v'}$ and $-\overline{v'T'}$ are often expressed as $\varepsilon_M \cdot \left(\partial \bar{u}/\partial r\right)$ and $\varepsilon_H \cdot \left(\partial \bar{T}/\partial r\right)$ respectively. The turbulent shearing stress and that of the heat transfer is usually described as a flux of momentum & heat. Unlike the molecular counter-part (ν and k), the eddy diffusivity is not a fluid property because it is a function of position and flow condition.

For the momentum equation, Prandtl [38] hypothesized that the behavior of the apparent shear stress was similar to the laminar stress, and proposed the identity:

$$-\overline{u'v'} = \varepsilon_M\left(\frac{\partial \bar{u}}{\partial r}\right) \tag{2.8}$$

and for the energy equation is:

$$-\overline{v'T'} = \varepsilon_H\left(\frac{\partial \bar{T}}{\partial r}\right) \tag{2.9}$$

With Eq. (2.8), Eq. (2.6) yields:

$$\bar{u}\frac{\partial \bar{u}}{\partial x}+\bar{v}\frac{\partial \bar{u}}{\partial r}+\frac{1}{\rho}\frac{\partial \bar{p}}{\partial x}=\frac{1}{r}\frac{\partial}{\partial r}\left[r\left(\nu+\varepsilon_M\right)\frac{\partial \bar{u}}{\partial r}\right] \tag{2.10}$$

and with Eq. (2.9), Eq. (2.7) becomes:

$$\bar{u}\frac{\partial \bar{T}}{\partial x}+\bar{v}\frac{\partial \bar{T}}{\partial r}=\frac{1}{r}\frac{\partial}{\partial r}\left[r\left(\alpha+\varepsilon_H\right)\frac{\partial \bar{T}}{\partial r}\right] \tag{2.11}$$

The corresponding equations in the rectangular coordinates are:

$$\bar{u}\frac{\partial \bar{u}}{\partial x}+\bar{v}\frac{\partial \bar{u}}{\partial y}+\frac{1}{\rho}\frac{\partial \bar{p}}{\partial x}=\frac{\partial}{\partial y}\left[\left(\nu+\varepsilon_M\right)\frac{\partial \bar{u}}{\partial y}\right] \tag{2.12}$$

and

$$\bar{u}\frac{\partial \bar{T}}{\partial x}+\bar{v}\frac{\partial \bar{T}}{\partial y}=\frac{\partial}{\partial y}\left[\left(\alpha+\varepsilon_H\right)\frac{\partial \bar{T}}{\partial y}\right] \tag{2.13}$$

2.2 Governing Equations: Turbulent Boundary Layer Flow in a Concentric Annulus

In an axisymmetric turbulent boundary layer flow on a circular cylindrical body in a zero pressure gradient, the distribution of the shear stress, τ, and heat flux, q, can be derived from the equations of momentum and energy. The time rate change of momentum in the cylindrical fluid element is:

$$\rho\frac{d}{dt}\left\{\left[\left(u+\frac{\partial u}{\partial x}dx\right)-u\right]+\left[\left(u+\frac{\partial u}{\partial r}dr\right)-u\right]\right\}2\pi r\,dr\,dx = \rho\left(u\frac{\partial u}{\partial x}+v\frac{\partial u}{\partial r}\right)2\pi r\,dr\,dx \tag{2.14}$$

Employing the momentum theorem, the rate of creation of momentum is equal to the external forces and yields the following:

$$-\frac{\partial p}{\partial x}+\frac{1}{r}\frac{\partial}{\partial r}(\tau\cdot r) = \rho\left(u\frac{\partial u}{\partial x}+v\frac{\partial u}{\partial r}\right) \tag{2.15}$$

Rearranging Eq. (2.15) becomes:

$$\left(u\frac{\partial u}{\partial x}+v\frac{\partial u}{\partial r}\right)+\frac{1}{\rho}\frac{\partial p}{\partial x} = \frac{1}{\rho r}\frac{\partial}{\partial r}(\tau\cdot r) \tag{2.16}$$

If there is no pressure gradient, the boundary layer equation for the mean flow from Eq. (2.16) is:

$$u\frac{\partial u}{\partial x}+v\frac{\partial u}{\partial r}=\frac{1}{\rho r}\frac{\partial(r\cdot\tau)}{\partial r} \tag{2.17}$$

The energy balance of a cylindrical fluid element in the fully developed region described gives:

$$-2\pi r\,dr\,\rho u c_P \frac{\partial T}{\partial x}dx \;-\; 2\pi r\,dr\,\rho v c_P \frac{\partial T}{\partial r}dr \;= \\ 2\pi dx\{(r+dr)\left(q+\frac{\partial q}{\partial r}dr\right) - qr\} \tag{2.18}$$

The equation of energy then becomes:

$$u\frac{\partial T}{\partial x} + v\frac{\partial T}{\partial r} = -\frac{1}{\rho c_P r}\frac{\partial}{\partial r}(q\cdot r) \tag{2.19}$$

and the continuity equation is:

$$\frac{\partial(r\cdot u)}{\partial x}+\frac{\partial(r\cdot v)}{\partial r}=0 \tag{2.20}$$

where the shear stress is defined as:

$$\tau = \mu\frac{\partial \bar{u}}{\partial r} - \rho\overline{u'v'} \tag{2.21}$$

Eqs. (2.17) and (2.19) in combination with Eqs. (2.8) and (2.9) yield:

$$\frac{\tau}{\rho} = \left(\nu + \varepsilon_M\right)\frac{\partial u}{\partial r} \tag{2.22}$$

and

$$-\frac{q}{c_P\rho} = \left(\alpha + \varepsilon_H\right)\frac{\partial T}{\partial r} \tag{2.23}$$

For the momentum equation, the behaviour of the apparent shear stress was proposed by Prandtl [38] as the identity:

$$-\overline{u'v'} = \varepsilon_M\left(\frac{\partial \bar{u}}{\partial r}\right) = l^2\left(\frac{\partial \bar{u}}{\partial r}\right)^2 \tag{2.24}$$

where Prandtl's mixing theory [34] is:

$$l = k\cdot y$$

and κ is von Kármán constant. The velocity and temperature distributions, u and T, for a given wall heat flux and fluid flow can be determined from Eqs. (2.22) and (2.23) if both the momentum eddy diffusivity, ε_M, and thermal eddy diffusivity, ε_H, are known.

2.3 Variable von Kármán Constants, κ_i: A New Modified Model

Consider a turbulent shear flow which is steady and two-dimensional on average. Let u(x,y) and v(x,y) be the mean velocity in the direction of increasing rectangular coordinates x and y, respectively. Experiments with turbulent shear flow have shown that the mean-velocity profile in the region near the surface can be described by a relationship, $\frac{u}{u_\tau} = f\left(\frac{yu_\tau}{\nu}\right)$, called the " law of the wall". For the special case of steady two-dimensional mean flow of an incompressible fluid, the form of the universal law is well established as:

$$\frac{u}{u_\tau} = \frac{1}{\kappa}\ln\left(\frac{yu_\tau}{\nu}\right) + C \tag{2.25}$$

where κ, the von Kármán constant, and C are to be determined experimentally. Prandtl's mixing length theory [39, 40] can be employed to obtain Eq. (2.25).

In the study of Yu [41] and Rao [42], variations in the value of the von Kármán constant, κ, have been observed in the turbulent boundary layer, and it was found that the von Kármán constant, κ, varied with the Reynolds number based on the radius of the circular cylinder, Re_{r_i}. Rao and Keshavan [43] suggested that as the Reynolds number becomes larger, the von Kármán constant, κ, has a tendency to reach a value of approximately 0.4.

In previous literature [2, 17, 21, 44, 45] of turbulent boundary layer flow on a cylindrical body, near the wall surface, the velocity gradient, $\left(\frac{\partial u}{\partial y}\right)$, becomes steeper and the value of the von Kármán constant, κ, increases as the radius becomes smaller. This

implies that the turbulent eddies are strongly affected by the change in the value of the transverse convex wall curvature, i.e, the cylinder radius, R_t.

To characterize the effect of transverse convex surface curvature, it is proposed in the study of Kim et al. [1] that the von Kármán constant, κ_t, not be a fixed value and it may take the following form:

$$\kappa_t = \kappa_o \cdot F(R_t) \tag{2.26}$$

$F(R_t)$ was approximated in the following form of a hyperbolic tangent function of the radius of a cylindrical body, R_t, with the experimental data of Kim & Lee [17], and Willmarth et al. [45]:

$$F(R_t) = 1 + 1.5 \cdot \tanh\left(0.0064 / R_t^{0.72} \right) \tag{2.27}$$

Even though the Eq. (2.27) is adequate, it is still in a dimensional form. To transform Eqs. (2.26) and (2.27) to dimensionless form, Eq. (2.27) is normalized by R_t=1.0m as:

$$\kappa_t = \kappa_o \cdot F(R_t / R_{ref}) \tag{2.28}$$

where $\kappa_o = 0.4$ and $R_{ref} = 1.0m$.

The value of $R_{ref} = 1.0m$ was taken because it was noted by Kim & Lee [17] that when $R_t \geq 1.0m$, no effect of the transverse surface convex curvature was observed. Therefore Eq. (2.27) becomes:

$$F(R_t^*) = 1 + 1.5 \cdot \tanh\left(0.0064 / R_t^{*0.72} \right) \tag{2.29}$$

where $R_i^* = R_i / R_{ref}$.

Kim et al. [1] assumed that measurements of values of y^+ $(= y \cdot u_\tau / \nu)$ less than 100 approximately would be unreliable as a result of large fluctuations in velocity, wall interference, poor probe sensitivity at low velocities, probe position error, or uncertainty in static pressure.

Eq. (2.28) shows that the value of κ_i increases with the decreasing value of the cylinder radius, R_i , or R_i^* suggesting that the length scale distribution of the turbulent eddies, which is a function of wall shear stress is strongly affected by the change in the value of R_i (i.e., the transverse convex surface curvature) while over a flat plate with $\frac{dp}{dx} < 0$, the range of the von Kármán constant, κ, is fixed at 0.4 to 0.41. Therefore, by the slope in the logarithmic region of non-dimensionalized velocity profiles, physically known as the von Kármán constant as shown in Eq. (2.25), you might be able to find out the involved physical mechanism.

Eqs. (2.28) and (2.29) form the basis of this analytical study, and the results from the analysis will be explained in terms of the modified von Kármán constant, κ_i.

2.4 Analysis: Fully Developed Turbulent Fluid Flow in a Concentric Annulus with a moving core

2.4.1 Problem definition and Assumptions

In order to predict temperature distribution and heat transfer rates, it is necessary to predict velocity field and shear stress distribution in the gap between the stationary core and the moving core. The physical model selected for a study of the development of the velocity and temperature profiles in the fully developed region for a concentric annulus has a series of assumptions, and the analysis for the fluid flow and heat transfer is subjected to the following conditions:

(1) The annulus is concentric and both the wall surfaces are smooth. The inner core is uniformly heated with constant heat flux while the outer wall is insulated.

(2) Velocity and temperature fields in the annulus are fully developed.

(3) The axial pressure gradient is sufficiently large so that there exists a maximum velocity within the annulus.

(4) The line of the maximum velocity coincides with the line of the zero shear stress.

(5) For the momentum eddy diffusivity, ε_M, the model by van Driest for the sublayer and that of Reichardt for the fully turbulent region are used.

(6) The thermodynamic properties (density, viscosity, specific heat, etc.) of the fluid are constant. The turbulent Prandtl number Pr_t is assumed 1.0.

(7) The flow is steady and turbulent at all points along the flow channels.

(8) The flow fields can be divided into two regions such as the sublayer and the fully turbulent region.

The assumption that the point where the radius of maximum velocity coincides with the point where zero shear stress is seen is not necessarily true [19, 46]. On the other hand, it is not possible to theoretically calculate the radius of zero shear or the shear stress at the radius of maximum velocity. However, the radius of zero shear will very likely be a radius not too different from the radius of the maximum velocity for a smooth concentric annulus [2].

2.4.2 Velocity Distribution

From the basic equations, Eq. (2.16), the governing turbulent transport equation for momentum can be written in dimensionless parameters as:

$$\frac{\partial u_j^+}{\partial \zeta_j^+} = \delta_j^+ \left[\frac{(\tau/\tau_R)_j}{1+(\varepsilon_M/\nu)_j} \right] \qquad (0 \le \zeta \le 1) \tag{2.30}$$

To solve Eq. (2.30), information on the eddy diffusivity and the shear stress distribution are needed. Once the eddy diffusivity for momentum, $\left(\varepsilon_M/\nu\right)_j$, and the shear stress ratio, $\left(\tau/\tau_R\right)_j$, are known for the entire fluid region, the velocity profiles can be derived. The details of the derivation of Eq. (2.30) are given in Appendix 2.

2.4.3 Eddy Diffusivity for Momentum, ε_M

To perform turbulent boundary-layer calculations, either information or a theory to evaluate the term $\overline{u'v'}$ is required. This is frequently referred to in the literature as the turbulence "closure" problem, and it is usually solved by solving an algebraic equation, or a differential equation, for $\overline{u'v'}$ which is defined as an apparent turbulent shear stress. It seems plausible that it should go to zero if there is no gradient in the mean velocity

profile, just as the viscous shear stress goes to zero. In fact, this is not precisely so, but it is close enough for many practical applications. It seems reasonable to state that:

$$\overline{u'v'} \propto \frac{\partial \bar{u}}{\partial y}$$

As a proportionality factor, the eddy diffusivity for momentum, ε_M, is defined as:

$$\overline{u'v'} = -\varepsilon_M \frac{\partial \bar{u}}{\partial y} \tag{2.31}$$

This is nothing more than a definition; there are still some problems in evaluating ε_M.

In this study, the eddy diffusivity models for momentum are originally from van Driest [5] and Reichardt [6] for sublayer regions and fully turbulent regions, respectively. Those models were modified for the present flow channel geometry with the variable von Kármán constant, κ_i, proposed by Kim et al [1]. It is assumed that the von Kármán constant, κ_i, for the inner core of transverse convex surface curvature, is a function of the radius of an inner core in a concentric annulus, R_i, or R_i^*, as was discussed in Section 2.3.

The concept of a sublayer [34] is used for regions close to each wall. This concept demands the sublayer model for which the eddy diffusivity retains a small maginitude throughout the sublayer and goes to zero only at the wall itself. The van Driest hypothesis [34] is to provide an eddy diffusivity in the sublayer that becomes zero at y = 0. It has the virtue that it allows a continuous calculation through the sublayer and into the fully turbulent region. With this, the Prandtl mixing length [34] can be used all the way to the wall. For simulating the sublayer, a damping function is needed in the mixing length equation, given as:

$$l = \kappa\, y\left(1 - e^{-y^+/A^+}\right) \tag{2.32}$$

where A^+ is the damping constant, which is determined empirically. To describe Eq. (2.32) in terms of the eddy diffusivity for momentum, ε_M is:

$$\frac{\varepsilon_M}{\nu} = \frac{l^2}{\nu}\frac{du}{dy} = l^{+2}\frac{du^+}{dy^+} \tag{2.33}$$

Rearranging Eq. (2.33) with the proposed variable von Kármán constant, κ_t, the modified eddy diffusivity distributions, $\left(\frac{\varepsilon_M}{\nu}\right)_j$, for regions close to each wall, $\left(0 \le y_j^+ \le y_\mu^+\right)$, becomes:

$$\left(\frac{\varepsilon_M}{\nu}\right)_j = \kappa_j^2\, y_j^{+2}\left[1 - \exp\left(-\frac{y_j^+}{A_j^+}\right)\right]^2\left|\frac{\partial u_j^+}{\partial y_j^+}\right| \tag{2.34}$$

Eq. (2.34) may be further expressed for $\left(0 \le \zeta_j \le \zeta_{j\delta}\right)$ as (see Appendix 3):

$$\left(\frac{\varepsilon_M}{\nu}\right)_j = \frac{1}{2}\left[-1 + \left\{1 + 4\left(\kappa_j \delta_j^+\right)^2 \zeta_j^2\left[1 - \exp\left(-\frac{\delta_j^+ \zeta_j}{A_j^+}\right)\right]^2\left(\frac{\tau}{\tau_R}\right)_j\right\}^{0.5}\right] \tag{2.35}$$

Since the velocity profile outside the viscous sublayer should differ from the law of the wall, the logarithmic law of the wall can not be used. For the fully developed regions outside the sublayer, Reichardt [6] proposed the following expression for ε_M based on experimental data for the turbulent core in a smooth pipe:

$$\frac{\varepsilon_M}{\nu} = \frac{\kappa R^+}{6}\left[1 - \left(\frac{r}{R}\right)^2\right]\left[1 + 2\left(\frac{r}{R}\right)^2\right] \tag{2.36}$$

where $r = R_o - y$ and κ is assumed to be a constant and equal to 0.4.

Assuming that the expression of Eq. (2.36) would be applicable in a modified form, Levy [16] and Roberts [29] both derived expressions for the velocity profiles in the turbulent flow through the fully developed region of a concentric annulus, and their expressions were seen to be valid for all the regions of a concentric annulus, provided appropriate values were given to the constant κ_i for the inner wall regions.

In this study, it is further postulated that Reichardt's expression [6] for the eddy diffusivity for momentum can be applied to the entire fully developed turbulent flow regions on both sides of the concentric annulus with proper modification for the regions outside the sublayer, $\left(y_{js}^{+} \le y_j^{+} \le \delta_j^{+}\right)$, as:

$$\left(\frac{\varepsilon_M}{\nu}\right)_j = \frac{\kappa_j \delta_j^{+}}{6}\left[1-\left(1-\frac{y_j^{+}}{\delta_j^{+}}\right)^2\right]\left[1+2\left(1-\frac{y_j^{+}}{\delta_j^{+}}\right)^2\right] \tag{2.37}$$

where j refers to region i (inner) or o (outer) and further reduced to for $\left(\zeta_{js} \le \zeta_j \le 1\right)$ as:

$$\left(\frac{\varepsilon_M}{\nu}\right)_j = \frac{\kappa_j \delta_j^{+}}{6}\zeta_j\left(2-\zeta_j\right)\left(3-4\zeta_j+2\zeta_j^2\right) \tag{2.38}$$

where $\zeta_{js} = y_{js}^{+}/\delta_j^{+}$.

2.4.4 Friction Factor and Reynolds Number

The friction factor may be defined by:

$$f_j = \frac{\tau_{R_j}}{\frac{1}{2}\rho u_b^2} \tag{2.39}$$

Since it is assumed that the pressure gradient is constant, the force balance yields the following equation:

$$\frac{dp}{dx}\pi(R_o^2 - R_i^2) = 2\pi(\tau_{Ro}R_o + \tau_{Ri}R_i) \tag{2.40}$$

Therefore, the friction factor, f, can be obtained from the definition as:

$$f = \frac{(R_o - R_i)}{\rho u_b^2}\left(-\frac{dp}{dx}\right) \tag{2.41}$$

Substituting Eq. (2.41) into Eq. (2.40), and after some rearrangement using dimensionless parameters, the friction factor becomes (see Appendix 4):

$$f = 8\left[\frac{\left\{1-\left(\frac{1}{\alpha}\right)\right\}^2\left\{1+\left(\frac{1}{\alpha}\right)\left(\frac{\tau_{R_o}}{\tau_{R_i}}\right)\right\}}{\left\{1+\left(\frac{1}{\alpha}\right)\right\}}\right]\left(\frac{R_i^+}{\mathrm{Re}}\right)^2 \tag{2.42}$$

where the shear stress distribution based on shear stress for the outer region is given as (see Appendix 1):

$$\frac{\tau_{R_i}}{\tau_{R_o}} = \left(\frac{1}{\alpha}\right)\left(\frac{R_m^2 - R_i^2}{R_o^2 - R_m^2}\right) \tag{2.43}$$

The Reynolds number is defined in the usual way as:

$$\mathrm{Re} = \frac{\rho u_b De}{\mu} = \frac{u_b De}{\nu} \tag{2.44}$$

where u_b is the average bulk velocity defined by:

$$u_b = \frac{\int_A u\, dA}{\int_A dA} \tag{2.45}$$

The bulk velocity is derived from the definition as:

$$u_b = \frac{1}{\pi(R_o^2 - R_i^2)}\left[\int_{R_i}^{R_m} u_i 2\pi r dr + \int_{R_m}^{R_o} u_o 2\pi r dr\right] \tag{2.46}$$

which can be written in the dimensionless form as:

$$u_b = \left(\frac{\nu}{R_o}\right)\left[\frac{2\alpha}{1-\alpha^2}\right]\left[\delta_j^+ \int_0^1 (1+\Delta_i\zeta_i)u_i^+ d\zeta_i + \frac{1}{\alpha}\delta_o^+ \int_0^1 (1-\Delta_o\zeta_o)u_o^+ d\zeta_o\right] \tag{2.47}$$

Substituting Eq. (2.47) into Eq. (2.44) with some rearrangement yields:

$$\mathrm{Re} = \left[\frac{4}{1+\alpha}\right]\left[\alpha\delta_i^+ \int_0^1 (1+\Delta_i\zeta_i)u_i^+ d\zeta_i + \delta_o^+ \int_0^1 (1-\Delta_o\zeta_o)u_o^+ d\zeta_o\right] \tag{2.48}$$

The method for non-dimensionalization for Eq. (2.47) and Eq. (2.48) is given in Appendix 4.

2.5 Relative Velocity

In the Section 2.4, the relationship between the average velocity, u_b, and Reynolds number is defined by Eq. (2.44). This Eq. (2.44) can be rearranged as:

$$u_b = \frac{\mathrm{Re}\cdot\nu}{De} = \frac{\mathrm{Re}\cdot\nu}{2(R_o - R_i)} \tag{2.49}$$

The relative velocity may be defined in the usual way as:

$$U^* = \frac{U}{u_b} \tag{2.50}$$

where U is the velocity of the moving inner core.

Substituting Eq. (2.49) into Eq. (2.50) with some rearrangement yields:

$$U^* = \frac{2U(R_o - R_i)}{\mathrm{Re}\cdot\nu} \tag{2.51}$$

which can be written in the dimensionless form as:

$$U^* = \frac{2(1-\alpha)U^+ \cdot R_i^+}{\alpha \cdot \mathrm{Re}} \tag{2.52}$$

2.6 Diabatic Turbulent flow in the Fully Developed Regions of a Concentric Annulus with a moving core

In the previous section, the turbulent flow velocity profiles of a concentric annulus were developed from a eddy diffusivity of momentum. Now the problems of the thermal boundary layer development where both the fluid velocity and temperature profiles are fully developed will be considered. Employing the turbulent Prandtl number for unit value, the temperature distribution in these regions will be developed. The ratio of eddy diffusivities for momentum and heat will be discussed in some detail. The energy integral equation will then be applied. Finally, the Nusselt numbers will be obtained for the various Reynolds numbers, Prandtl numbers, radius ratios and the relative velocity of the moving inner cores.

2.6.1 Eddy diffusivity for Heat

In order to perform turbulent boundary-layer heat-transfer calculations, some methods for evaluating $\overline{v'T'}$ are required. A theory can be sought for direct evaluation of $\overline{v'T'}$, or alternatively an eddy diffusivity can be introduced, analogous to the eddy diffusivity for momentum. $\overline{v'T'}$ is an apparent turbulent heat flux in the direction normal to the main flow. It seems plausible that it goes to zero if there is no mean temperature gradient in the normal direction, for otherwise a violation of the second law of thermodynamics becomes possible. Thus it seems reasonable to state that:

$$\overline{v'T'} \propto \frac{\partial \overline{T}}{\partial y}$$

As a proportionality factor, the eddy diffusivity for heat transfer, ε_H, is defined:

$$\overline{v'T'} = \varepsilon_H \frac{\partial \overline{T}}{\partial y} \tag{2.53}$$

Similarly, the ratio of the eddy diffusivity for momentum and heat, $\varepsilon_M / \varepsilon_H$, which is called the turbulent Prandtl number, Pr_t, can be defined as:

$$Pr_t = \frac{\mu_t c}{k_t} = \frac{\varepsilon_M}{\varepsilon_H} \tag{2.54}$$

where μ_t and k_t are eddy viscosity and eddy conductivity, respectively. Knowing ε_M at every point, the thermal boundary layer can be solved with the appropriate information on Pr_t. The turbulent Prandtl number, Pr_t, plays a crucial role in the analytical studies to predict heat transfer coefficients in turbulent convective heat transfer [8]. To simplify the mathematical manipulation, many of these analytical results are based on the assumption that this ratio is equal to unity. The simple assumption, $Pr_t = 1$, is equivalent to Reynolds analogy [34]. According to the experimental works reported in the references [11, 19, 28, 34, 47, 48], it appears that the Pr_t is not equal to unity, but varies with the distance from the wall and has a complicated relationship with other variables such as y^+, Pr, Re, α, etc.

In the supporting investigation performed for the unity value of turbulent Prandtl number [40], Ludwieg [24] found that the ratio, $\varepsilon_H / \varepsilon_M = 1 / Pr_t$, varies from about unity at the wall to about 1.5 in the centre of a pipe and is independent of the Mach number. Similar results were reported by Johnson [49] who made measurements in a boundary layer on a heated wall. According to these, the ratio $\varepsilon_H / \varepsilon_M$ increases from about unity at the wall to approximately 2 at the edge of the boundary layer. Page [47] and Reichardt [40] reported the measurement of 2, the former in the wake behind a circular cylinder, and the latter in a free jet, both in an incompressible fluid flow. According to the

preceding measurements, the ratio, $\varepsilon_H/\varepsilon_M$, is smaller in a boundary layer than in a free stream, due to the influence of the wall on the boundary layer. Therefore, it seems plausible that the ratio, $\varepsilon_H/\varepsilon_M$, has a value of unity at the wall (according to Ludwieg [24], the value is 1.08 at $Pr_t = 0.9$) and increases to a value of 2 ($Pr_t = 0.5$) away from the wall. In practice, frequently, a constant value of $\varepsilon_H/\varepsilon_M = 1$ ($Pr_t = 1$) or of 1.3 (Reichardt [40], giving $Pr_t = 0.77$) is assumed. In this study the value of unity for the turbulent Prandtl number is used and this is because of the following facts.

From the experimental works [34], it is at least clear that the Pr_t, the ratio of the eddy diffusivity for momentum and heat, $\varepsilon_M/\varepsilon_H$, is,

(1) smaller than unity for air

(2) greater than unity for liquid metal.

However, it must be pointed that the available experimental evidence is not sufficiently consistent to arrive at any concrete conclusion.

Some workers such as Leung et al. [23] in their analysis on heat transfer with turbulent flow in concentric annuli with constant and variable heat flux used the theoretical treatment of Jenkins [50]. Jenkins considered the heat conduction to or from an element of an eddy during its transverse to the main flow direction. From this consideration, a correlation for Pr_t was obtained. However, Leung et al. [23] used a multiplying factor of 1.2 to fit the expression better to their experimental data.

In his study of the thermal entrance problems of concentric annuli, Lee [18] divided the annular passage into two regions and allowed the variation of $\varepsilon_H/\varepsilon_M$ based on his

previous experimental measurements. Park [28] formulated an empirical correlation of the turbulent Prandtl number, $\varepsilon_H / \varepsilon_M$, as a function of y^+ and radius ratio, α from the results of his experimental work as:

$$\sigma\left(y_j^+\right) = \frac{\varepsilon_H}{\varepsilon_M}\left(y_j^+\right) = 0.968\ \alpha^{-0.045}\ y_j^{+0.031} \tag{2.55}$$

In his analysis, Park [28] used Eq. (2.55) for the case of Prandtl numbers bigger than 0.5 because the experimental results were obtained using air as the working fluid.

The problem of the turbulent Prandtl number is still subject to further studies, both experimentally and analytically. The effects of turbulence structure, fluid properties and wall characteristics on eddy motion must be taken into consideration.

2.6.2 Temperature Distribution

Temperature profiles can be derived from the energy equation governing the transport of heat, given by Eq. (2.23), if the functions for the heat flux and the eddy diffusivity for heat are known.

Eq. (2.23) can be written in non-dimensional parameters as (see Appendix 2):

$$\frac{\partial T_j^+}{\partial \zeta_j} = \pm\ \mathrm{Pr} \cdot \delta_j^+ \left[\frac{q_j / q_{R_i}}{1 + \left(\mathrm{Pr}/\mathrm{Pr}_t\right) \cdot \left(\varepsilon_M / \nu\right)_j} \right] \qquad \left(0 \le \zeta_j \le 1\right) \tag{2.56}$$

where the dimensionless temperature for each region is defined as:

$$T_j^+ = \frac{\left(T_{R_i} - T_j\right)\ c\ \tau_{R_j}}{q_{R_i}\left(\tau_{R_i}/\rho\right)^{0.5}} \tag{2.57}$$

where +ve for j = i and -ve for j = o.

The heating condition is a uniform heat flux at the core tube only and the heat flux distributions are obtained form an energy balance as (see Appendix 1):

$$q_i/q_{R_i} = \frac{1-\alpha^2\left(1+\Delta_i\zeta_i\right)^2}{\left(1-\alpha^2\right)\left(1+\Delta_i\zeta_i\right)} \qquad \left(0 \le \zeta_i \le 1\right) \tag{2.58}$$

and

$$q_o/q_{R_i} = \frac{\alpha\left(2-\Delta_o\zeta_o\right)\Delta_o\zeta_o}{\left(1-\alpha^2\right)\left(1-\Delta_o\zeta_o\right)} \qquad \left(0 \le \zeta_o \le 1\right) \tag{2.59}$$

The initial conditions for Eq. (2.56) are

$T_i^+ = 0$ at $\zeta_i = 0$ and $T_o^+ = T_{om}^+$ at $\zeta_o = 1$

The dimensionless velocity and temperature distributions in the inner and outer regions of the maximum velocity can now be obtained by solving this dimensionless differential equation, Eq. (2.56), respectively, once the eddy diffusivity and the matching conditions are established.

2.6.3 Nusselt Number

The Nusselt number is defined in the usual way as:

$$Nu = \frac{h \cdot 2(R_o - R_i)}{k} \tag{2.60}$$

and the convective heat transfer coefficient is defined as:

$$h = \frac{q_{R_i}}{(T_{R_i} - T_b)} \tag{2.61}$$

In dimensionless form, Eq. (2.60) becomes (see Appendix 4):

$$Nu = 2\left[\frac{1-\alpha}{\alpha}\right]\frac{R_i^+ \,\mathrm{Pr}}{T_b^+} \tag{2.62}$$

The bulk temperature, T_b, is defined as:

$$T_b = \frac{\int_{R_i}^{R_o} u(r) 2\pi r T dr}{\int_{R_i}^{R_o} u(r) 2\pi r dr} \tag{2.63}$$

T_b can be expressed in dimensionless form as:

$$T_b^+ = \left[\frac{4}{1+\alpha}\right]\left(\frac{1}{\mathrm{Re}}\right)[\alpha\delta_i^+ \int_0^1 (1+\Delta_i\zeta_i) u_i^+ T_i^+ d\zeta_i + \left(\frac{\tau_{R_i}}{\tau_{R_o}}\right)^{0.5} \delta_o^+ \int_0^1 (1-\Delta_o\zeta_o) u_o^+ T_o^+ d\zeta_o] \tag{2.64}$$

Therefore, the Nusselt number can be obtained by solving Eq. (2.64). The method of non-dimensionalization is given in Appendix 4.

2.7 Method of Solution

To obtain all the parameters such as u_j^+, T_j^+, Nu, Re, U^*, u_b, Pr, and so on for fully developed thermal boundary layer in a smooth concentric annulus with a moving core, the following calculation procedure are used:

(1) Input Parameters

$R_i^* = 0.005, 0.01, 0.02, 0.05, 0.1, 0.2, 0.5, 1.0$

$\alpha = 0.2, 0.5, 0.8$

$U^* = 0.0, 0.2, 0.4, 0.6, 0.8, 1.0$

$Pr = 0.01, 0.1, 0.72, 1.0, 2, 5, 10, 100$

$Pr_t = 1$

(2) Fixed Parameters

$\kappa_i = \kappa_o \cdot F(R_i^*)$ (calculated from Eq. (2.28))

$\kappa_o = 0.4$

$F(R_i^*) = 1 + 1.5\tanh(0.0064 / R_i^{*0.72})$ (calculated from Eq. (2.29))

$$A_i^+ = 22.70 + 0.634\left\{1 - \exp\left(-R_i^*/0.21\right)\right\} + 2.67\left\{1 - \exp\left(-R_i^*/0.02\right)\right\}$$

$A_o^+ = 26$

$y_{js}^+ = 26$ (sublayer thickness for inner and outer regions)

(3) Assume a value of R_m between R_o and R_i.

(4) The velocity profiles for the fully developed region are obtained from integration of Eq. (2.22) with Eqs. (2.35) and (2.38).

(5) From the continuity of velocities at the location of maximum velocity (r = R_m, or $\zeta_i = \zeta_o = 1$), the relationship between u_{im}^+ and u_{om}^+ is used as the

matching condition, shown below. If this equality works, the process will go on to the next step; if it does not, return to step (3) and reassume the value of R_m.

$$u^+_{om} = (\tau_{w_i}/\tau_{w_o})^{0.5}_d \cdot u^+_{im}$$

(6) The results from step (4) are substituted into Eq. (2.47) for bulk velocity, u_b, then friction factor, f, will be calculated from Eq. (2.42).

(7) The results from step (4) are substituted into Eq. (2.48) for Reynolds number, Re, then relative velocity will be calculated from Eq. (2.52). The initial velocity, U, can be calculated from the relative velocity, U^*, and bulk velocity, u_b, using Eq. (2.50). Once the velocity profiles are obtained in a concentric annulus with a moving core, one can move to the heat transfer calculations.

(8) Temperature distributions are computed from Eq. (2.56) with Eqs. (2.58) and (2.59) for the heat flux distributions and Eqs. (2.5) and (2.9) for the eddy diffusivity of momentum. Pr_t is assumed to be unit.

(9) The Nusselt number, Nu, is computed from Eq. (2.62) with bulk temperature from Eq. (2.64) and the given value of Pr Number.

CHAPTER 3
COMPUTATION

3.1 General Approach

Most of the theoretical calculation requires numerical integration where accuracy of the computation is very important. In most cases, "Simpson's rule" was used for the numerical integration and was checked by repeating the integration process with varying mesh sizes. The general methods used to solve this study are called "one-step methods" and all "one-step methods" can be expressed in the general form that is shown below, with variations in the manner in which the slope is estimated.

New value = old value + slope × step size.

According to this equation, the slope estimate is used to extrapolate from an old value to a new value over a distance d. This formula can be applied step-by-step to compute into the next step and hence, trace out the trajectory of the solution. The simplest approach is to use the differential equation to estimate the slope in the form of the first derivative at the previous point. In other words, the slope at the beginning of the interval is taken as an approximation of the average slope over the whole interval. This approach is called "Euler's method" [51] and it is extremely simple to program on a personal computer.

The numerical solution of ordinary differential equations (ODEs) involves two types of errors: round-off error and truncation error [51]. Round-off error is due to the fact that a computer can only represent quantities with a finite number of digits. Truncation error

is the discrepancy introduced by the fact that the numerical method employs an approximation to represent exact mathematical operations and quantities. It consists of two parts. The first is local truncation errors that result from an application of this method at each step. The second is to propagate truncation errors that result from the approximations produced during the previous steps. The sum of the two is the total or global truncation error.

As it is known with Euler's method, the source of errors is the fact that the derivative at the beginning of the interval is assumed to apply across the entire interval. Decreasing the step size may reduce these errors. However, to attain much better accuracy for the same computational effort we need to employ other one-step methods. For the calculations of this study the Runge-Kutta (RK) methods [51] are used. Among the higher-order techniques of the RK methods, the Butcher's Fifth-Order RK method is used.

To solve the governing differential equations for the fully developed turbulent flow in a smooth concentric annulus with a moving core, a set of grids with uniform spacing is first generated within the physical domain. Grid points are designed to have the same boundaries of the physical domain for consideration of boundary conditions.

To obtain the velocity profiles, u_j^+, Eq. (2.8) is used as the basic form and once a certain velocity profile is identified at a specific condition, other information such as friction factors, temperature profiles, and Nusselt numbers for momentum and heat transfer can then be produced.

The integration that we perform in this study for such values as the bulk velocity and bulk temperature, etc., is numerically calculated using Simpson's 1/3 rule [51]. While

there are higher-order formulas of Simpson's rules, we have used it in this study because of its simplicity and accuracy.

For the numerical calculations in the present study, using C++ language, a number of computer programs were prepared for the numerical evaluation of the theoretical expressions for the various parameters.

3.2 Calculation Procedure

The computer program developed for this study was partitioned into three sections:

Section 1: Assume a value of R_m, which is the position of the maximum velocity, and calculate the non-dimensional parameters, δ_j^+, R_j^+, and Δ_j, for a given set of input parameters (R_i, α, U*, Re, Pr, and ζ_j).

Section 2: Calculate the velocity and temperature distributions and the bulk parameters using the higher-order techniques of the RK methods, the Butcher's Fifth-Order RK method, to solve the governing differential equations and the higher-order formulas of Simpson's rules, Simpson's 1/3 rule [51], to solve integral equations.

Section 3: Calculate the friction factor, Nusselt numbers, influence coefficients and output the results

Section 1 is critical in determining all parameters and the validity of the results.

3.2.1 Methodology for Section 1

In Section 2.7, the input parameters and fixed parameters are already defined. For a given set of input parameters, the procedure for finding non-dimensional parameters is as follows:

(1) Assume a value of R_m between R_o and R_i.

(2) The values of α, R_j, R_j^+, Re, and Pr are prescribed.

(3) κ_i is calculated from Eqs. (2.26) and (2.27) with the inner radius, R_i.

(4) A_i^+ is calculated from the equation below:

$$A_i^+ = 22.70 + 0.634\left\{1-\exp\left(-R_i^*/0.21\right)\right\} + 2.67\left\{1-\exp\left(-R_i^*/0.02\right)\right\}$$

(5) δ_j^+ is calculated from the equation below:

$$\delta_j^+ = \left(|R_m - R_j| \left(\frac{\tau_R}{\rho} \right)_j^{0.5} \right) / \nu$$

(6) Δ_j is calculated from the equation below:

$$\Delta_j = \delta_j^+ / R_j^+ .$$

(7) ζ_j is calculated from the equation below:

$$\zeta_j = y_j^+ / \delta_j^+$$

3.2.2 Methodology for Sections 2 and 3

(1) The velocity profile

The velocity profile for each region is calculated by performing a numerical integration of the velocity gradient, Eq. (2.30) with Eq. (2.35) and Eq. (2.38), using Simpson's 1/3 rule.

(2) The temperature profile

Temperature distributions are computed from Eq. (2.56) with Eqs. (2.58) and (2.59) for the heat flux distributions and Eqs. (2.4) and (2.8) for the eddy diffusivity of momentum. Pr_t is assumed to be unit.

(3) The results from step 1 are substituted into Eq. (2.47) for bulk velocity, u_b, then friction factor, f, will be calculated from Eq. (2.42).

(4) The results from step 1 are substituted into Eq. (2.48) for Reynolds number, Re, then relative velocity will be calculated from Eq. (2.52). The initial velocity, U, can be calculated from the relative velocity, U^*, and bulk velocity, u_b, using Eq. (2.50).

Once the velocity profiles are obtained in a concentric annulus with a moving core, one can move to the heat transfer calculations.

(5) The Nusselt number, Nu, is computed from Eq. (2.62) with the bulk temperature from Eq. (2.64) and the given value of Pr.

3.3 Results of Computations

The governing differential equations have been solved by numerical procedure with the boundary conditions appropriate to the fully developed turbulent flows in a concentric annulus with a moving core.

The method to obtain the correct value of the van Driest Damping Parameters (effective thickness), A_i^+, at a given R_i^* of 0.005 is shown in Fig. 2.1. The two-layer model was given from the Prandtl mixing-length model for the sublayer and fully developed turbulent region, then compared to the van Driest model for velocity distributions [19]. Figs. 2.2, 2.3, 2.4 and 2.5 are for R_i^* of 0.01, 0.05, 0.1 and 1.0, respectively. From such figures, the variations of effective thickness, A_i^+, for different values of R_i^* were obtained as they are shown in Fig. 2.6, which demonstrates the effect of Transverse Convex Curvature. The effective values of A_i^+ is correlated and are given as:

$$A_i^+ = 22.70 + 0.634\left\{1 - \exp\left(-R_i^*/0.21\right)\right\} + 2.67\left\{1 - \exp\left(-R_i^*/0.02\right)\right\} \qquad (3.1)$$

The relationship between R_i^+ and Reynolds number for the value of U* = 0.0 is shown in Fig. 2.7, respectively. Radius ratio, α, is fixed at 0.5 and R_i^* are 0.005, 0.01, 0.05, 0.1, and 1.0, over the Reynolds ranges of about 10^4 to 10^5. It is compared with the case of Suk [2] for concentric annuli with the stationary core studied. The results shown in the figure validate the present study. The agreement is very good.

Figs. 2.8 and 2.9 show the predicted velocity distributions in the fully developed region at $R_i^* = 1.0$ with a fixed radius ratio of $\alpha = 0.5$ to compare with the case studied of Shigechi et al. [4]. Since there is no experimental data available for concentric annuli

with moving cores, this is the only way to test the validity of the present study. The comparisons of the predicted velocity distributions with those of the previous studies [2, 4] are shown in Fig. 2.10 at $R_i^* = 1.0$ with a fixed radius ratio of $\alpha = 0.5$ and different relative velocities of $U^* = 0.0$, 0.6 and 1.0. The agreement is very good.

The predicted maximum velocity profiles of the inner and outer cores with a fixed relative velocity of $U^* = 0.4$ and a fixed Reynolds number of Re = 100,0000 are shown in Figs. 2.11 and 2.12. Fig. 2.13 shows the predicted maximum velocity profiles of the inner core for a fixed relative velocity of $U^* = 0.8$ and a fixed Reynolds number of Re = 100,0000. The radius ratios are $\alpha = 0.2$, 0.5 and 0.8, respectively.

The predicted bulk velocity distributions for different relative velocities, U*, of 0.4 and 0.8 at a given Reynolds number, Re = 100,0000, are given in Figs. 2.14 and 2.15.

The friction factors, f, calculated from Eq. (2.39) for $R_i^* = 1.0$ and $\alpha = 0.999$ are plotted in Fig. 2.16, and compared with two empirical correlation for the fully developed turbulent flow between parallel plates for the Reynolds number ranging between 20,000 to 100,000 [34]. In Figs. 2.17 to 2.22, the normalized friction factors, $f^* (f/f_{1.0m})$, are plotted as a function of Re for three radius ratios, $\alpha = 0.2$, 0.5 and 0.8, and for R_i^* at 0.005, 0.01, 0.02, 0.05, 0.1, and 0.5.

The predicted temperature distributions in the fully developed region at $R_i^* = 1.0$ with a fixed radius ratio of $\alpha = 0.5$ and a fixed relative velocity of $U^* = 1.0$ to compare with that of Shigechi et al. [4] are shown in Figs. 2.23 and 2.24. They are for two Prandtl numbers of Pr = 0.72 and 5.0.

The predicted temperature distributions for three different radii of the inner cores are plotted in Fig. 2.25 with a fixed radius ratio of $\alpha = 0.5$ and a fixed relative velocity of U^*

= 1.0. The comparisons of the predicted temperature distributions with that of Shigechi et al. [4] are shown in Figs. 2.26 and 2.27 at $R_i^* = 1.0$ with a fixed radius ratio of $\alpha = 0.5$ and three different relative velocities of $U^* = 0.0$, 0.5 and 1.0. Both are for a fixed Reynolds number (Re = 100,0000) and two different Prandtl numbers of Pr = 0.72 and 5.0.

The predicted maximum temperature profiles of the inner core for a fixed Prandtl number of Pr = 0.72 and a fixed Reynolds number of Re = 100,0000 are shown in Figs. 2.28 and 2.29, and the radius ratios, α, are 0.2, 0.5 and 0.8, respectively.

Figs. 2.30 to 2.32 show the predicted Nusselt numbers for the value of $R_i^* = 1.0$ with a fixed radius ratio of $\alpha = 0.999$ to compare with the case of parallel plates [34]. The values of the Prandtl numbers, Pr, were 0.7, 1.0, and 10.0 and the range of Reynolds numbers was between 10^4 and 10^5. The Nusselt numbers, Nu, calculated from Eq. (2.62) for a fixed radius ratio of $\alpha = 0.5$, a fixed Prandtl number of Pr = 0.72, and three different relative velocities of $U^* = 0.0$, 0.5 and 1.0 are given in Figs. 2.33 and 2.34. The values of R_i^* are 0.005, 0.05, 0.2, 0.5, and 1.0 and the Reynolds numbers of Re are 20,000 and 100,000, respectively. The Nusselt numbers, Nu, for a fixed radius ratio of α = 0.5, a fixed Reynolds number of $Re = 10^5$, and different Prandtl number of Pr = 0.01, 0.72, 5.0, 10.0, 100.0 are given in Figs. 2.35 and 2.36. The values of R_i^* are 0.005, 0.05, 0.2, 0.5, and 1.0 and the relative velocities, U^*, are 0.5 and 1.0, respectively. Figs. 2.37 and 2.38 show the Nusselt numbers, Nu, for a fixed Prandtl number of Pr = 0.72 and different radius ratios of $\alpha = 0.2$, 0.5, 0.8. The values of R_i^* are 0.005, 0.05, 0.2, 0.5, and 1.0 and the relative velocities of $U^* = 0.5$ and 1.0, respectively. Figs. 2.39 and 2.40 show the Nusselt numbers, Nu, for a fixed radius ratio of $\alpha = 0.5$, a fixed Prandtl number of Pr

= 0.72, and three different Reynolds numbers of Re = 20,000, 50,000, and 100,000. The values of R_i^* are 0.005, 0.05, 0.2, 0.5, and 1.0 and the relative velocities, U^*, are 0.5 and 1.0, respectively. The Nusselt numbers for several cases of the inner core radii with a fixed radius ratio of α = 0.5, Reynolds number of Re = 20,000 and Prandtl number of Pr = 0.72 are shown in Fig. 2.41. Figs. 2.42 and 2.43 are graphs for the cases of Pr = 1.0 and Pr = 10.0, respectively.

CHAPTER 4
RESULTS AND DISCUSSTIONS

4.1 General Overview

The present study investigated the effect of Transverse Convex Surface Curvature (T.C.S.C) in concentric annuli with moving cores. The results for the characteristics of turbulent fluid flow and heat transfer can be evaluated through analytical studies. In the present study, the effect of Transverse Convex Surface Curvature (T.C.S.C) on the fluid flow characteristics in terms of the velocity distribution, friction factor, temperature distribution and heat transfer coefficients was predicted and investigated with numerical methods for the fully developed turbulent flow and heat transfer in a concentric annulus with a moving core. In the analysis, it was assumed that heat is generated uniformly at the moving inner core.

In the analytical study, i.e. Chapter 2, the analytical results were obtained through a mathematical model for turbulence models based on a variable van Driest Constant, A_t^+, [2] and a variable von Kármán constant, κ_t, proposed in the previous studies [7].

The numerical procedure given in Chapter 3 was conducted on the effects of the inner radius, R_i^*, with the annuli having different values for the radii of the inner cores, R_i^*. The values are between 0.005 and 1.0. The radius ratio, α, was fixed as a constant to demonstrate the effect of Transverse Convex Surface Curvature (T.C.S.C.) with the Reynolds number ranging from 20,000 to 100,000. Six different Prandtl numbers (0.01, 0.72, 1.0, 5.0, 10.0, and 100.0) were also used to view the T.C.S.C effect on heat transfer.

Because there are no results in the literature that have been produced on the fully developed region for turbulent flow in a concentric annulus with a moving core, the results from the present study were compared to the special cases against those previous studies, i.e., $U^* = 0.0$ and $R_i^* = 1.0$.

4.2 Turbulent Flow in the Fully Developed Regions

The original van Driest constant, A_i^+, of 26 [4] is an empirically determined effective sublayer thickness. The law of the wall is for the fully developed region in the two-layer model shown as follows [34]:

$$u^+ = y^+ \qquad \text{for} \quad 0 < y^+ < A^+$$

$$u^+ = (1/\kappa_i)\ln y^+ + 5.25 \qquad \text{for} \quad A^+ < y^+$$

The van Driest hypothesis is a sublayer scheme that provides for an eddy diffusivity that becomes 0 only at y = 0, and that also has the virtue that it allows a continuous calculation through the sublayer and into the fully turbulent region with no discontinuities. It does a reasonable job of predicting the various flow parameters throughout the entire sublayer region.

With this scheme, the concept of the Prandtl mixing length was used all the way to the wall instead of truncating it to zero at an assumed effective outer edge of the sublayer, but the Damping function was introduced for simulating the sublayer in the mixing-length equation. A_i^+ was used as Damping parameter in the equation.

In this study, the value of A^+ for the inner core, A_i^+, seems to change with the changing inner core radius, R_i^*, as with the von Kármán constant for the inner core, κ_i. The model from van Driest for velocity distribution [19] is:

$$u_i^+ = \int_0^{y_i^+} \frac{2}{1+\left\{1+4\kappa_i^2 y_i^{+2}\left[1-\exp\left(-y_i^+/A_i^+\right)\right]^2\right\}^{0.5}} dy_i^+ \qquad \text{for} \qquad 0 \le y_i^+$$

The comparison was made to the two-layer model as shown in Figs. 2.1 to 2.5 and the appropriate A_i^+ was given to each inner core radius, R_i^*. In Fig. 2.6, the results were

gathered on the A_i^+ vs. R_i^* graph to show A_i^+ approaching the fixed value of approximately 26. The correlative equation was given as Eq. (3.1) in Chapter 3.

4.2.1 Velocity Distribution

The present analytical velocity profiles were obtained for the fully developed turbulent boundary layer flows in a concentric annulus with a moving core at a Reynolds number of approximately 100,000 with a fixed radius ratio of $\alpha = 0.5$ and a fixed radius of $R_i^* =$ 1.0 and compared with the previous work [4], respectively in Figs. 2.8 and 2.9. Since there are no experimental data available for concentric annuli with moving cores, this is the only way to prove the validity of the present study.

Most of the velocity profiles are plotted as dimensionless velocity, u_j^+, in order to plot all curves on the same basis. Since the shear stress at the walls of both tubes is constant for the fully developed turbulent flows in a concentric annular duct, the friction velocities, u_{τ_j}, for the inner region of the flow field can be determined. The conventional dimensionless parameters, u_i^+ and y_i^+ can be obtained from these friction velocities.

In Figs. 2.8 and 2.9, the predicted velocity distribution and the previous work [4] of the fully developed turbulent flow with a fixed relative velocity, $U^* = 0.5$ and 1.0, and a fixed radius of the inner core, R_i^*, at a given Reynolds number are shown where α is kept at 0.5. The values of present analytical velocity distributions are almost identical to the results of the previous analytical data [4].

The predicted velocity profiles and those of the previous studies [2, 4] of the fully developed turbulent boundary layer flows with a fixed radius of the inner core, $R_i^* =1.0$,

and a fixed radius ratio, α = 0.5, at a given Reynolds number, Re = 100,000, are shown in Fig. 2.10, in which the predicted velocity profiles with three different relative velocities, U* = 0.0, 0.6, and 1.0, are plotted with the comparison of the previous studies [2, 4]. The data for a relative velocity, U* = 0.0, of the present analysis are almost identical to the values of the previous analytical data [2] and for a relative velocity, U* = 1.0, are almost identical to the results of Shigechi et al. [4]. Throughout the evaluation of predicted velocity profiles and velocity distribution, the results of Figs. 2.8 to 2.10 demonstrate the accuracy of the present analysis.

Figs. 2.11 and 2.12 show the predicted maximum velocity profiles in the fully developed region with a fixed relative velocities of U^* = 0.4 and a fixed Reynolds number of Re = 100,0000 over the radius ranges of the inner cores, R_i^* = 0.005, 0.01, 0.02, 0.05, 0.1, 0.2, 0.5, and 1.0. They are for different radius ratios of α = 0.2, 0.5 and 0.8. The dimensionless velocity at the location of the maximum velocity does not coincide with the given condition shown in Figs. 2.11 and 2.12. This is due to the different values of the wall shear stress at the walls, i.e. at $r = R_m$, or $\zeta_i = \zeta_o = 1$, the dimensionless velocity $u_{om}{}^+$ is related to $u_{im}{}^+$ through the equation of $u_{om}^+ = (\tau_{w_i}/\tau_{w_o})_d^{0.5} \cdot u_{im}^+$ and

$$\left.\frac{\partial u_o^+}{\partial \zeta_o}\right]_{\zeta_o=1} = \left.\frac{\partial u_i^+}{\partial \zeta_i}\right]_{\zeta_i=1} = 0.$$

In Fig. 2.13, the predicted velocity profiles with three different radius ratios, α = 0.2, 0.5, and 0.8, a fixed relative velocity of U^* = 0.8, and a fixed Reynolds number of Re = 100,0000 over the radius ranges of the inner cores, R_i^* = 0.005, 0.01, 0.02, 0.05, 0.1, 0.2, 0.5, and 1.0, are shown which at a relative velocity, U^* = 0.8, shows the difference of the predicted velocity profiles from Fig. 2.11 with a relative velocity, U^* = 0.4.

The predicted bulk velocities for the fully developed turbulent boundary layer flows in a concentric annulus with a moving core for a Reynolds number of approximately 100,000 with three different radius ratios, α = 0.2, 0.5, and 0.8, are seen in Figs. 2.14 and 2.15. They are for different relative velocities of U* = 0.4 and 0.8 over the radius ranges of the inner cores, R_i^* = 0.005, 0.01, 0.02, 0.05, 0.1, 0.2, 0.5, and 1.0. The results show that the predicted average velocities, u_b^+, increase with the increase of the relative velocities, U*.

Throughout the evaluation of predicted velocity profiles and velocity distribution, it is evident that the velocity profiles deviate with changing inner core radii, R_i^*, for the fully developed turbulent flow in a concentric annulus with a moving core. The transverse convex surface curvature, therefore, is one of the factors which affects the characteristics of turbulent fluid flow in addition to the radius ratio, α, and relative velocities, U*.

4.2.2 Friction Factor

The theoretical skin friction coefficients for the fully developed turbulent flows in a concentric annulus with a moving core, f, calculated from Eq. (2.39) with the inner core radius, R_i^*=1.0, and a fixed radius ratio of α = 0.999 are shown in Fig. 2.16. Having the radius ratio, α, of 0.999 and the inner core radius, R_i^*, of 1.0, the geometry of the concentric annulus can be regarded as parallel plates and therefore, the experimental results for the fully developed turbulent flow in the parallel plates are compared with the results of the present analysis. As can be seen in the figure, the calculation is in a good agreement with the experimental data of Reynolds number, Re > 20,000.

Fig. 2.17 illustrates friction factors vs. Reynolds numbers for the fully developed turbulent flow at a fixed radius ratio, α = 0.2. The values from the calculations made for several radii of the inner cores, R_i^*, are normalized by the case of an inner core radius, R_i^* = 1.0, which are indicated as f*. It shows that the normalized friction factor, f*, increases with a decreasing value of the inner core radius, R_i^*. This implies that as R_i^* decreases, the shear stress at the inner wall increases for a given Reynolds number at a fixed value of α. This must be the fact that, since the velocity gradient, $\left(\partial u/\partial y\right)$, near the wall surface for the inner region becomes flatter as the inner core radius, R_i^*, becomes smaller, the wall shear stress of the inner core, τ_{W_i}, increases with a decreasing value of the inner core radius, R_i^*. The turbulence production, $-\rho\overline{u'v'}\left(\partial u/\partial y\right)$, increases with a decreasing value of R_i^*, because the velocity gradient, $\left(\partial u/\partial y\right)$, near the wall

surface for the inner core becomes flatter with a decreasing value of R_i^*. The same trend for the fully developed turbulent flow with a fixed radius ratio, α, which Kim [7] proved experimentally, can be seen in Fig. 2.18. The effects of transverse convex curvature at the radius ratio, $\alpha = 0.5$ on the friction factor calculated for different values of inner core radii R_i^* are shown in Figs. 2.19 and 2.20. Figs. 2.21 and 2.22 show the same for α = 0.8. It is seen that the effect of Re on f* for a given value R_i^* is very small.

4.3 Turbulent Flow and Heat Transfer in the Fully Developed Regions

4.3.1 Temperature Distribution

The effects of the transverse convex surface curvature for a Reynolds number of approximately 100,000 with a fixed radius ratio of $\alpha = 0.5$, a fixed radius of $R_i^* = 1.0$, and a fixed relative velocity of U* = 1.0 for two different Prandtl number of 0.72 and 5.0 obtained in this analysis on temperature distributions are shown in Figs. 2.23 and 2.24, respectively. The conditions for both figures are for uniform heat flux at the core. In the figures, the predicted temperature distributions are compared with those of Shigechi et al. [4] for the values of the present theoretical temperature distributions are almost identical to the results of Shigechi et al. [4], which indicates that the analysis is correct.

In Fig. 2.25, the predicted temperature profiles for the fully developed turbulent boundary layer flows in a concentric annulus with a moving core are shown with different radii of the inner cores with the fixed values of $\alpha = 0.5$, Pr = 0.72, Re = 100,000, and U* = 1.0. The figure illustrates that, as the inner core radius, R_i^*, becomes smaller, the value of the dimensionless temperature, T_i^+, becomes smaller and it is evident from Eq. (2.56) that for given values of α, Pr and Re, the turbulent heat transfer becomes more vigorous with a decreasing value of R_i^*. The abscissa of the curve in the figure is chosen to be a non-dimensional distance, $(r - R_i)/(R_o - R_i)$, because annuli of different inner core radii, R_i^*, are considered.

The predicted temperature profiles obtained in this study are compared with those of Shigechi et al. [4] in Figs. 2.26 and 2.27. Since there are no experimental data available for concentric annuli with moving cores, this is the only way to evaluate the validity of

the present study. Each figure shows the predicted temperature profiles at a fixed radius ratio of $\alpha = 0.5$, a fixed Reynolds number of Re = 100,000, and a fixed inner core radius of $R_i^* = 1.0$ with three different relative velocities, U* = 0.0, 0.5, and 1.0. They are for different Prandtl numbers of Pr = 0.72 and 5.0, respectively. They demonstrate that as the relative velocities, 'U*', becomes larger, the value of the dimensionless temperature, 'T_i^+', becomes larger. Similar to Fig. 2.25, it is evident from Eq. (2.56) that at given fixed values of α, Pr and Re, the turbulent heat transfer becomes more vigorous with a increasing value of U*. The values of the present analytical temperature distributions are almost identical to the results of the previous analytical data [4]. The accuracy for the effect of transverse convex curvature on temperature distribution of the present analysis is well shown in Figs. 2.26 to 2.27.

Figs. 2.28 and 2.29 show the effect of R_i^* on the predicted maximum dimensionless temperature, T_{im}^+, in the fully developed region for a fixed Reynolds number of Re = 100,000 and a fixed Prandtl number of Pr = 0.72 for the range of α at 0.2, 0.5 and 0.8. They are for different relative velocities, U* = 0.4 and 0.8, respectively. It is seen that the maximum temperature increases with the increase of the radius ratios, α, indicating that the turbulent heat transfer becomes higher with a increasing value of U*. This is because at a higher relative velocity, the heat is diffused rapidly over the entire fluid, whereas at a low relative velocity it is distributed over the entire flow cross section. This is explained by Eq. (2.31) and Eq. (2.56).

4.3.2 Nusselt Number

The comparison between the Nusselt number for the fully developed turbulent flow of the parallel plates and the results of the present analysis is made as it was explained for the case of the friction factor in Section 4.2.2. Figs. 2.30, 2.31, and 2.32 are plotted for different Prandtl numbers, Pr = 0.7, 1.0, and 10.0, respectively. The present study uses an input of $\alpha = 0.999$ and $R_i^* = 1.0$ to closely simulate parallel plates geometry. The Nusselt numbers from this input for the fully developed turbulent flow is comparable to those reported by Kays and Leung [33] with Pr = 0.7 and $Pr_t = 0.9$. It is seen that the agreement is very good.

4.3.3 Relationship between Non-Dimensional Parameters and the Convex Curvature of the Inner Core

The analytical results on the effect of the transverse convex surface curvature, R_i^*, on the heat transfer coefficients in terms of the Nusselt number for the fully developed turbulent flow in a concentric annulus with a moving core are shown in Figs. 2.33 to 2.34. In Figs. 2.33 and 2.34, the Nusselt numbers are shown for three different relative velocities, U* = 0.0, 0.5 and 1.0, at a given Prandtl number of Pr = 0.72 with a fixed radius ratio of $\alpha = 0.5$. The figures illustrate that as the relative velocities, U*, increase, Nusselt number decreases over the range of inner core radii, R_i^* = 0.005, 0.05, 0.2, 0.5, and 1.0. For Figs. 2.33 and 2.34, with the increase of Reynolds number, Nusselt number calculated from Eq. (2.60) increases. It shows that the effect of the transverse convex surface curvature is similar to the case of the friction factor: as the radius of the inner core is smaller, the heat transfer rate is higher. This is because the smaller the value of the inner core radius, R_i^*, the smaller the bulk temperature, T_b^+, due to the increase of the

production term of turbulent heat convection, $-c_p\rho\overline{v'T'}\left(\partial T/\partial y\right)$, at fixed values of α, Pr, and Re, resulting in greater heat transfer near the wall surface. Therefore, the Nusselt number for the fully developed turbulent flows in a concentric annulus with a moving core with the smaller inner core diameter is always greater than that of the annulus with the larger inner core radius.

The effects of the Prandtl number, Pr, are shown in Figs. 2.35 and 2.36 for five Prandtl numbers, Pr = 0.01, 0.72, 5.0, 10.0, and 100.0 with a fixed radius ratio, $\alpha = 0.5$ and a fixed Reynolds number, Re = 100,000. Figures show that when the Prandtl number increases, the heat transfer becomes higher. This is because the turbulent thermal diffusion is higher for an increasing value of the Prandtl number as discussed earlier.

The effects of the transverse convex surface curvature, R_i^*, on the fully developed heat transfer coefficients in terms of the Nusselt number at a given Reynolds number, Re = 100,000, and a given Prandtl number, Pr = 0.72, with three different radius ratios, α = 0.2, 0.5, and 0.8 at U* = 0.5 and 1.0 are shown in Figs. 2.37 and 2.38, respectively. As seen in the figures, the smaller the radius ratios and R_i^*, the higher the heat transfer. The physical meaning was already discussed in the previous related figures.

In Figs. 2.39 and 2.40, the Nusselt numbers were obtained for the fully developed turbulent flow in concentric annular tubes with moving cores for increasing value of Reynolds number of Re = 20,000, 50,000, and 100,000 on the effect of the transverse convex surface curvature, R_i^*, with a fixed radius ratio, $\alpha = 0.5$, and Prandtl number, Pr = 0.72, respectively. They are for two different relative velocities, U* = 0.5 and 1.0. Figures show that as the Reynolds number increases, the Nusselt number increases, and

the effect of the transverse convex surface curvature due to the relative velocities seems to have minor effect on the heat transfer rate.

In Figs. 2.41 to 2.43, the Nusselt number is calculated from Eq. (2.62) for six different radii of the inner cores, R_i^* = 0.005, 0.01, 0.02, 0.05, 0.1, and 1.0, with a fixed radius ratio of α = 0.5 and a fixed Reynolds number of Re = 20,000 at the different relative velocities of U* = 0.0, 0.25, 0.5, 0.75, and 1.0. They are for different Prandtl numbers of Pr = 0.72, 1.0, and 10.0 which show that the effects of the transverse convex surface curvature are similar to the case of the friction factor. That is, the smaller the radius of the inner core, the higher the heat transfer rate.

Throughout the analytical results on the effect of the transverse convex surface curvature, R_i^*, on the fully developed heat transfer coefficients for fully developed turbulent flow in a concentric annulus with a moving core as mentioned earlier, the heat transfer rates in terms of the Nusselt number are affected by α, U*, Pr, and Re on the effect of the transverse convex surface curvature, R_i^*.

CHAPTER 5
CONCLUSION

The present study investigated the effect of the transverse convex surface curvature on the fully developed turbulent flows and heat transfer in a concentric annulus with a moving core. The effects of the transverse convex surface curvature on the fluid flow and heat transfer, i.e., velocity distribution, friction factor, eddy diffusivity, van Driest Damping constant, temperature distribution, and heat transfer coefficient, have been studied. The analytical predictions were obtained through a mathematical model for turbulence based on the variable van Driest damping constant, A_i^+, and the variable von Kármán constant, κ_i, proposed in the previous studies [2, 7].

The computer program for the present study employs an iterative process to match the velocity and temperature profiles with force and energy balances and calculates the desired momentum and thermal characteristics. It is assumed that thermodynamic fluid properties in the analysis were independent of temperature.

The following conclusions are reached:

(1) Transverse convex surface curvature significantly affects the velocity and temperature distributions of the fully developed turbulent flow in a concentric annulus with a moving core.

(2) The friction factor increases with the decreasing values of the inner core radii and the shear stress at the inner wall increases for a given Reynolds number at fixed

radius ratios. The effect of Reynolds number on the friction factor for given values of the inner core radii is very small.

(3) Nusselt number decreases with the increasing values of relative velocities over the range of inner core radii and Nusselt number increases with the value of increasing Reynolds number. The smaller the radius ratios and R_i^*, the higher the heat transfer rate.

(4) The effect of the relative velocities on the transverse convex surface curvature of the fully developed turbulent flow and heat transfer affects little on heat transfer rate.

(5) The effects of the transverse convex curvature on heat transfer increase with increasing Prandtl number.

APPENDIX 1
Distribution of Shear Stress and Radial Heat Flux in a Concentric Annulus with a moving core

A.1.1 Shear Stress Distribution

The schematic geometry of a concentric annulus with smooth surfaces is shown in Fig. A1.1.

The distribution of shear stress, τ_i, is derived using the momentum equation. Referring to Fig. A1.1, a force balance for cylindrical fluid element in the inner region is:

$$-\tau_{Ri}(2\pi r)dx + \left(\tau_{Ri} + \frac{\partial \tau_{Ri}}{\partial r}\right)2\pi(r+dr)dx + p(2\pi r)dr - \left(p + \frac{\partial p}{\partial x}dx\right)2\pi r\,dr = 0 \qquad \text{(A1.1)}$$

On simplifying Eq. (A1.1) as:

$$\frac{\partial}{\partial r}\left(\tau_{Ri}\cdot r\right) = \frac{\partial p}{\partial x}\,r \qquad \text{(A1.2)}$$

and integrating Eq. (A1.2) as:

$$\left(\tau_{Ri}\cdot r\right) = \frac{\partial p}{\partial x}\int_{R_i}^{r} r\,dr \qquad R_i \le r \le R_m \qquad \text{(A1.3)}$$

which is:

$$\tau_{Ri}\cdot r = \frac{\partial p}{\partial x}\frac{1}{2}\left(r^2 - R_i^2\right) + C \qquad \text{(A1.4)}$$

with the boundary condition ; $\tau_i = 0$ at $r = R_i + \delta_i$:

$$0 = \frac{\partial p}{\partial x}\frac{1}{2}\left\{(R_i + \delta_i)^2 - R_i^2\right\} + C \qquad \text{(A1.5)}$$

Rearranging Eq. (A1.5) yields:

$$C = -\frac{\partial p}{\partial x}\cdot\frac{1}{2}\left[\left(R_i+\delta_i\right)^2 - R_i^2\right] \tag{A1.6}$$

Substitution of Eq. (A1.6) into (A1.4) yields:

$$\tau_{Ri} = \frac{1}{2r}\frac{\partial p}{\partial x}\left[r^2 - \left(R_i+\delta_i\right)^2\right] \tag{A1.7}$$

at inner core wall (subscript w), $r = R_i$:

$$\tau_{R_i} = \frac{1}{2R_i}\frac{\partial p}{\partial x}\left[R_i^2 - \left(R_i+\delta_i\right)^2\right] \tag{A1.8}$$

Divide Eq. (A1.7) by Eq. (A1.8) and with $r = R_i + y_i$ to obtain:

$$\left(\frac{\tau}{\tau_R}\right)_i = \frac{R_i}{R_i+y_i}\frac{\left(y_i-\delta_i\right)\left(2R_i+y_i+\delta_i\right)}{\left(2R_i+\delta_i\right)\left(-\delta_i\right)} \tag{A1.9}$$

Rearrange Eq. (A1.9) with $\zeta_i = {y_i^+}/{\delta_i^+}$ and $\Delta_i = {\delta_i^+}/{R_i^+}$:

$$\left(\frac{\tau}{\tau_R}\right)_i = \frac{\left(1-\zeta_i\right)\left[1+\Delta_i\zeta_i/\left(2+\Delta_i\right)\right]}{1+\Delta_i\zeta_i} \tag{A1.10}$$

Similarly for the outer region:

$$\left(\frac{\tau}{\tau_R}\right)_o = \frac{\left(1-\zeta_o\right)\left[1-\Delta_o\zeta_o/\left(2-\Delta_o\right)\right]}{1-\Delta_o\zeta_o} \tag{A1.11}$$

Rearranging Eq. (A1.10) and Eq. (A1.11) yields:

$$\left(\frac{\tau}{\tau_R}\right)_j = \frac{\left(1-\zeta_j\right)\left[1\pm\Delta_j\zeta_j/\left(2\pm\Delta_j\right)\right]}{1\pm\Delta_j\zeta_j} \tag{A1.12}$$

We can apply Eq. (A1.12) to Eq. (2.30) to get the velocity profiles, +ve for j = i and

- ve for j = o.

$$\frac{\partial u_j^+}{\partial \zeta_j^+} = \delta_j^+ \left[\frac{(\tau/\tau_R)_j}{1+(\varepsilon_M/\nu)_j} \right] \tag{2.30}$$

To obtain the ratio of the shear stress, integration of Eq. (A1.1) for the outer region:

$$(\tau_{Ro} \cdot r) = \frac{\partial p}{\partial x} \int_r^{R_o} r\, dr \qquad R_m \le r \le R_o \tag{A1.13}$$

and boundary condition, $\tau_o = 0$ at $r = R_m$ gives:

$$\tau_{Ro} = \frac{1}{2r} \frac{\partial p}{\partial x} \left(R_m^2 - r^2 \right) \tag{A1.14}$$

At the outer wall, $r = R_o$, Eq. (A1.14) gives the shear stress as:

$$\tau_{R_o} = \frac{1}{2R_o} \frac{\partial p}{\partial x} \left(R_m^2 - R_o^2 \right) \tag{A1.15}$$

and inner wall, $r = R_i$, from Eq.(A1.8):

$$\tau_{R_i} = \frac{1}{2R_i} \frac{\partial p}{\partial x} \left(R_i^2 - R_m^2 \right) \tag{A1.16}$$

Divide Eq. (A1.8) by Eq. (A1.14) to obtain the ratio of the shear stress, Eq. (2.43):

$$\frac{\tau_{R_i}}{\tau_{R_o}} = \left(\frac{1}{\alpha} \right) \left(\frac{R_m^{\,2} - R_i^{\,2}}{R_o^{\,2} - R_m^{\,2}} \right) \tag{2.43}$$

and for annular flow, with over $R_m = R_i + \delta_i$ and under $R_m = R_o - \delta_o$:

$$\left(\frac{\tau_{R_i}}{\tau_{R_o}} \right)_x = \frac{1}{\alpha} \left(\frac{2R_i \delta_i + \delta_i^2}{2R_o \delta_o - \delta_o^2} \right) \tag{A1.17}$$

A.1.2 Radial Heat Flux Distribution

In a concentric annulus, the heating condition considered is such that the core surface is heated and the outer surface is insulated. The heat analysis can be carried out by calculating the heat balance. The control volume for the heat balance is also expressed in Figure A1.1.

Consider a small cylindrical control volume as indicated in Figure. A1.1. If the axial thermal diffusion is negligible, according to the steady flow energy equation, the net heat transfer equals the enthalpy change in the present case as:

$$\rho c_p u T 2\pi r\,dr + q 2\pi r\,dx = \rho c_p u\left(T + \frac{\partial T}{\partial x}dx\right)2\pi r\,dx + \left(q + \frac{\partial q}{\partial r}dr\right)2\pi(r + dr)dx \tag{A1.18}$$

(1) For Inner Region

The Eq. (A1.18) can be simplified as:

$$-\frac{\partial}{\partial r}(q_i \cdot r) = \rho c_p r u_i \frac{\partial T_i}{\partial x} \tag{A1.19}$$

Integration of Eq. (A1.19) yields:

$$q_i \cdot r = -\rho c_p \frac{\partial T_i}{\partial x}\int_{R_i}^{r} r\,u_i(r)\,dr \tag{A1.20}$$

Assume, $u_i(r) = u_{ib}$, which is bulk motion:

$$q_i \cdot r = -\rho c_p \frac{\partial T_i}{\partial x} u_{ib} \frac{1}{2}\left(r^2 - R_i^2\right) + C \tag{A1.21}$$

with the boundary condition $q_i = 0$ at $r = R_o$:

$$C = \rho c_p \frac{\partial T_i}{\partial x} u_{ib} \frac{1}{2}\left(R_o^2 - R_i^2\right) \tag{A1.22}$$

Substitution of Eq. (A1.22) into Eq. (A1.21) yields:

$$q_i \cdot r = -\rho c_p \frac{\partial T_i}{\partial x} \cdot \frac{1}{2}\left(r^2 - R_o^2\right) u_{ib} \tag{A1.23}$$

For inner core wall ; $r = R_i$:

$$q_{R_i} \cdot R_i = -\rho c_p \frac{\partial T_i}{\partial x} \cdot \frac{1}{2}\left(R_i^2 - R_o^2\right) u_{ib} \tag{A1.24}$$

Divide Eq. (A1.23) by Eq. (A1.24) to obtain:

$$\frac{q_i}{q_{R_i}} = \frac{R_i}{r} \cdot \frac{\left(r^2 - R_o^2\right)}{\left(R_i^2 - R_o^2\right)} \tag{A1.25}$$

Rearrange Eq. (A1.25) with $r = R_i + y_i$, $\zeta_i = {y_i^+}/{\delta_i^+}$ and $\Delta_i = {\delta_i^+}/{R_i^+}$ to obtain Eq. (2.58).

$$q_i/q_{R_i} = \frac{1 - \alpha^2\left(1 + \Delta_i \zeta_i\right)^2}{\left(1 - \alpha^2\right)\left(1 + \Delta_i \zeta_i\right)} \qquad \left(0 \le \zeta_i \le 1\right) \tag{2.58}$$

(2) For Outer Region

Simplify Eq. (A1.18) and integrate to obtain:

$$q_o \cdot r = -\rho c_p \frac{\partial T_o}{\partial x} \int_r^{R_o} r\, u_o(r)\, dr \tag{A1.26}$$

Assumption of $u_o(r) = u_{ob}$, which is bulk motion:

$$q_o \cdot r = -\rho c_p \frac{\partial T_o}{\partial x} u_{ob} \frac{1}{2}\left(R_o^2 - r^2\right) + C \tag{A1.27}$$

with the boundary condition, $q_o = 0$ at $r = R_o$, C = 0.

Similarly as the inner region:

$$\frac{q_o}{q_{R_i}} = \frac{R_i}{r}\frac{\left(R_o^2 - r^2\right)}{\left(R_i^2 - R_o^2\right)} \tag{A1.28}$$

and with $r = R_o - y_o$, $\zeta_o = {y_o^+}/{\delta_o^+}$ and $\Delta_o = {\delta_o^+}/{R_o^+}$ to obtain Eq. (2.59):

$$q_o/q_{R_i} = -\frac{\alpha\left(2 - \Delta_o\zeta_o\right)\Delta_o\zeta_o}{\left(1-\alpha^2\right)\left(1-\Delta_o\zeta_o\right)} \qquad \left(0 \le \zeta_o \le 1\right) \tag{2.59}$$

APPENDIX 2
Non-Dimensionalized Forms of the Velocity and Temperature Equation for Concentric Annular Geometry

A.2.1 Velocity Profile

The radial velocity of fluid, u(r), can be derived from the definition of total shear stress as:

$$\tau = \mu \frac{\partial u}{\partial y} - \rho \overline{u'v'} \tag{A2.1}$$

From the Prandtl mixing length hypothesis, the turbulent fluctuation term becomes:

$$-\overline{u'v'} = l^2 \left| \frac{\partial u}{\partial y} \right|^2 \tag{A2.2}$$

Substituting Eq. (A2.2) into Eq. (A2.1) becomes:

$$\frac{\tau}{\rho} = \nu \frac{\partial u}{\partial y} + l^2 \left| \frac{\partial u}{\partial y} \right|^2 \tag{A2.3}$$

As a proportionality factor, the eddy diffusivity for momentum, ε_M, is defined by Eq. (2.31) as:

$$\overline{u'v'} = -\varepsilon_M \frac{\partial \bar{u}}{\partial y} \tag{2.31}$$

Rearranging Eq. (A2.3) with Eq. (2.31) yields:

$$\frac{\tau_j}{\rho} = \left(\nu + \varepsilon_M\right)_j \frac{\partial u_j}{\partial y_j} \tag{A2.4}$$

The definition of friction velocity, u_τ, is:

$$u_\tau = \sqrt{\left(\frac{\tau_R}{\rho}\right)} \tag{A2.5}$$

Non-dimensionalize the velocity gradient:

$$\frac{\partial u_j}{\partial y_j} = \frac{\partial u_j^+}{\partial y_j^+}\left(\frac{u_\tau^2}{\nu}\right)_j \tag{A2.6}$$

where $\partial u_j = u_{\tau_j}\partial u_j^+, \partial y_j = \left(\nu/u_\tau\right)_j \partial y_j^+, \partial y_j^+ = \delta_j^+ \, \partial \zeta_j^+$

Eq. (A2.4) can be transformed into dimensionless form as:

$$\frac{\partial u_j^+}{\partial \zeta_j} = \delta_j^+ \frac{\left(\tau/\tau_R\right)_j}{\left(1+\varepsilon_M/\nu\right)_j} \tag{A2.7}$$

A.2.2 Temperature Profile

The equation of a temperature profile across a flow cross-section can be derived from the basic heat transport equation in Eq. (2.23) as:

$$-\frac{q}{c_p \rho} = \left(\alpha + \varepsilon_H\right)\frac{\partial T}{\partial r} \tag{2.23}$$

where ε_H is the thermal diffusivity.

Eq. (2.23) can be made dimensionless by introducing a non-dimensionalized temperature, T_j^+, written in Eq. (2.57) as:

$$T_j^+ = \frac{\left(T_{R_i} - T_j\right) \, c \, \tau_{R_j}}{q_{R_i}\left(\tau_{R_j}/\rho\right)^{0.5}} \tag{2.57}$$

Using Eq. (2.57), the partial derivative for T can be transformed as:

For inner region:

$$\partial T_i = -\frac{q_{R_i} u_{\tau_i}}{c\tau_{R_i}} \partial T_i^+ \tag{A2.8}$$

From $r = R_i + y_i$, ∂r is given as:

$$\partial r = \frac{1}{u_{\tau_i}} \delta_i^+ \partial \zeta_i \nu \tag{A2.9}$$

The dimensionless form of Eq. (2.23) combined with Eqs. (A2.8) and (A2.9) in the inner region is:

$$\frac{\partial T_i^+}{\partial \zeta_i} = \mathrm{Pr} \cdot \delta_i^+ \frac{\left(q/q_R\right)_i}{\left(1 + \mathrm{Pr}/\mathrm{Pr}_t \cdot \varepsilon_M/\nu\right)_i} \tag{A2.10}$$

For outer region:

In the same way as the inner region:

$$\frac{\partial T_o^+}{\partial \zeta_o} = -\mathrm{Pr} \cdot \delta_o^+ \frac{\left(q_o/q_{R_i}\right)}{\left(1 + \mathrm{Pr}/\mathrm{Pr}_t \cdot \varepsilon_M/\nu\right)_o} \tag{A2.11}$$

Therefore, we can obtain:

$$\frac{\partial T_j^+}{\partial \zeta_j} = \pm \mathrm{Pr} \cdot \delta_j^+ \frac{\left(q_j/q_{R_i}\right)}{\left(1 + \mathrm{Pr}/\mathrm{Pr}_t \cdot \varepsilon_M/\nu\right)_j} \tag{A2.12}$$

APPENDIX 3
Non-Dimensionalized Forms of the Turbulence Model for Concentric Annular Geometry

To solve the closure problems that arise in turbulence fluctuation terms, the eddy viscosity term, ε_M/ν, requires mathematical modelling because it cannot be determined analytically. The term will exhibit different behaviours, depending on the state of the boundary layers. Usually, the boundary layer can be regarded as consisting of two layers.

The first one, the viscous sublayer, is confined to a region of flow near a solid boundary. Beyond of the viscous sublayer lays the fully turbulent regions. Therefore, both regions require the turbulence models, respectively.

A.3.1 Viscous Sublayer

In the viscous sublayer, the turbulence model proposed by van Driest [5] is used in the present analysis. The van Driest hypothesis is a sublayer scheme that provides for an eddy diffusivity that is zero at y = 0. It has the virtue that it allows a continuous calculation through the sublayer and into the fully turbulent region with no discontinuity.

In this scheme, the Prandtl mixing length can be used to the wall instead of truncating it to zero at an assumed outer edge of the sublayer with a damping function.

Van Driest proposed that:

$$l = \kappa\, y\left(1 - e^{-y^+/A^+}\right) \tag{2.32}$$

where A^+ is the damping constant determined empirically. Eq. (2.32) in a form of eddy viscosity, ε_M/ν,

$$\frac{\varepsilon_M}{\nu} = \frac{l^2}{\nu}\frac{du}{dy} = l^{+2}\frac{du^+}{dy^+} \tag{2.33}$$

The combination of Eqs. (2.23) and (2.33) yields:

$$\left(\frac{\varepsilon_M}{\nu}\right)_j = \kappa_j^2 y_j^{+2}\left[1 - \exp\left(-\frac{y_j^+}{A_j^+}\right)\right]^2\left|\frac{\partial u_j^+}{\partial y_j^+}\right| \tag{2.34}$$

where

$$\frac{\partial u_j^+}{\partial \zeta_j^+} = \delta_j^+\left[\frac{(\tau/\tau_R)_j}{1+(\varepsilon_M/\nu)_j}\right] \qquad (0 \le \zeta \le 1) \tag{2.30}$$

Substitution of Eq. (2.30) into Eq. (2.34) gives:

$$\left(\frac{\varepsilon_M}{\nu}\right)_j^2 + \left(\frac{\varepsilon_M}{\nu}\right)_j = \left(\kappa_j y_j^+\right)^2\left[1 - \exp\left(-\frac{y_j^+}{A_j^+}\right)\right]^2\left(\frac{\tau}{\tau_R}\right)_j \tag{A3.1}$$

Eq. (A3.1) is a form of an incomplete square polynomial about ε_M/ν:

$$ax^2 + bx + c = 0 \tag{A3.2}$$

The solutions are:

$$x = \frac{\varepsilon_M}{\nu},\ a = 1,\ b = 1 \text{ and } c = \left(\kappa_j y_j^+\right)^2\left[1 - \exp\left(-\frac{y_j^+}{A_j^+}\right)\right]^2\left(\frac{\tau}{\tau_R}\right)_j$$

The positive root of the polynomial is:

$$\left(\frac{\varepsilon_M}{\nu}\right)_j = \frac{1}{2}\left[-1 + \left\{1 + 4\cdot\left(\kappa_j\delta_j^+\zeta_j\right)^2\left[1 - \exp\left(1 - \frac{\delta_j^+\zeta_j}{A_j^+}\right)\right]\left(\frac{\tau}{\tau_R}\right)_j\right\}^{0.5}\right] \tag{A3.3}$$

With the variable von Kármán constant, κ_i , proposed in Kim's research [7], the expression of $(\varepsilon_M/\nu)_j$ becomes:

For the viscous sublayer of an inner region of the annular flow:

$$\left(\frac{\varepsilon_M}{\nu}\right)_i = \frac{1}{2}\left[-1+\left\{1+0.64\cdot\left[F(R_i^*)\delta_i^+\zeta_i\right]^2\left[1-\exp\left(1-\frac{\delta_i^+\zeta_i}{A_i^+}\right)\right]\left(\frac{\tau}{\tau_R}\right)_i\right\}^{0.5}\right] \quad \text{(A3.4)}$$

For the viscous sublayer of an outer region of the annular flow:

$$\left(\frac{\varepsilon_M}{\nu}\right)_o = \frac{1}{2}\left[-1+\left\{1+0.64\cdot\left(\delta_o^+\zeta_o\right)^2\left[1-\exp\left(1-\frac{\delta_o^+\zeta_o}{A_o^+}\right)\right]\left(\frac{\tau}{\tau_R}\right)_o\right\}^{0.5}\right] \quad \text{(A3.5)}$$

A.3.2 Fully Turbulent Regions

Since the velocity profiles outside the viscous sublayers should differ from the law of the wall, the logarithmic law of the wall cannot be used. In fully turbulent regions, the empirical model originally proposed by Reichardt [6] is used in a modified form, Eq. (2.37), as:

$$\left(\frac{\varepsilon_M}{\nu}\right)_j = \frac{\kappa_j\delta_j^+}{6}\left[1-\left(1-\frac{y_j^+}{\delta_j^+}\right)^2\right]\left[1+2\left(1-\frac{y_j^+}{\delta_j^+}\right)^2\right] \quad \text{(2.37)}$$

and non-dimensionalized as follows:

$$\left(\frac{\varepsilon_M}{\nu}\right)_j = \frac{\kappa_j\delta_j^+}{6}\zeta_j\left(2-\zeta_j\right)\left(3-4\zeta_j+2\zeta_j^2\right) \quad \text{(2.38)}$$

For the fully turbulent layer of an inner region:

$$\left(\frac{\varepsilon_M}{\nu}\right)_i = \frac{1}{15}f\left(R_i^*\right)\delta_i^+\left[\zeta_i\left(2-\zeta_i\right)\left(3-4\cdot\zeta_i+2\cdot\zeta_i^2\right)\right] \quad \text{(A3.6)}$$

where the variable von Kármán constant, κ_i, proposed in this study was applied.

For the fully turbulent layer of an outer region:

$$\left(\frac{\varepsilon_M}{\nu}\right)_o = \frac{1}{6}\kappa_o \delta_o^+ \left[\zeta_o(2-\zeta_o)(3-4\cdot\zeta_o+2\cdot\zeta_o^2)\right] \qquad \text{(A3.7)}$$

where κ_o is a constant, 0.4, in this analysis.

APPENDIX 4
Non-Dimensionalized Forms of Other Fluid Parameters for Concentric Annular Geometry

A.4.1 Bulk Velocity

The schematic geometry of an idealized model of a concentric annulus with smooth surfaces is shown in Fig. A4.1.

The bulk velocity of the fluid across the concentric annulus cross-section is defined as:

$$u_b = \frac{\int_{dA} u(r)2\pi r\, dA}{\int_{dA} 2\pi r dA} = \frac{\int_{R_i}^{R_m} u(r) r\, dr + \int_{R_m}^{R_o} u(r) r\, dr}{\frac{1}{2}\cdot\left(R_o^2 - R_i^2\right)} \qquad \text{(A4.1)}$$

Introducing the dimensionless parameter, u_b can be rewritten as:

For the inner region of the concentric annulus, $r = R_i + y_i$.

From the Fig. A4.1, $y_i = 0$ at the $r = R_i$ and $y_i = \delta_i$ at the $r = R_m$.

For the outer region of the concentric annulus, $r = R_o - y_o$.

Similarly, $y_o = 0$ at the $r = R_o$ and $y_o = \delta_o$ at the $r = R_m$.

Developing the parameters in the dimensionless form as:

$$dr = \delta_j^+ \zeta_j \text{ and } \Delta_j = \frac{\delta_j^+}{R_j^+}, \zeta_j = \frac{y_j^+}{\delta_j^+}, \alpha = \frac{R_i}{R_o}$$

Substitute the parameters into the Eq. (A4.1):

$$u_b = \left(\frac{\nu}{R_o}\right)\left[\frac{2\alpha}{1-\alpha^2}\right]\left[\delta_j^+ \int_0^1 (1+\Delta_i\zeta_i)u_i^+ d\zeta_i + \frac{1}{\alpha}\delta_o^+ \int_0^1 (1-\Delta_o\zeta_o)u_o^+ d\zeta_o\right] \tag{A4.2}$$

A.4.2 Reynolds Number

The Reynolds number for a concentric annulus cross section is defined as:

$$\mathrm{Re} = \frac{\rho\, u_b De}{\mu} = \frac{u_b De}{\nu} = \frac{u_b 2(R_o - R_i)}{\nu} \tag{A4.3}$$

Eq. (A4.3) can be further reduced as:

$$\mathrm{Re} = \frac{u_b 2R_i(1-\alpha)}{\alpha\nu} \tag{A4.4}$$

Substituting the bulk velocity, u_b, given in Eq. (A4.2) into Eq. (A4.4) and rearranging it in dimensionless terms yields:

$$\mathrm{Re} = \left[\frac{4}{1+\alpha}\right]\left[\alpha\delta_i^+ \int_0^1 (1+\Delta_i\zeta_i)u_i^+ d\zeta_i + \delta_o^+ \int_0^1 (1-\Delta_o\zeta_o)u_o^+ d\zeta_o\right] \tag{2.48}$$

A.4.3 Friction Factor

The friction factor is defined as:

$$f_j = \frac{\tau_{R_j}}{\frac{1}{2}\rho\, u_b^2} \tag{2.39}$$

For a concentric annulus cross-section, it becomes:

$$f = \frac{(R_o - R_i)}{\rho u_b^{\,2}}\left(-\frac{dp}{dx}\right) \tag{2.41}$$

A force balance made for an element of fluid in the annulus gives:

$$\frac{dp}{dx}\pi\left(R_o^{\,2} - R_i^{\,2}\right) = 2\pi(\tau_{Ro}R_o + \tau_{Ri}R_i) \tag{A4.5}$$

Substituting Eq. (A4.5) into Eq. (2.41) yields:

$$f = -\frac{(R_o - R_i)}{\rho u_b^2}\frac{2(\tau_{Ro}R_o + \tau_{Ri}R_i)}{(R_o^2 - R_i^2)} \tag{A4.6}$$

where the bulk velocity, u_b can be expressed as:

$$u_b = \frac{\mathrm{Re}.\nu}{2(R_o - R_i)} \tag{A4.7}$$

Substituting Eq. (A4.7) into Eq.(A4.6) yields:

$$f = -\frac{4(R_o - R_i)(R_o - R_i)^2}{\rho\,\mathrm{Re}^2\,\nu^2}\frac{2(\tau_{Ro}R_o + \tau_{Ri}R_i)}{(R_o^2 - R_i^2)} = -\frac{8(R_o - R_i)^2}{\rho\,\mathrm{Re}^2\,\nu^2}\frac{(\tau_{Ro}R_o + \tau_{Ri}R_i)}{(R_o + R_i)}$$

$$= -\frac{8(R_o - R_i)}{\mathrm{Re}^2}\left[R_i + \left(\frac{\tau_{Ro}}{\tau_{Ri}}\right)R_o\right]\left(\frac{\tau_{Ri}/\rho}{\nu^2}\right) \tag{A4.8}$$

or

$$f = -\frac{8(1-\alpha)}{\mathrm{Re}^2\,\alpha}R_i^2\left[1 + \left(\frac{\tau_{Ro}}{\tau_{Ri}}\right)\alpha\right]\left(\frac{\tau_{Ri}/\rho}{\nu^2}\right) \tag{A4.9}$$

Finally, the last expression of Eq.(A4.9) can be rearranged in dimensionless form as:

$$f = -8\left[\frac{\left\{1 + \left(\tau_{Ri}/\tau_{Ro}\right)\alpha\right\}(1-\alpha)^2}{(1+\alpha)}\right]\left(\frac{R_o^+}{\mathrm{Re}}\right)^2 \tag{A4.10}$$

where the shear stress distribution in dimensionless parameters is given in Eq. (2.43) as:

$$\frac{\tau_{R_i}}{\tau_{R_o}} = \left(\frac{1}{\alpha}\right)\left(\frac{R_m^2 - R_i^2}{R_o^2 - R_m^2}\right) \tag{2.43}$$

A.4.4 Bulk Temperature

The bulk temperature of the fluid across the concentric annulus cross-section is defined as:

$$T_b = \frac{\int_{R_i}^{R_o} 2\pi\, r\, u(r)\, T\, dr}{\int_{R_i}^{R_o} 2\pi r\, u(r)\, dr} \tag{A4.11}$$

The dimensionless temperatures, T_j^+ is defined as:

$$T_j^+ = \frac{(T_{R_j} - T_j)\, c_p\, \tau_{R_j}}{q_{R_i} u_{\tau_j}} \tag{A4.12}$$

Substitution of Eq.(A4.12) into Eq.(A4.11) and rearranging would yield:

$$T_b = \frac{T_R \int_{R_i}^{R_o} u(r) r dr}{\int_{R_i}^{R_o} u(r) r dr} - \frac{q_{R_i} u_{\tau_j}}{c_p \tau_{R_j}} \frac{\int_{R_i}^{R_o} u(r) T_j^+ r dr}{\int_{R_i}^{R_o} u(r) r dr} \tag{A4.13}$$

Which can be reduced to:

$$T_b = T_R - \frac{q_{R_i} u_{\tau_j}}{c_p \tau_{R_j}} \frac{\int_{R_i}^{R_o} u(r) T_j^+ r dr}{\int_{R_i}^{R_o} u(r) r dr} \tag{A4.14}$$

or

$$T_R - T_b = \frac{q_{R_i} u_{\tau_j}}{c_p \tau_{R_j}} \frac{\int_{R_i}^{R_o} u(r) T_j^+ r dr}{\int_{R_i}^{R_o} u(r) r dr} \tag{A4.15}$$

The dimensionless temperatures, T_b^+ is defined as:

$$T_b^+ = \frac{(T_{R_i} - T_b) c_p \tau_{R_i}}{q_{R_i} u_{\tau_i}} \tag{A4.16}$$

Now, the bulk velocity, u_b is:

$$u_b = \frac{2}{(R_o^2 - R_i^2)}\left[\int_{R_i}^{R_o} u(r) r dr\right] \tag{A4.17}$$

and

$$\int_{R_i}^{R_o} u(r) r dr = \frac{u_b (R_o + R_i)(R_o - R_i)}{2} = \frac{2u_b (R_o - R_i)}{\nu} \frac{(R_o + R_i)\nu}{4}$$

$$= \mathrm{Re}\cdot \nu \cdot R_o \frac{1+\alpha}{4} \tag{A4.18}$$

Rearrange Eq. (A4.12) and integrate it as Eq. (A4.13) to obtain:

$$\frac{\int_{R_i}^{R_o} r u_j \frac{q_{R_i} u_{\tau_j}}{c\tau_{R_j}} T_j^+ dr}{\int_{R_i}^{R_o} r u_j dr} = \frac{\int_{R_i}^{R_o} r u_j T_{R_i} dr}{\int_{R_i}^{R_o} r u_j dr} - \frac{\int_{R_i}^{R_o} r u_j T_j dr}{\int_{R_i}^{R_o} r u_j dr} = T_{R_i} - T_b \tag{A4.19}$$

multiply $\left(c\tau_{R_j} / q_{R_i} u_{\tau_j}\right)$ to both hand sides:

$$\frac{c\tau_{R_j}}{q_{R_i} u_{\tau_j}} \cdot \frac{\int_{r_i}^{r_o} r u_j \frac{q_{R_i} u_{\tau_j}}{c\tau_{R_j}} T_j^+ dr}{\int_{r_i}^{r_o} r u_j dr} = \frac{c\tau_{R_j}}{q_{R_i} u_{\tau_j}} \cdot \left(T_{R_i} - T_b\right) = T_{bj}^+ \tag{A4.20}$$

Non-dimensionalize Eq. (A4.20):

$$T_{bj}^+ = \frac{\int_{R_i}^{R_o} r u_j T_j^+ dr}{\int_{R_i}^{R_o} r u_j dr} = \frac{\int_{R_i^+}^{R_o^+} r^+ u_j^+ T_j^+ dr^+}{\int_{R_i^+}^{R_o^+} r^+ u_j^+ dr^+} \tag{A4.21}$$

where

$$\int_{R_i}^{R_o} u(r)T_j^+ rdr = \int_{R_i}^{R_m} u(r)T_i^+ rdr + \int_{R_m}^{R_o} u(r)T_o^+ rdr$$

$$= R_i\delta_i^+ \nu \int_0^1 (1+\Delta_i\zeta_i)u_i^+ T_i^+ d\zeta_i + R_o\delta_o^+ \nu \int_0^1 (1-\Delta_o\zeta_o)u_o^+ T_o^+ d\zeta_o \qquad \text{(A4.22)}$$

Substitution of Eq.(A4.15) and (A4.18) into Eq.(A4.16) yields:

$$T_b^+ = \left[\frac{4}{1+\alpha}\right]\left(\frac{1}{\mathrm{Re}}\right)\left[\alpha\delta_i^+ \int_0^1 (1+\Delta_i\zeta_i)u_i^+ T_i^+ d\zeta_i + \left(\frac{\tau_{R_i}}{\tau_{R_o}}\right)^{0.5} \delta_o^+ \int_0^1 (1-\Delta_o\zeta_o)u_o^+ T_o^+ d\zeta_o\right] \qquad \text{(A4.23)}$$

A.4.5 Nusselt Number

The Nusselt number is defined as:

$$Nu = \frac{hDe}{k} = \frac{h\cdot 2(R_o - R_i)}{k} \qquad \text{(A4.24)}$$

where h is defined as:

$$h = \frac{q_{R_i}}{(T_{R_i} - T_b)} \qquad \text{(A4.25)}$$

From the definition of T_b^+, $(T_{R_i} - T_b)$ can be be obtained:

$$T_b^+ = \frac{(T_{R_i} - T_b)\, c\, \tau_{R_i}}{q_{R_i} u_{\tau_i}} \qquad \text{(A4.26)}$$

Substitution of Eqs. (A4.24) and (A4.25) in to Eq. (A4.23) yields:

$$\mathrm{Nu} = \frac{c\,\tau_{R_i}}{u_{\tau_i}} \frac{1}{T_b^+} \frac{2\cdot(R_o - R_i)}{k} \qquad \text{(A4.27)}$$

Eq. (A4.27) can be further reduced with $u_{\tau_i} = \sqrt{\frac{\tau_{R_i}}{\rho}}$ as:

$$\mathrm{Nu} = 2\left(\frac{1-\alpha}{\alpha}\right)\frac{1}{T_b^+} R_i^+ \nu \frac{\rho c}{k} \qquad \text{(A4.28)}$$

Transform Eq. (A4.28) with Prandtl number, $\mathrm{Pr} = \frac{\nu}{k/\rho c}$, where $\left(k/\rho c\right)$ is thermal diffusivity to obtain Eq. (2.62):

$$\mathrm{Nu} = 2\left(\frac{1-\alpha}{\alpha}\right)\frac{R_i^+ \mathrm{Pr}}{T_b^+} \tag{A4.29}$$

REFERENCES

1. Kim, M.W. Kim, K.C. and Lee, Y., "Effect of Transverse Convex Surface Curvature on Fluid Flow and Heat Transfer for Turbulent Boundary Layer Flow Longitudinal to a Circular Cylinder: Analysis and Experiment," *Conference of Heat Transfer in Turbulent Flows ASME.*, HTD., San Francisco, vol. 318, pp. 137-144, 1995.

2. Suk, E., "Effect of Transverse Convex Surface Curvature on Fluid Flow and Heat Transfer in the Entrance Region of Concentric Annuli," *M.A.Sc. Thesis*, University of Ottawa, 1998.

3. Lee, Y. and Kim, K.H., "Inverted Annular Flow Boiling," *Int. J. Multiphase Flow*, vol. 13, pp. 345-355, 1987.

4. Shigechi, T., Kawae, N., and Lee, Y., "Turbulent fluid flow and heat transfer in concentric annuli with moving cores," *Heat and Mass Transfer*, vol. 33, pp. 2029-2037, 1990.

5. Van Driest, E.R., "On Turbulent Flow Near a Wall," *J. Aero. Sci.*, vol. 23, pp. 1007-1012, 1956.

6. Reichardt, H., "Die Wärmeübertragung in turbulenten Reibungschichten," *Z. Angew. Math. Mech.*, vol. 20, pp. 297, 1940, Available in English translation as NACA TM1047, 1943.

7. Kim, M.W., "Effect of Transverse Convex Curvature on Turbulent Flow and Heat Transfer," *Ph.D. Thesis*, University of Ottawa, 1996.

8. Knudsen, J.G. and Katz, D.L., *Fluid Dynamics and Heat Transfer*, McGraw-Hill, 1958.

9. Quamby, A. and Anard, R.K., "Fully Developed Turbulent Heat Transfer in Concentric Annuli with Uniform Wall Heat Fluxes," Chem. Eng. Sci., vol. 24, pp. 156-166, 1971.

10. Rothfus, R.R., Monrad, C.C., Sikchi, K.G., and Keideger, W.J., "Isothermal Skin Friction in Flow through Annular Sections," *Indus. and Eng. Chem.*, vol. 47, pp. 913, 1955.

11. Mizushina, T., Ito, R. and Ogino, F., "Eddy Diffusivity Distribution Near the Wall,"*4th Int. Heat Transfer Conference*, vol. 2, FC 218, 1970.

12. Bailey, R.V., "Heat Transfer to Liquid Metals in Concentric Annuli," *Oak Ridge Nat. Lab. Report ORNL-521*, 1964.

13. Barrow, H. and Pope, C.W., "A simple analysis of flow and heat transfer in railway tunnels," *Heat Fluid Flow*, vol. 8, pp. 119-123, 1987.

14. Barrow, H., Lee, Y., and Roberts, A., "The Similarity Hypothesis Applied to Turbulent Flow in an Annulus," *Int. J. Heat Mass Transfer*, vol. 8, pp. 1499, 1965.

15. Brighton, J.A. and Jones, J.B., "Fully Developed Turbulent Flow in Annuli," *J. of Basic Eng., Trans. ASME, Sec. D.*, vol. 86, pp. 835-844, 1964.

16. Levy, S., "Turbulent Flow in an Annulus," *J. Heat Transfer*, ASME, vol. 89, pp. 25-31, Feb., 1967.

17. Kim, K.C., Lee, Y. and Ma, E, "Effect of Transverse Convex Curvature on Turbulent Flow and Heat Transfer," *First International Symposium on Experimental and Computational Aerothermodynamics of Internal Flows*, Beijing, pp. 202-207, 1990.

18. Lee, Y. "Turbulent Heat Transfer from the Core Tube in Thermal Entrance Regions of Concentric Annuli," *Int. J. of Heat and Mass Transfer*, vol. 11, pp. 509-522, 1968.

19. Lee, Y., "Turbulent Flow and Heat Transfer in Concentric and Eccentric Annuli," *Ph.D. Thesis*, University of Liverpool, 1964.

20. Lee, Y. and Barrow, H., "Turbulent Flow and Heat Transfer in Concentric and Eccentric Annuli," *Proceedings, I. Mech. E.*, vol. 178, pp. 1-16, 1964.

21. Lee, Y. and Kim, K.C., "An Analysis on Effect of Transverse Convex Curvature on Turbulent Flow and Heat Transfer," *Wärme-und Stoffübertragung*, vol. 28, pp. 89-95, 1993.

22. Lee, Y. and Park, S.D., "Developing Turbulent Flow in Concentric Annuli: An Analytical and Experimental Study," *Wärme-und Stoffübertragung*, vol. 4, pp. 156-166, 1971.

23. Leung, E.Y., Kays, W.M. and Reynolds, W.C., "Heat Transfer with Turbulent Flow in Concentric and Eccentric Annuli with Constant and Variable Heat Flux," *Report AHT4*, Stanford University, 1962.

24. Ludwieg, H., "Bestimmung des Verhältnisses der Austauschkoeffizienten für Wärme und Impuls bei turbulenten Grenzschichten," ZFW 4, pp. 73-81, 1956.

25. Okiishi, T.H. and Serovy, G.K., "An Experimental Study of the Turbulent Flow Boundary-Layer Development in Smooth Annuli," *J. of Basic. Eng. Trans. ASME,* vol. 89, pp. 823-836, 1967.

26. Olson, R.M. and Sparrow, E.M., "Measurements of Turbulent Flow Development in Tubes and Annuli with Square or Round Entrances," *A. I. CH. E. Jour.*, vol. 9, pp. 766-770, Nov, 1963.

27. Park, S.D. and Lee, Y., "Diabatic Turbulent Flow in the Entrance Region of Concentric Annuli", *84th Annual Meeting*, The Eng. Inst. Canada, Paper No. 70-CSME-9, 1970.

28. Park, S.D., "Developing Turbulent Flow and Heat Transfer in Concentric Annuli; An Analytical and Experimental Study," *Ph.D. Thesis*, University of Ottawa, 1971.

29. Roberts, A., "A Comment on the Turbulent Flow Velocity Profile in a Concentric Annulus," *Int. J. Heat and Mass Transfer*, vol. 10, pp. 709-712, 1967.

30. Roberts, A. and Barrow, H., "Turbulent Heat Transfer to Air in the Vicinity of the Entry of an Internally Heated Annulus," *Proceedings, Thermodynamics and Fluid Mechanics Conv., Bristol*, 1968.

31. Shigechi, T. and Lee, Y., "An Analysis on Fully Developed Laminar Fluid Flow and Heat Transfer in Concentric Annuli with moving cores," *Heat and Mass Transfer*, vol. 34, pp. 2593-2601, 1991.

32. Cebeci, T. and Smith, A.M.O., "Analysis of Turbulent Boundary Layers," Academic Press, New York, U.S.A., pp. 47-56, 62-77, 106, 191, 1974.

33. Kays, W.M. and Leung, E.Y., "Heat Transfer in Annular Passage Hydrodynamically Developed Turbulent Flow with Arbitrarily Prescribed Heat Flux," *Int J. of Heat & Mass Transfer*, vol. 6, pp. 537-557, 1963.

34. Kays, W.M. and Crawford, M.E., *Convective Heat and Mass Transfer*, 3rd ed, McGraw-Hill, New York, 1993.

35. Reynolds, W.C., Lundberg, R.E., and McCuen, P.A., "Heat Transfer in Annular Passages. General Formulation of the Problem for Arbitrarily Prescribed Wall Temperatures or Heat Fluxes," *J. Heat Mass Transfer*, vol. 6, pp. 483-493, 1963.

36. Wilson, N.W. and Medwell, J.O., "An analysis of the Developing Turbulent Hydrodyanmic and Thermal Boundary Layers in an Internally Heated Annulus," *Paper No. 70-HT-9, Trans. ASME*, pp. 1-7, 1970.

37. Deissler, R.G., "Analytical Investigation of Turbulent Flow in Smooth Tubes with Heat Transfer with Variable Fluid Properties for Prandtl Number of 1," *NACA TN-2242*, December, 1950

38. Prandtl, L., "Über Flüssigkeitsbewegung bei sehr kleiner Reibung," *Proc. 3rd. Int. Math. Cong. Heidelberg*, 1904, Reprinted in NACA TM 452, 1928.

39. Holman, J.P., *Heat Transfer*, 8th ed., McGraw-Hill, New York, 1997.

40. Schlichting, H., *Boundary Layer Theory*, 7th ed., McGraw-Hill, New York, 1979.

41. Yu, Y.S., "Effect of Transverse Curvature on Turbulent Boundary Layer Characteristics," *J. Ship Research*, vol. 2, pp. 33-51, 1958.

42. Rao, G.N.V., "The Law of The Wall in a Thick Axisymmetric Turbulent Boundary Layer," *J. Appl. Mech.*, vol. 34, pp. 237-238, 1967.

43. Rao, G.N.V. and Keshavan, N.R., "Axisymmetric Turbulent Boundary Layers in Zero Pressure Gradient Flows," *J. Appl. Mech.*, vol. 39, pp. 25-32, 1972.

44. Coles, D., "The Law of the Wake in the Turbulent Boundary Layer," *J. of Fluid Mechanics*, vol. 1, pp. 191-226, 1956.

45. Willmarth, W.W. and Yang, C.S., "Wall Pressure Fluctuations beneath Turbulent Boundary Layers on a Flat plate and a Cylinder," *J. Fluid Mech.*, vol 41, pp. 47-80, 1970.

46. Kjellström, B. and Hedberg, S., "On Shear Stress Distributions for Flow in Smooth or Partially Rough Annuli," *AE-243*, Aktiebolaget, Atomenergi, Stockholm, Sweden, 1966.

47. Page, F., Schlinger, W.G., Breaux, D.K. and Sage, B.H., "Point Values of Eddy Conductivity and Viscosity in Uniform Flow Between Parallel Plates," *Ind. Eng. Chem.*, vol. 44, pp. 424-430, 1952.

48. Sleicher, C. and Tribus, M., "Heat Transfer to a Pipe with Turbulent Flow and Arbitrary Wall Temperature Distribution," *Trans. ASME*, vol 79, pp.789, 1957.

49. Johnson, D.S., "Velocity and Temperature Fluctuation Measurements in a Turbulent Boundary Layer Downstream for Stepwise Discontinuity in Wall Temperature," *Trans. ASME. 61*, pp. 705-710, 1939.

50. Jerkins, R., "Variation of the Eddy Conductivity with Prandtl Modules and it's Use in Prediction of Turbulent Heat Transfer Coefficients," *Heat Transfer and Fluid Mechanics Inst.*, 147, Stanford Univ. Press, Stanford, California, 1951.

51. Chapra, S.C. and Canale, R.P., *Numerical Methods for Engineers*, 2nd ed., McGraw-Hill, New York, 1990.

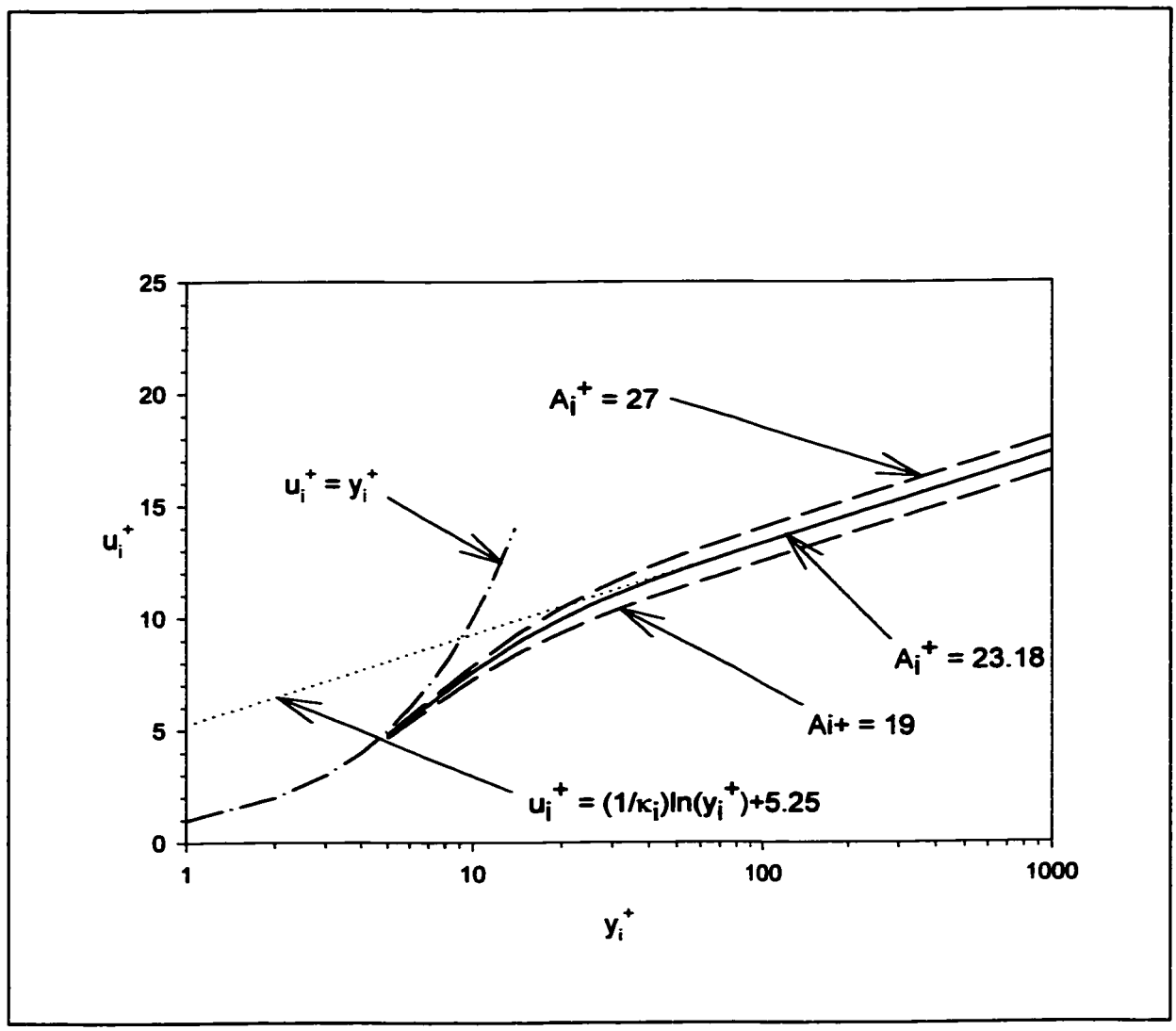

Figure 2.1 Determination of the van Driest Damping Parameter, A_i^+ ; $R_t^* = 0.005$

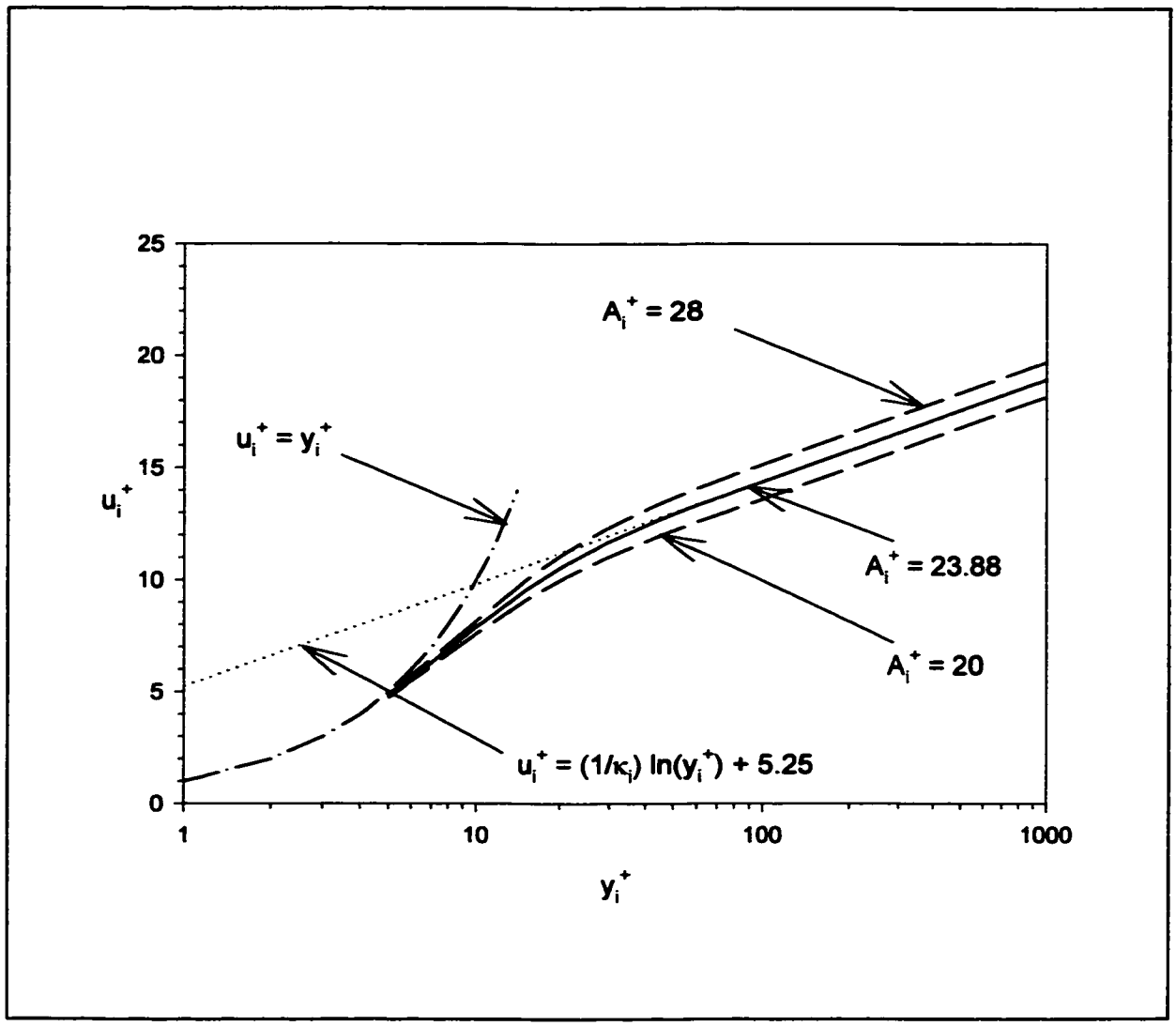

Figure 2.2 Determination of the van Driest Damping Parameter, A_i^+; $R_t^* = 0.01$

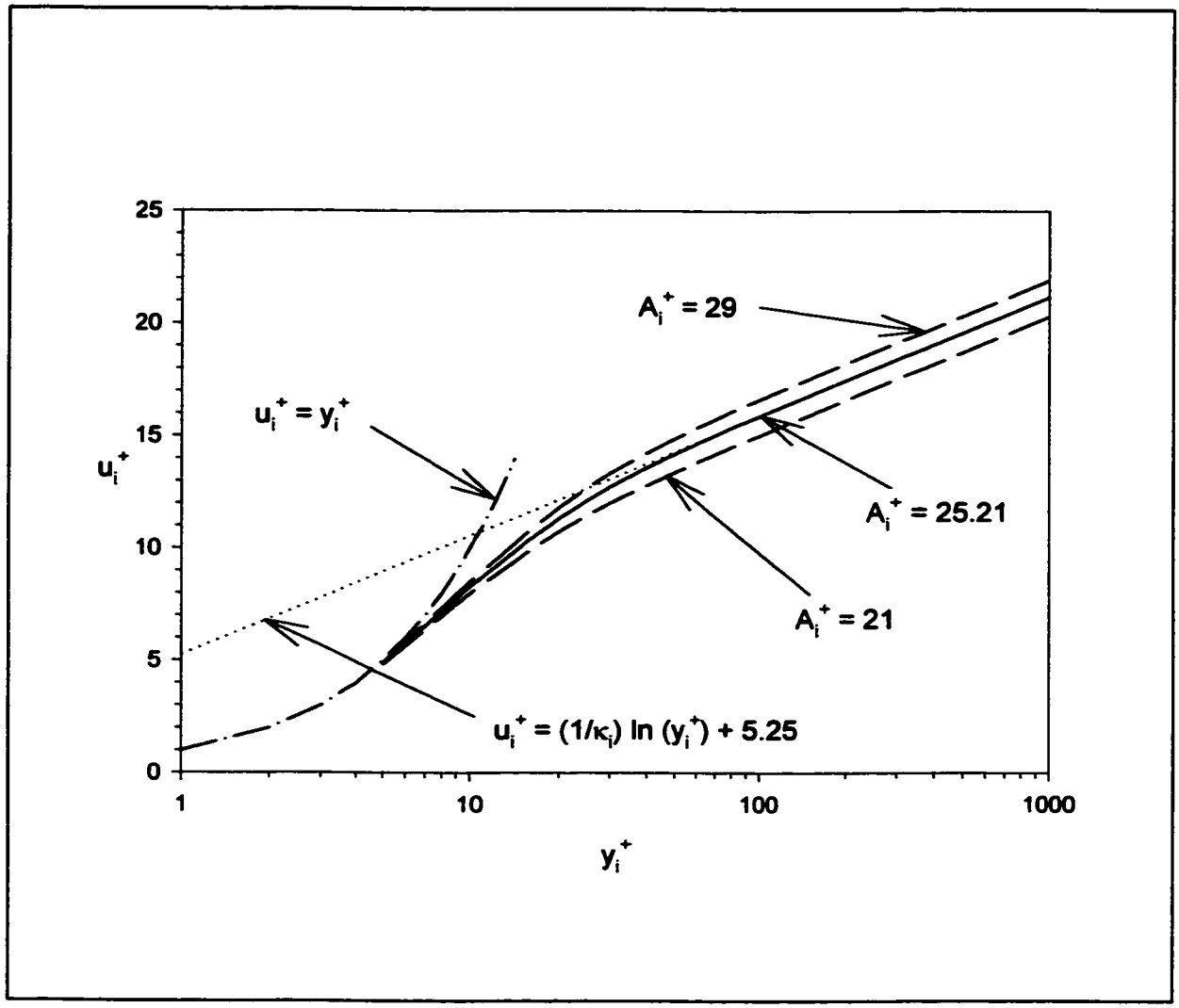

Figure 2.3 Determination of the van Driest Damping Parameter, A_i^+ ; $R_i^* = 0.05$

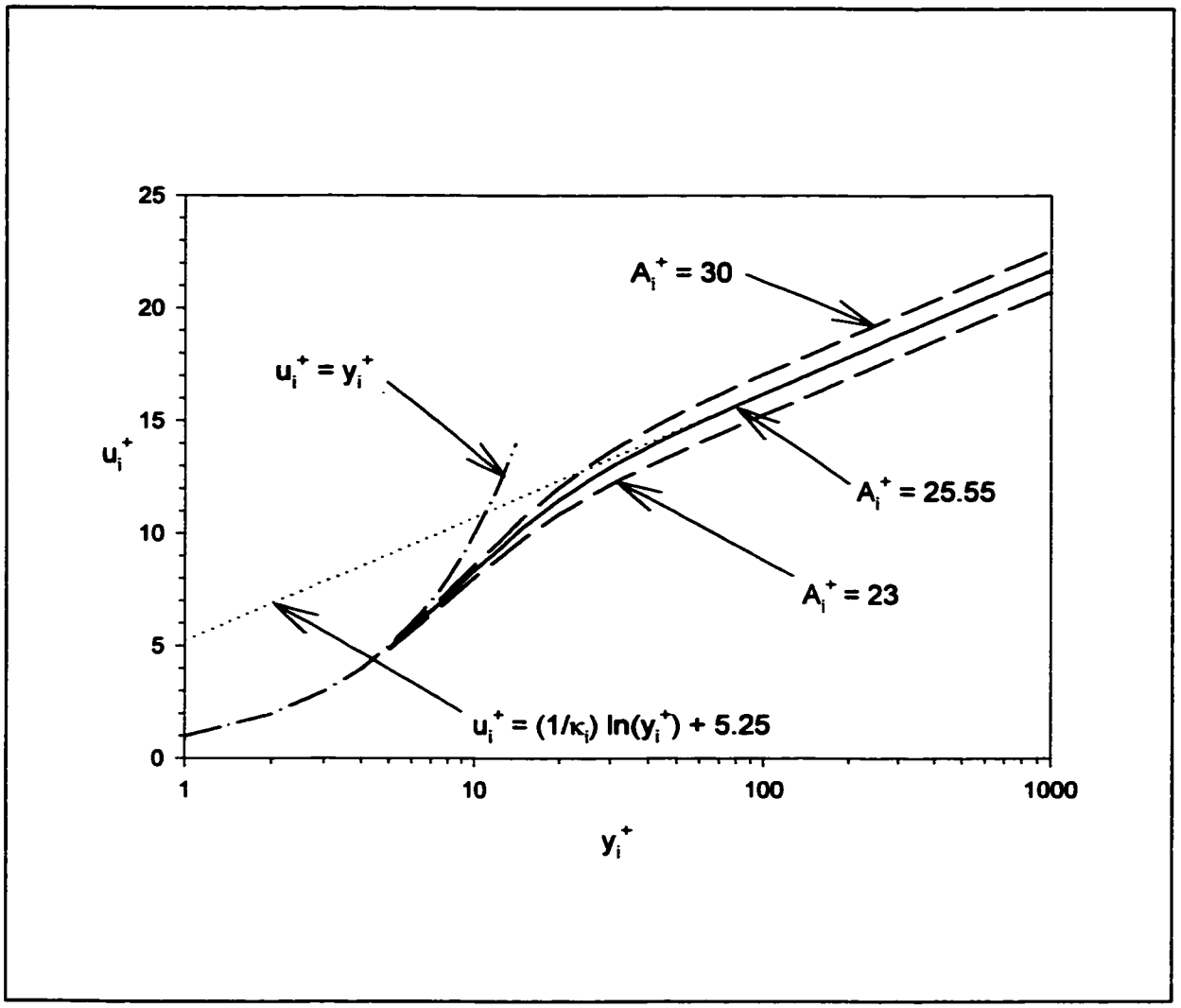

Figure 2.4 Determination of the van Driest Damping Parameter, A_i^+; $R_i^\bullet = 0.1$

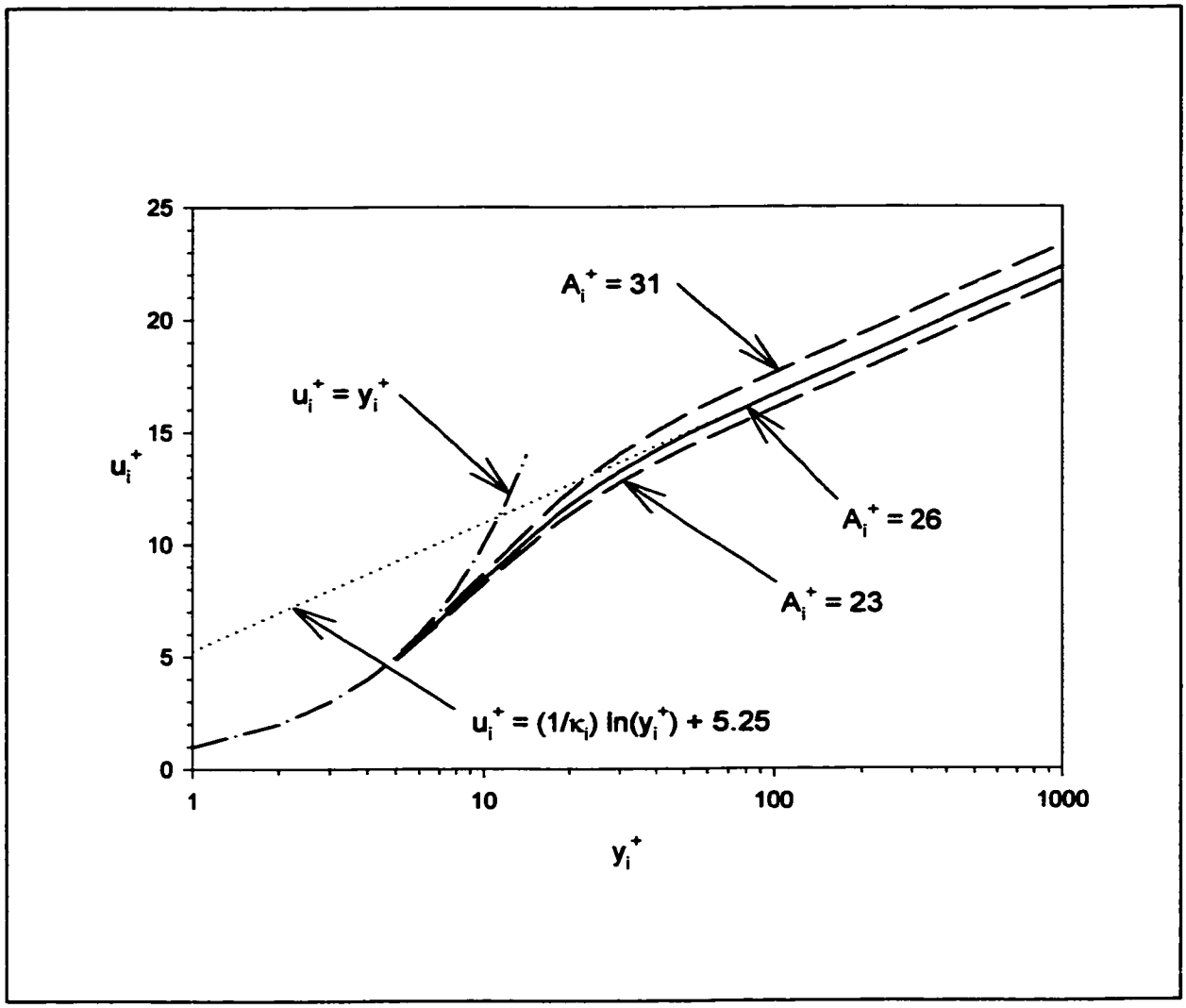

Figure 2.5 Determination of the van Driest Damping Parameter, A_i^+; $R_t^\bullet = 1.0$

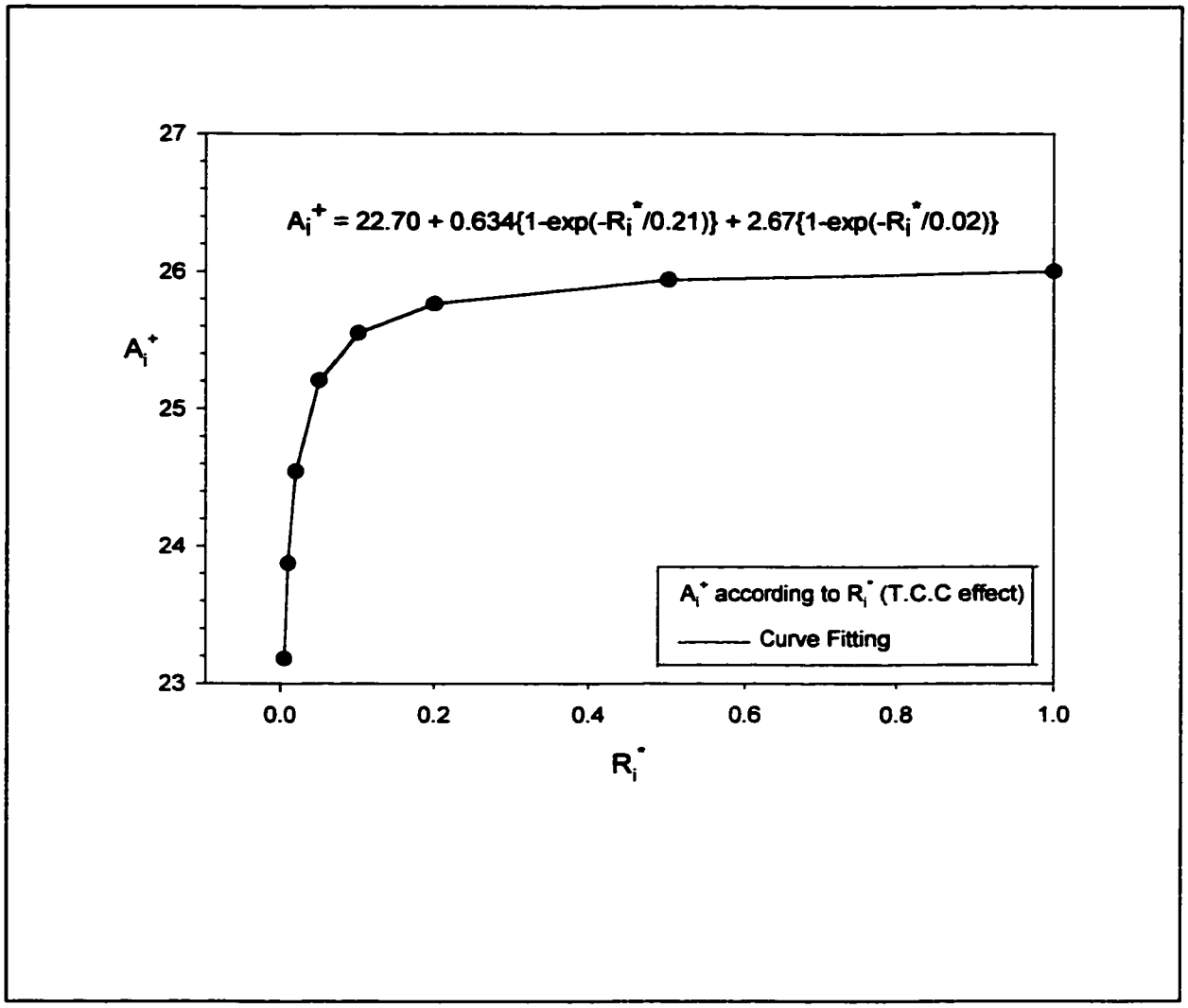

Figure 2.6 Effect of R_i^* on the variation of the van Driest Damping Parameter for Inner Region, A_i^+

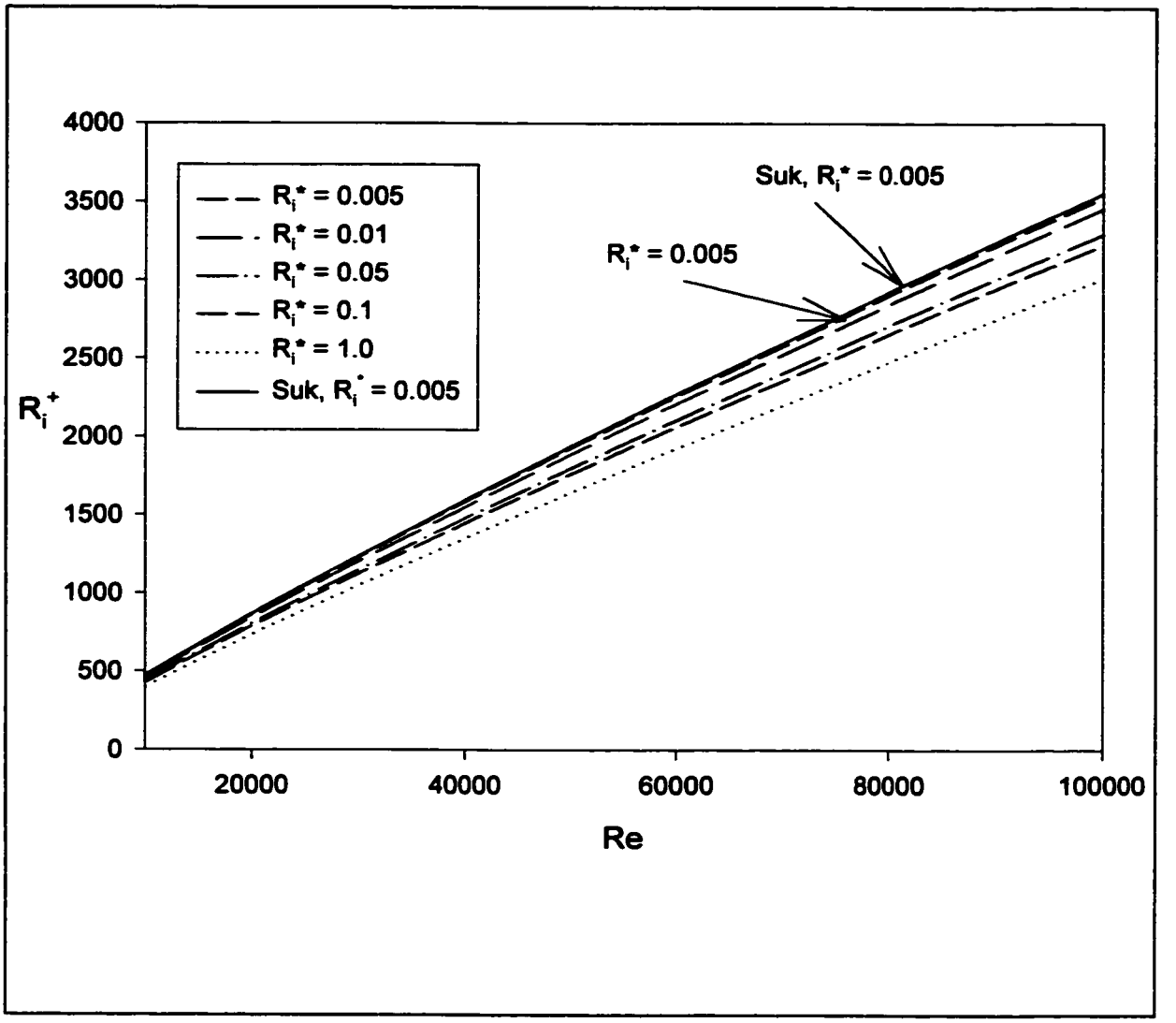

Figure 2.7 Effect of R_i^+ on the Reynolds Number, $\mathrm{Re} = u_b \cdot 2(R_o - R_i)/\nu$

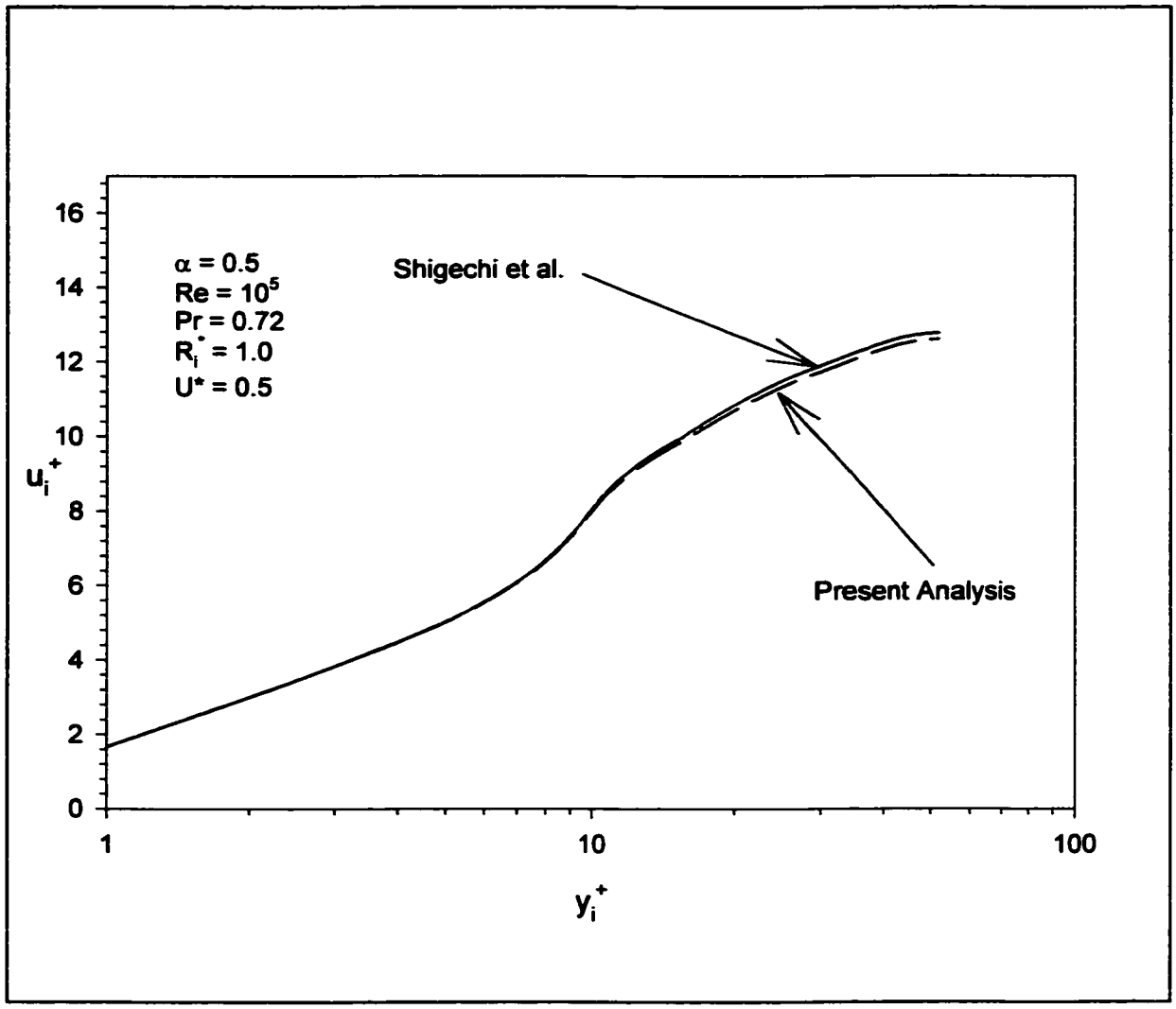

Figure 2.8 Velocity Distribution; U* = 0.5

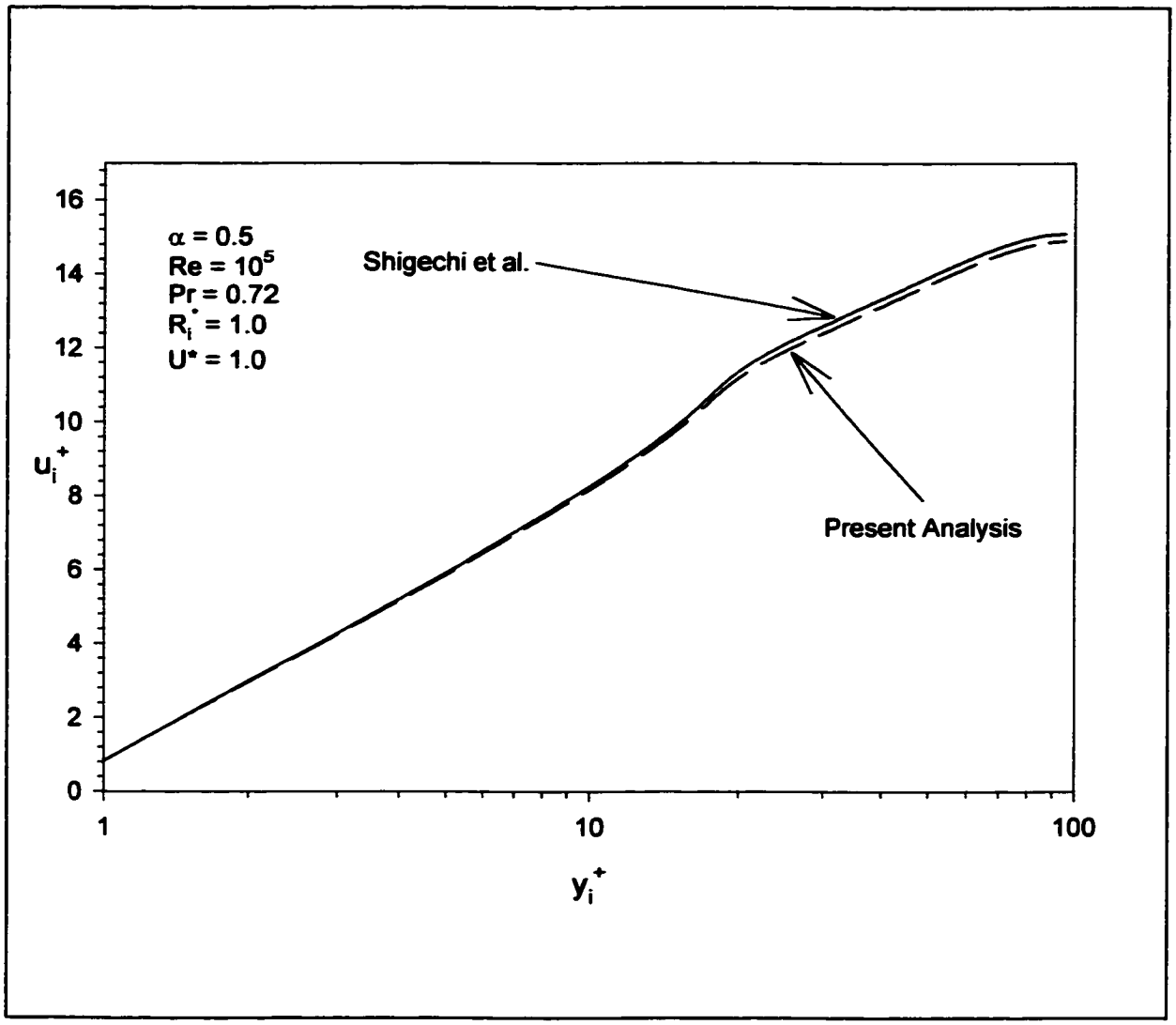

Figure 2.9 Velocity Distribution; U* = 1.0

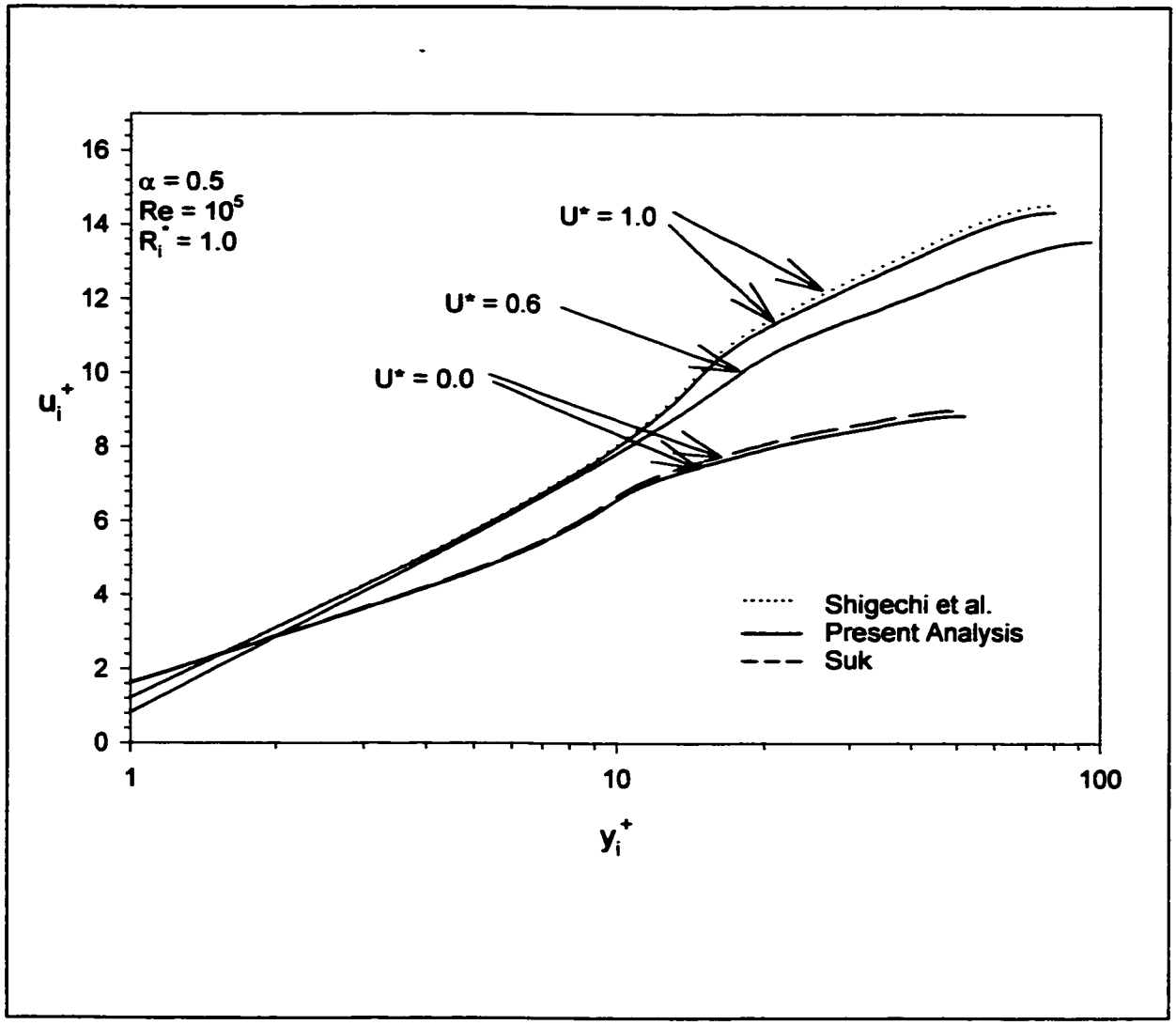

Figure 2.10 Dimensionless Velocity Profiles

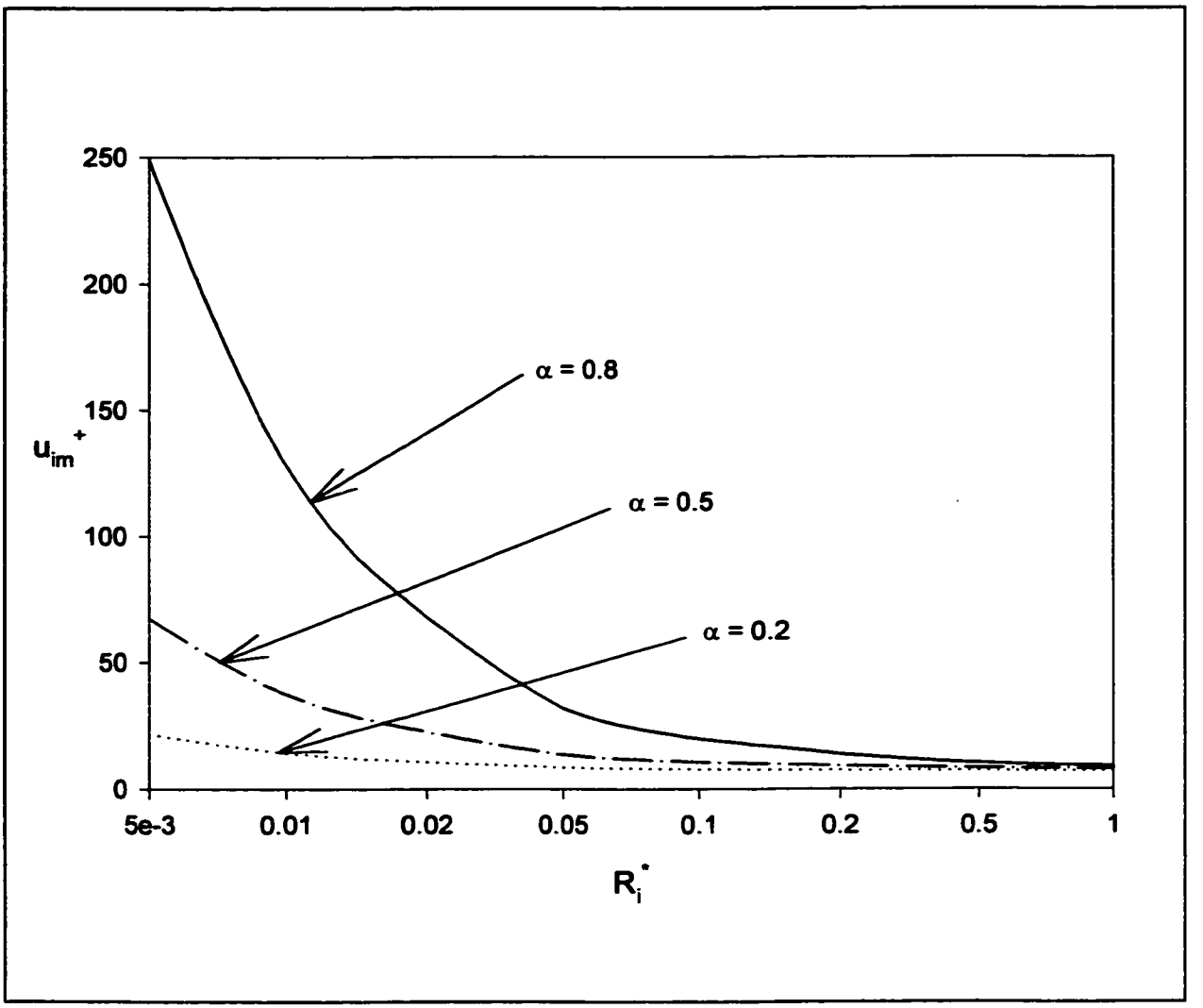

Figure 2.11 Effect of R_i^* on Maximum Velocity; Re = 10^5 and U* = 0.4

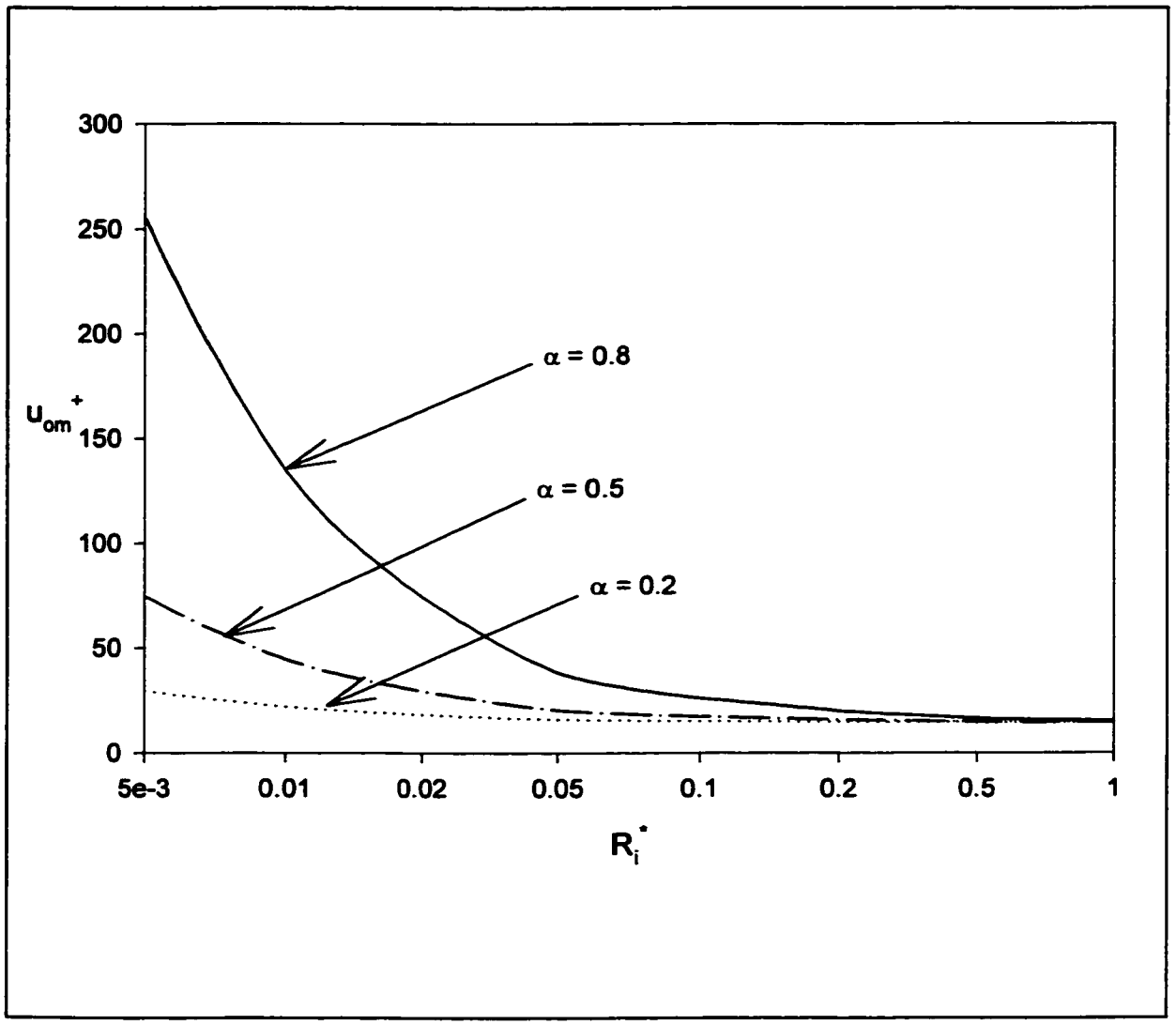

Figure 2.12 Effect of R_i^* on Maximum Velocity; Re = 10^5, and U* = 0.4

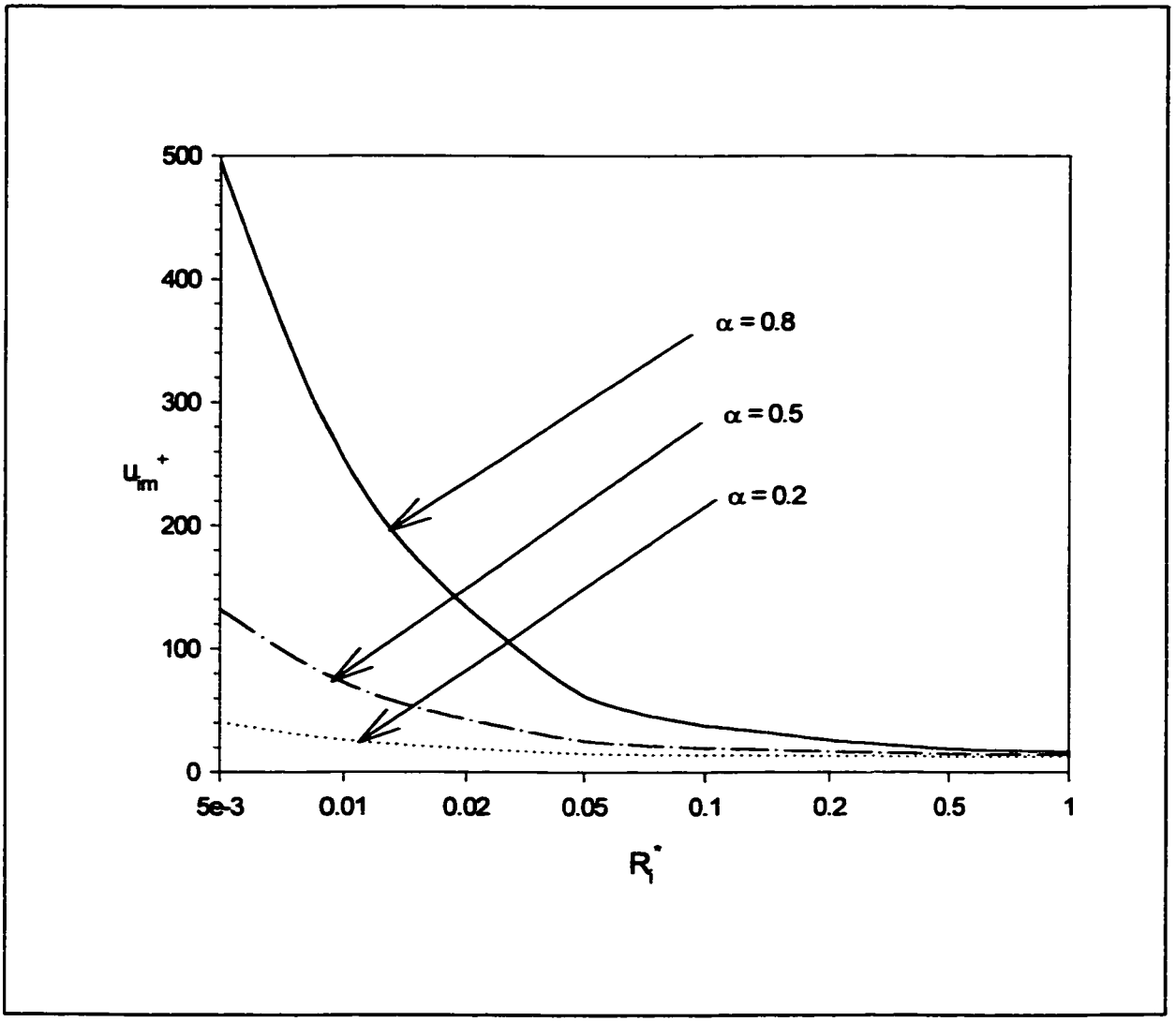

Figure 2.13 Effect of R_i^* on Maximum Velocity; Re = 10^5, and U* = 0.8

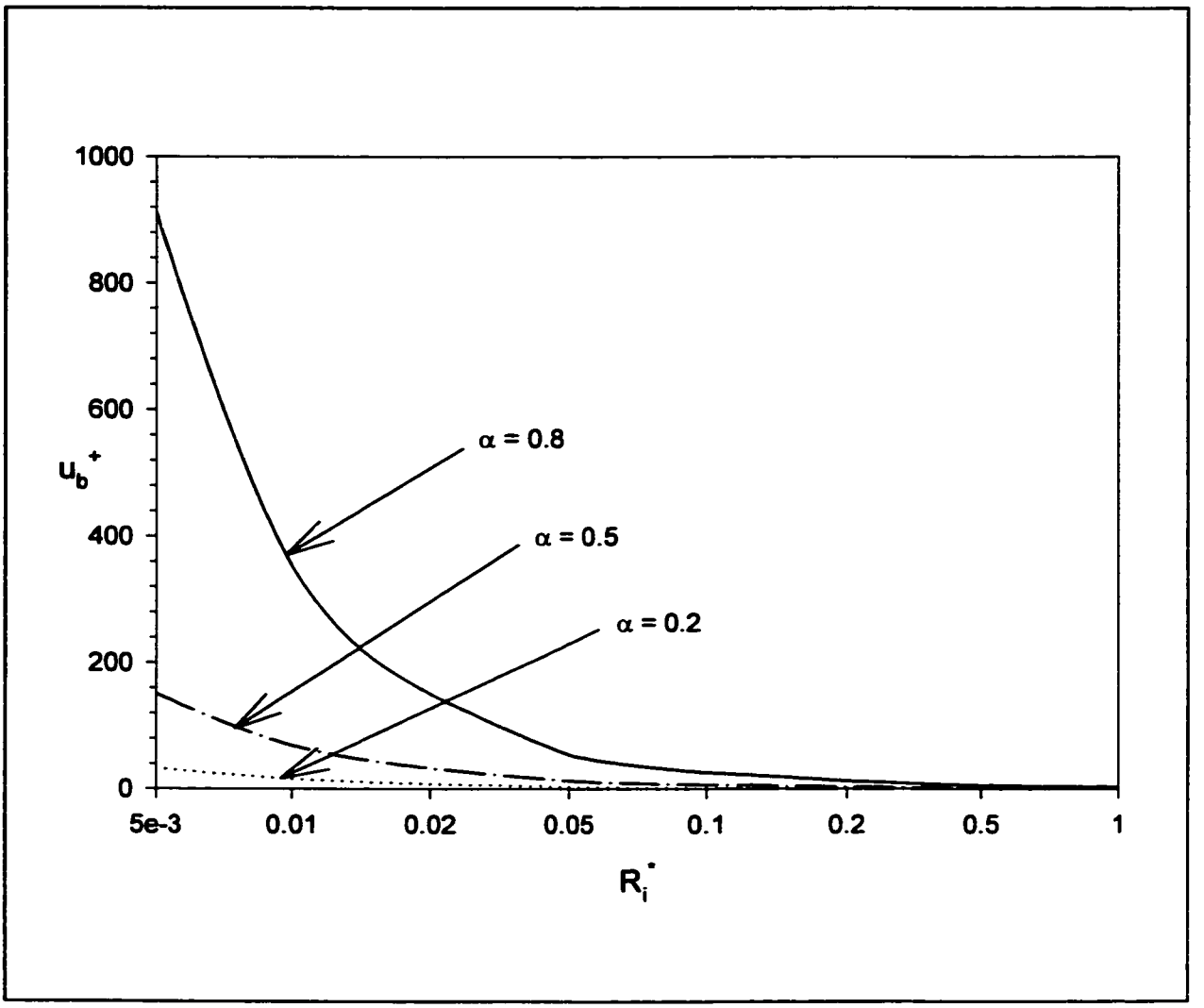

Figure 2.14 Effect of R_i^* on Dimensionless Bulk Velocity; U* = 0.4 and Re = 10^5

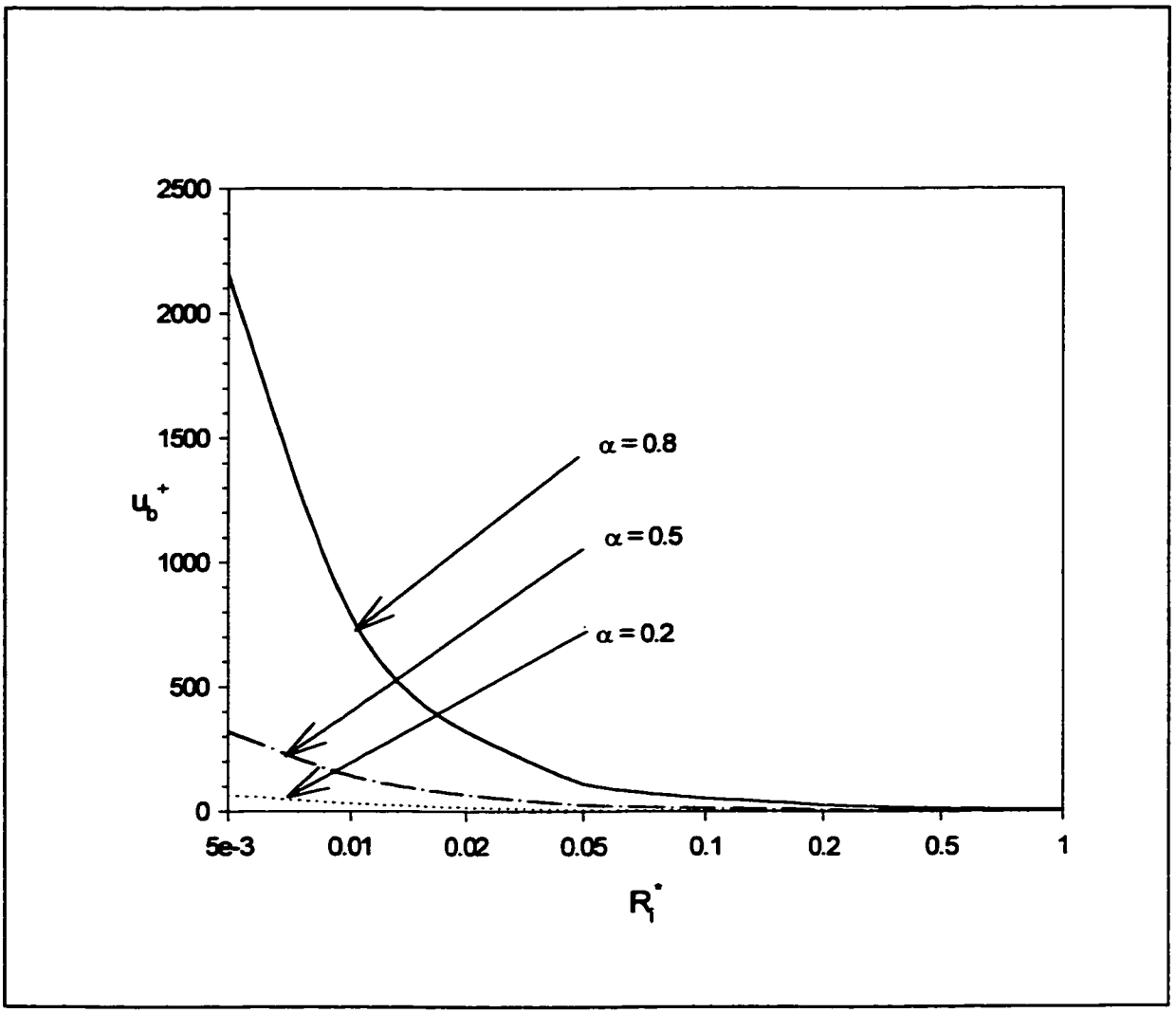

Figure 2.15 Effect of R_t^* on Dimensionless Bulk Velocity; U* = 0.8 and Re = 10^5

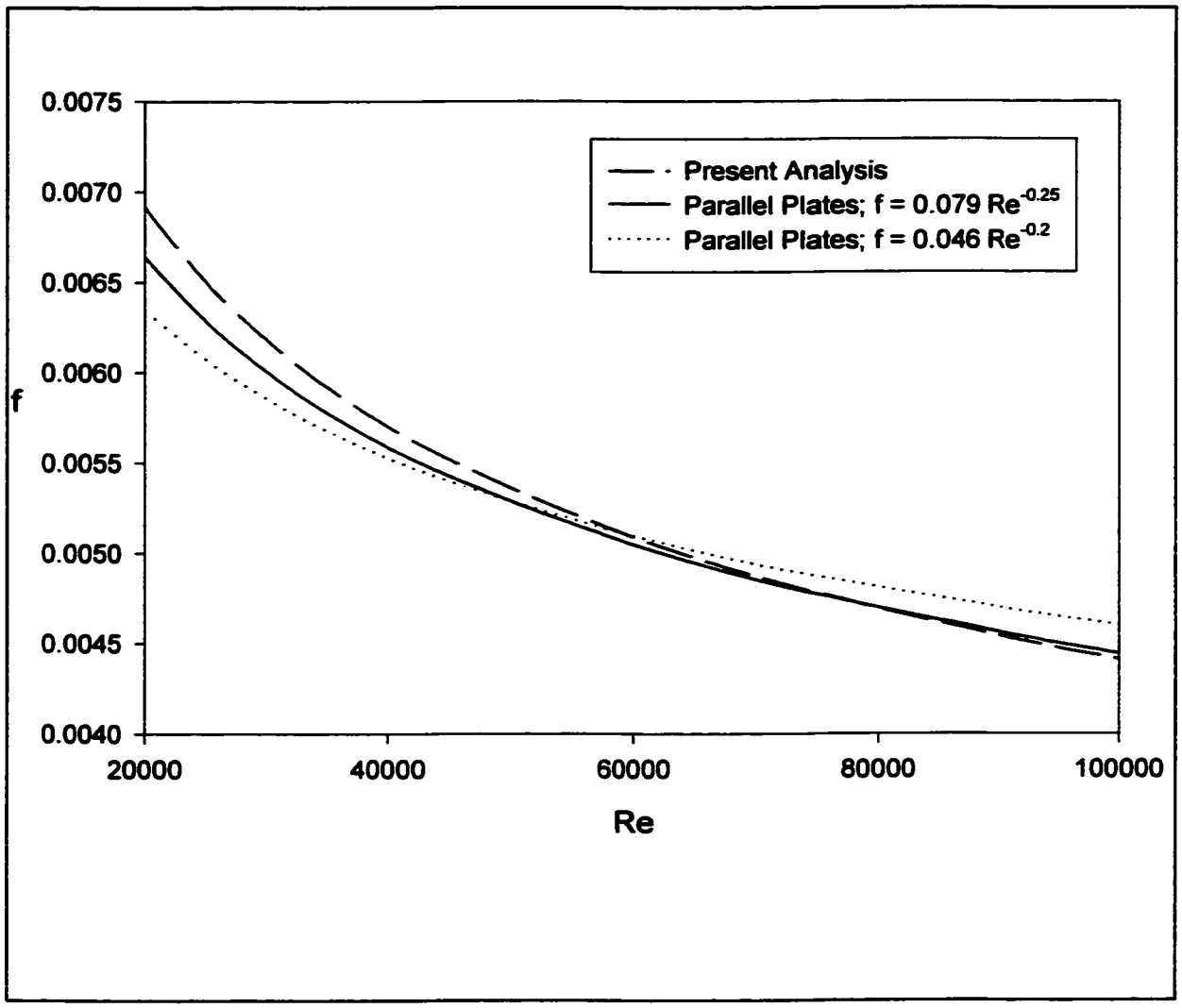

Figure 2.16 Friction Factors; $R_i^* = 1.0$, $\alpha = 0.999$ and U*=0.0; $\mathrm{Re} = u_b \cdot 2(R_o - R_i)/\nu$

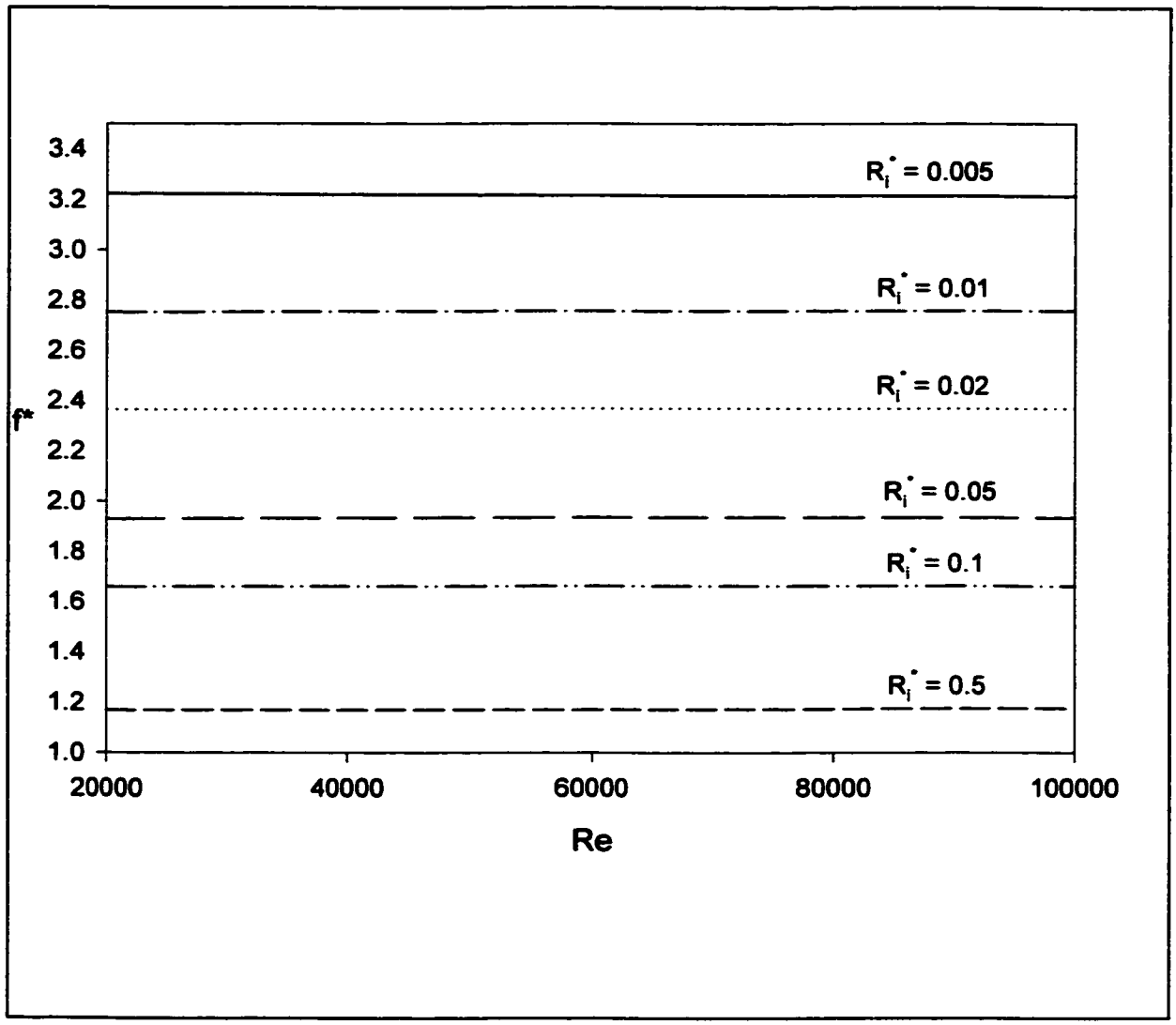

Figure 2.17 Effect of R_i^* on Normalized Friction Factors ($f^* = f / f_{1.0m}$); $\alpha = 0.2$, U* = 0.5; Re = $u_b \cdot 2(R_o - R_i)/\nu$

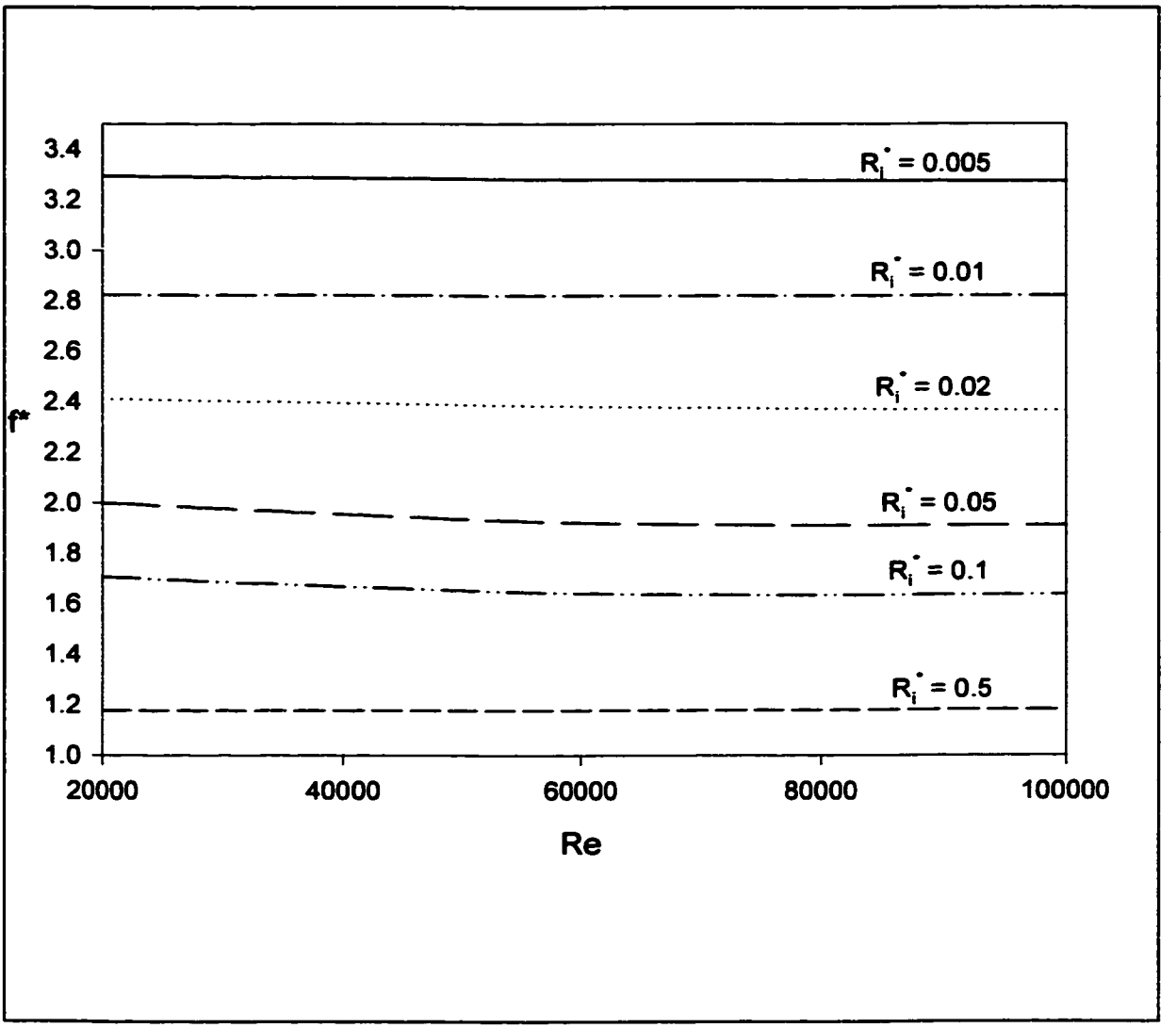

Figure 2.18 Effect of R_i^* on Normalized Friction Factors ($f^* = f / f_{1.0m}$); $\alpha = 0.2$, U* = 1.0; Re = $u_b \cdot 2(R_o - R_i)/\nu$

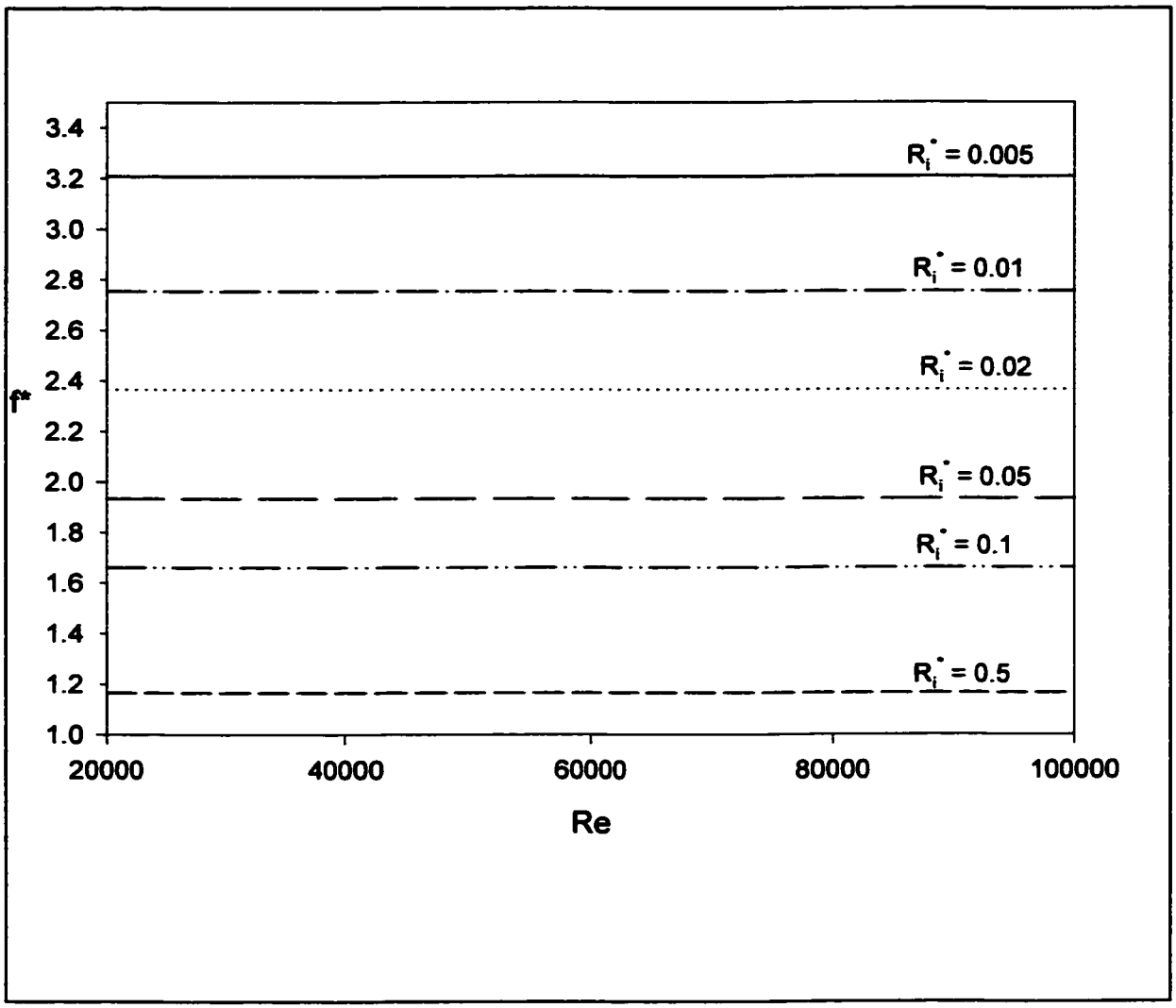

Figure 2.19 Effect of R_i^* on Normalized Friction Factors ($f^* = f / f_{1.0m}$); $\alpha = 0.5$, U* = 0.5; Re = $u_b \cdot 2(R_o - R_i)/\nu$

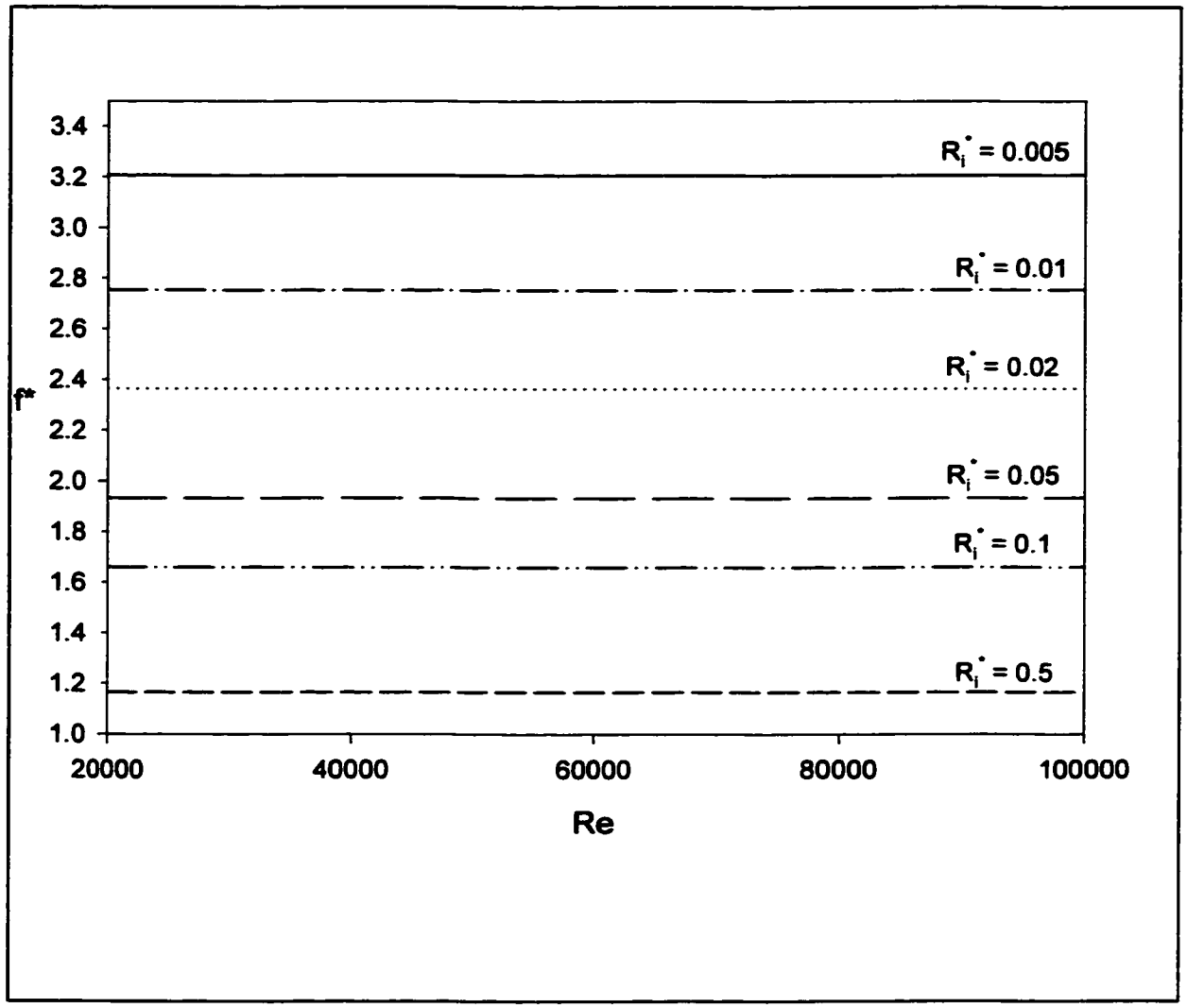

Figure 2.20 Effect of R_i^* on Normalized Friction Factors ($f^* = f / f_{1.0m}$); $\alpha = 0.5$, U* = 1.0; Re = $u_b \cdot 2(R_o - R_i)/\nu$

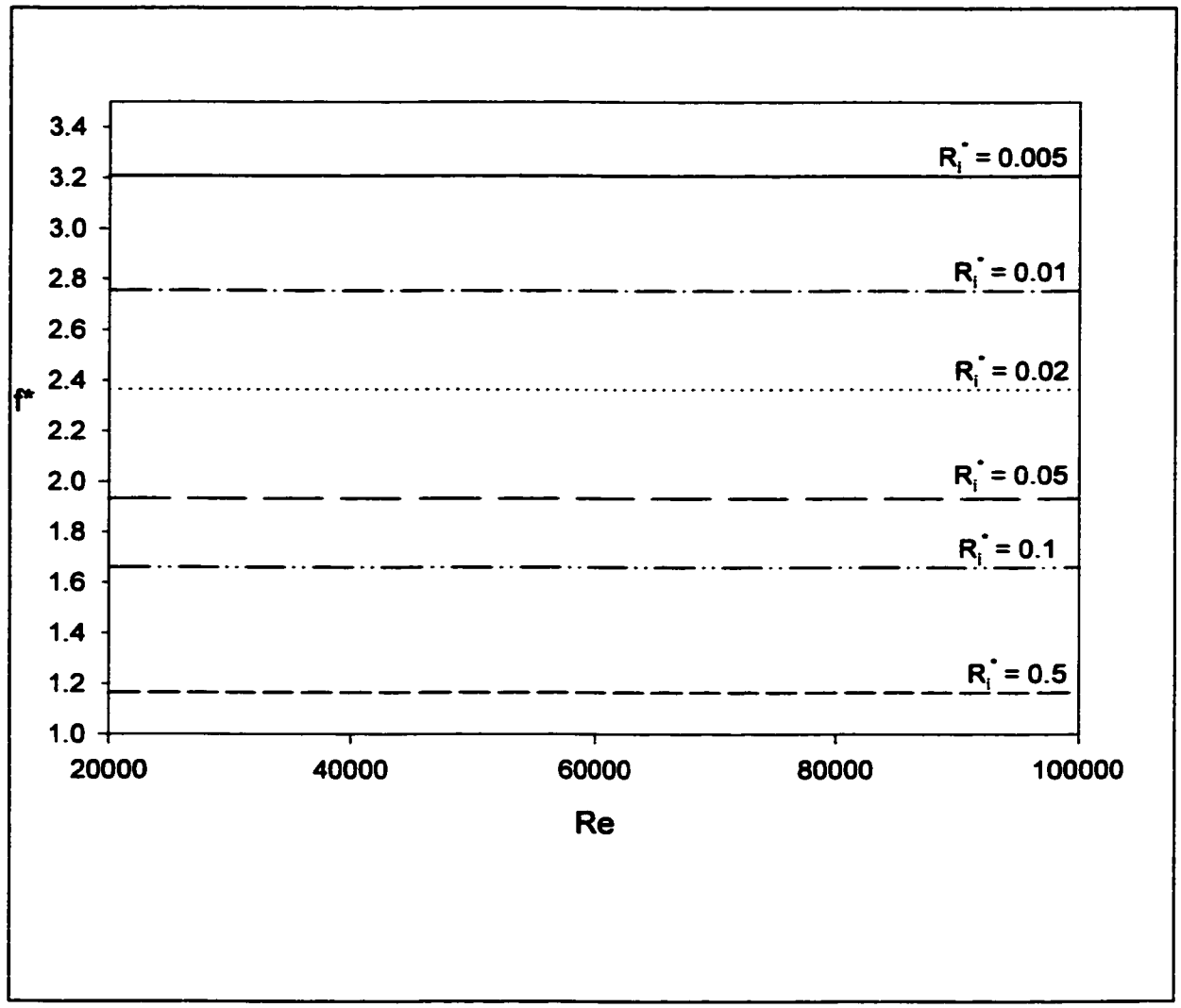

Figure 2.21 Effect of R_i^* on Normalized Friction Factors ($f^* = f / f_{1.0m}$); $\alpha = 0.8$, U* = 0.5; Re = $u_b \cdot 2(R_o - R_i)/\nu$

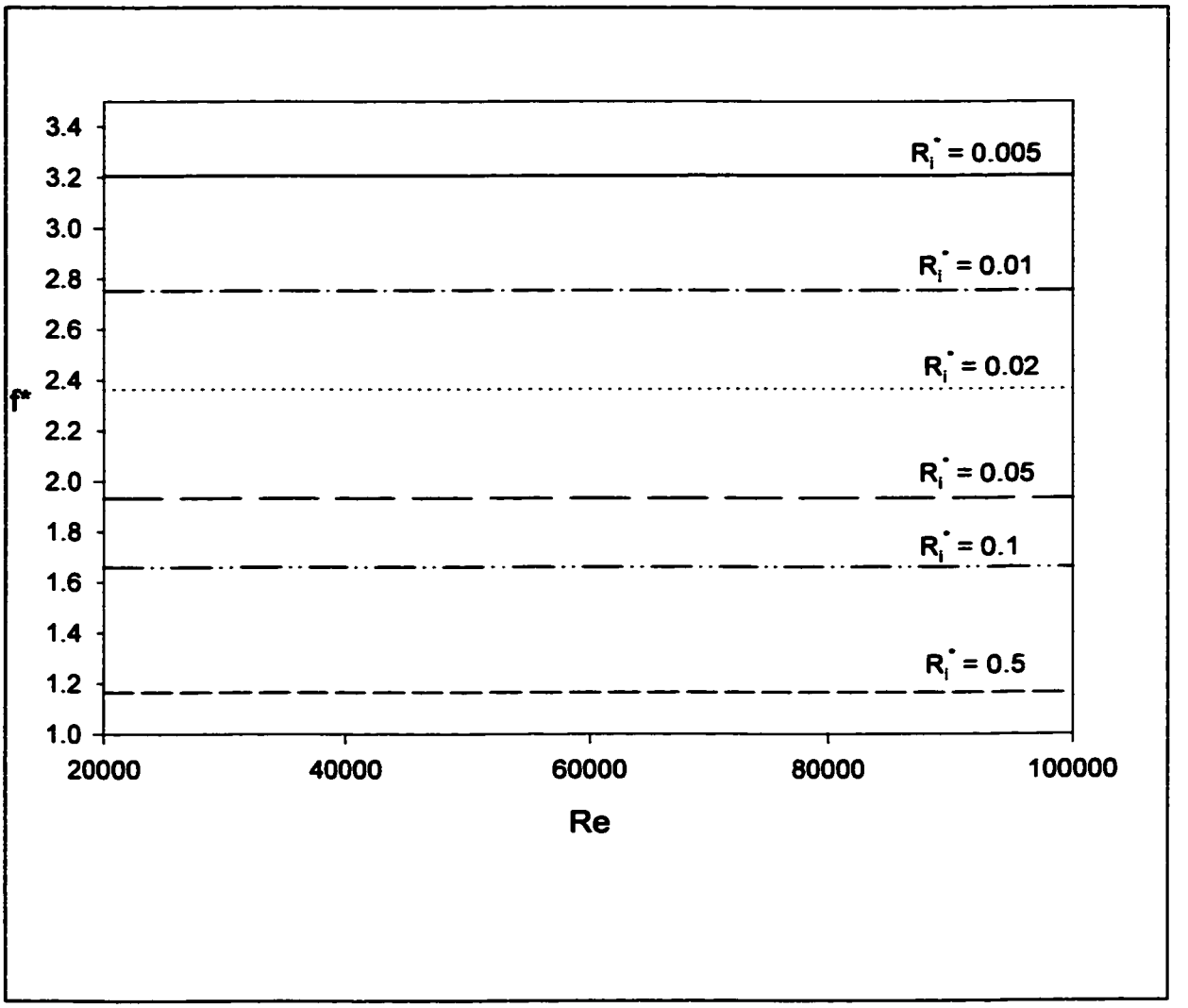

Figure 2.22 Effect of R_i^* on Normalized Friction Factors ($f^* = f / f_{1.0m}$); $\alpha = 0.8$, U* = 1.0; Re = $u_b \cdot 2(R_o - R_i)/\nu$

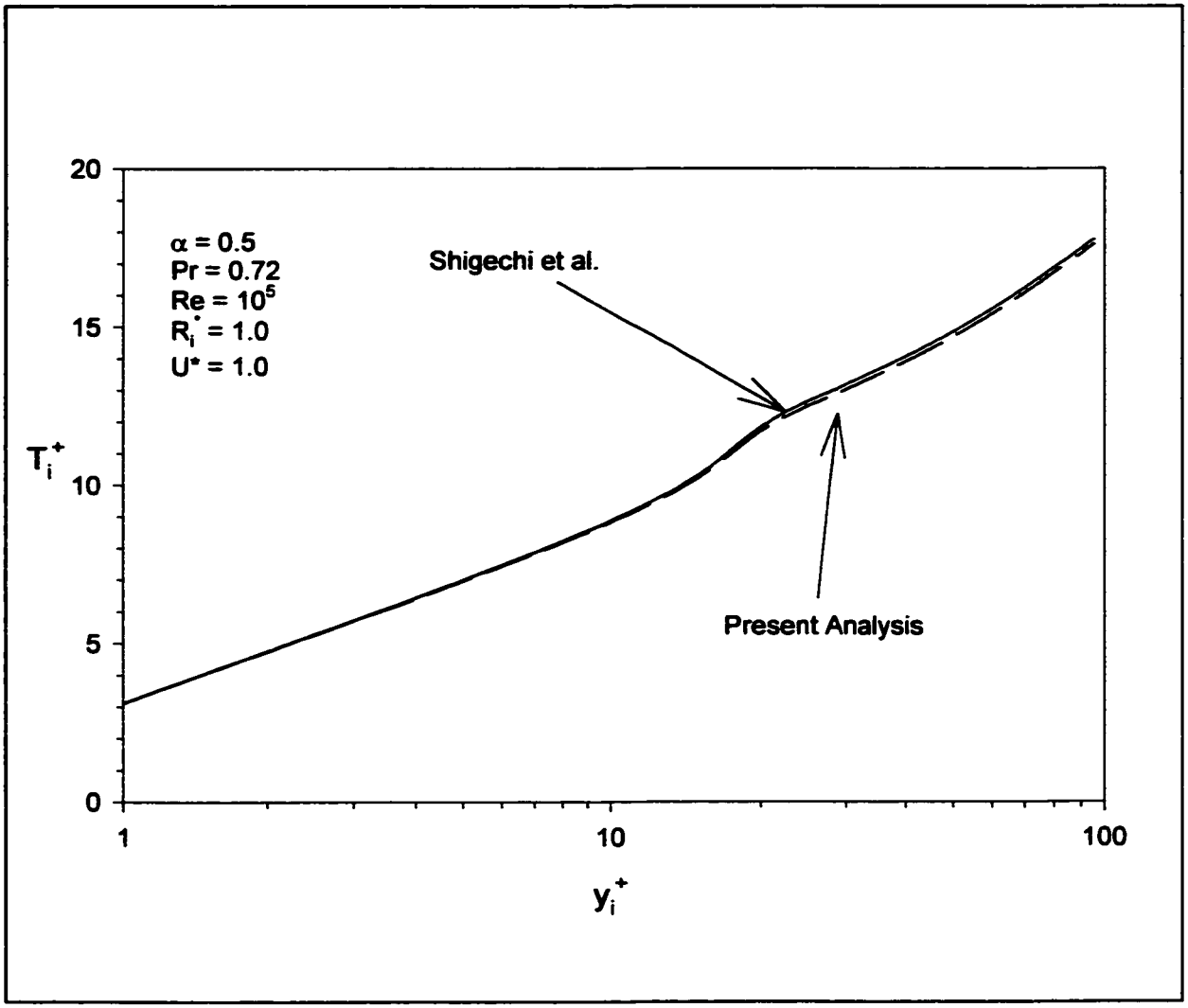

Figure 2.23 Dimensionless Temperature Profile; U* = 1.0 and Pr = 0.72

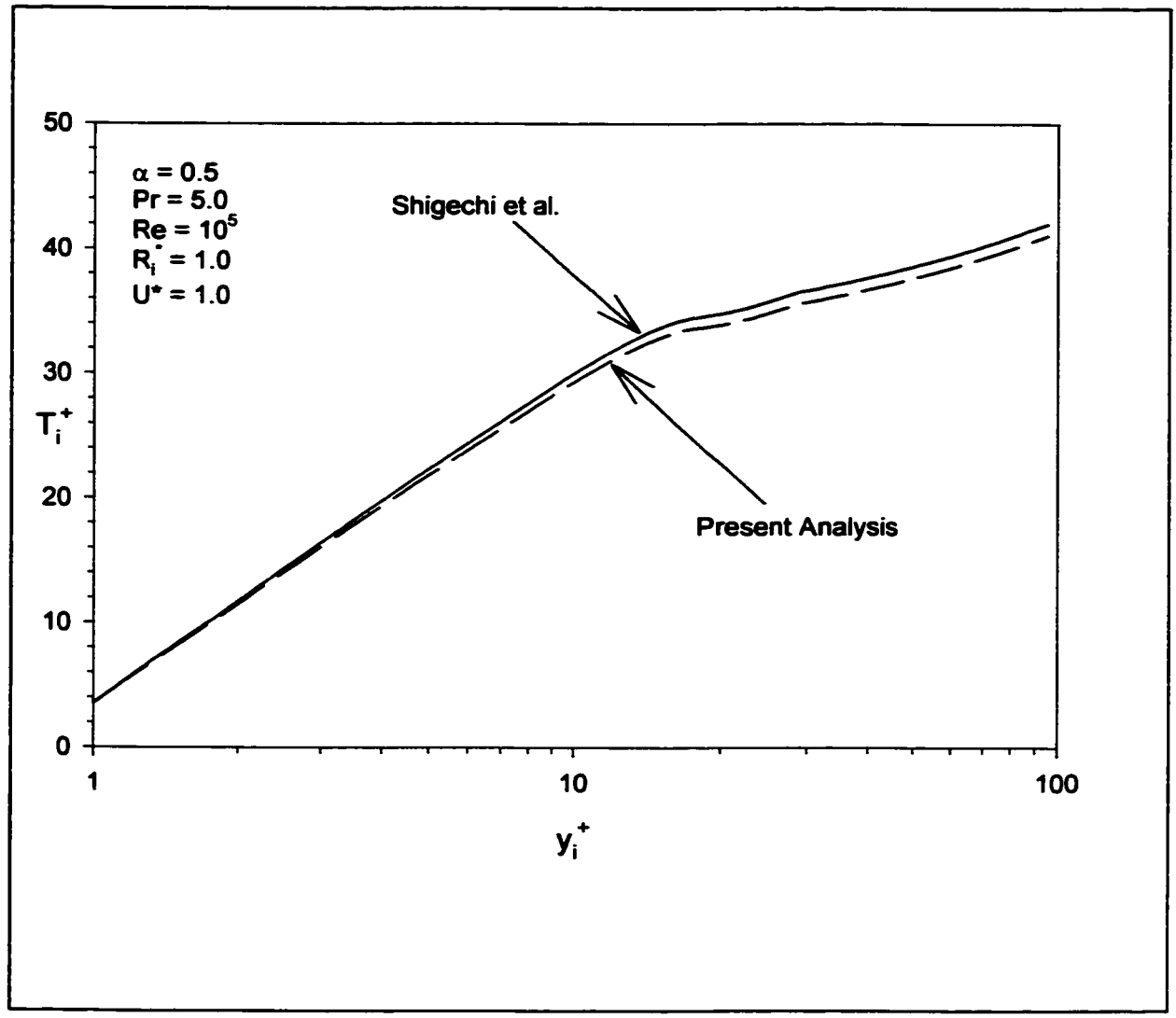

Figure 2.24 Dimensionless Temperature Profile; U* = 1.0 and Pr = 5.0

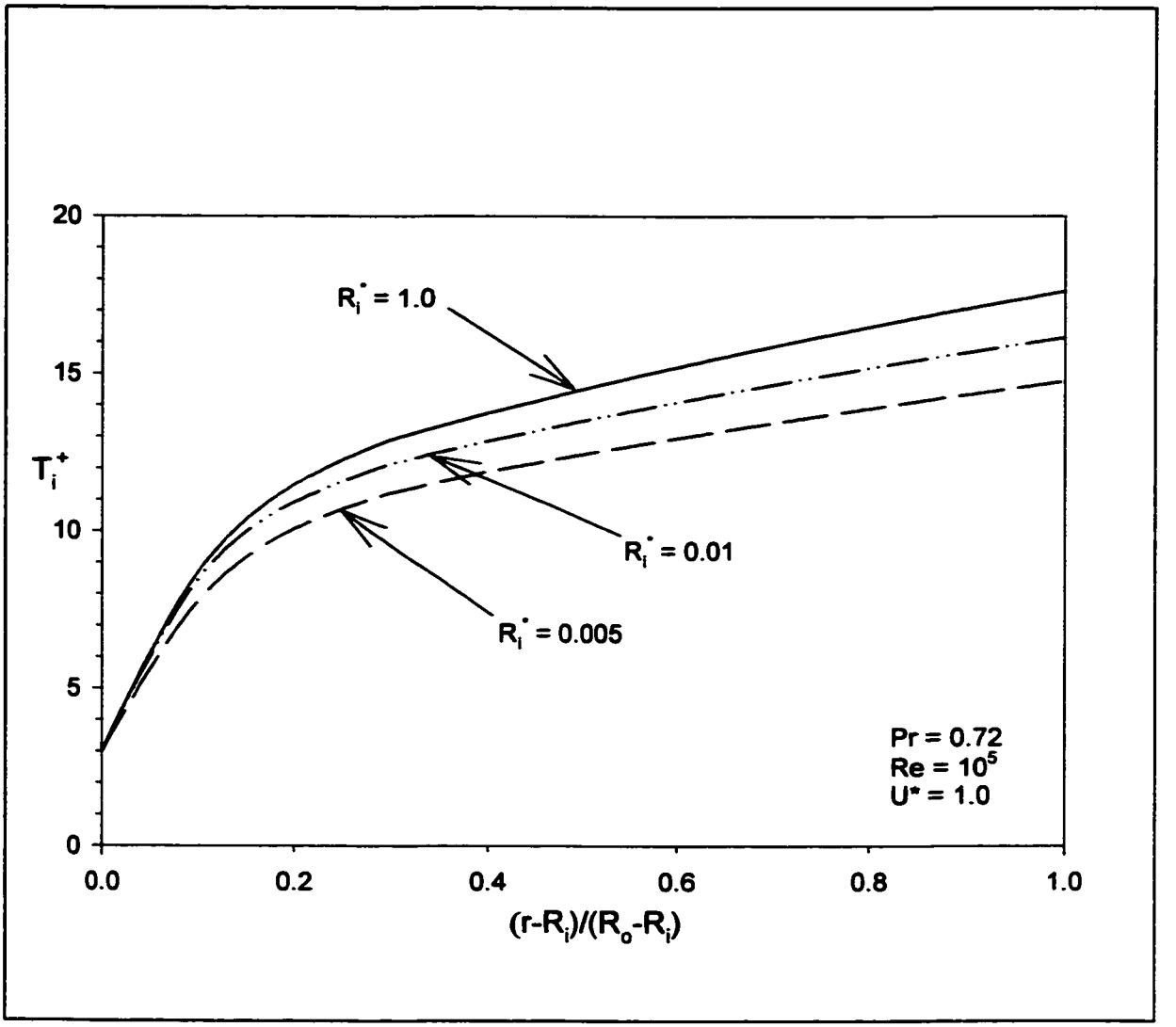

Figure 2.25 Effect on R_i^* on Temperature Distribution; $\alpha = 0.5$ and U* = 1.0

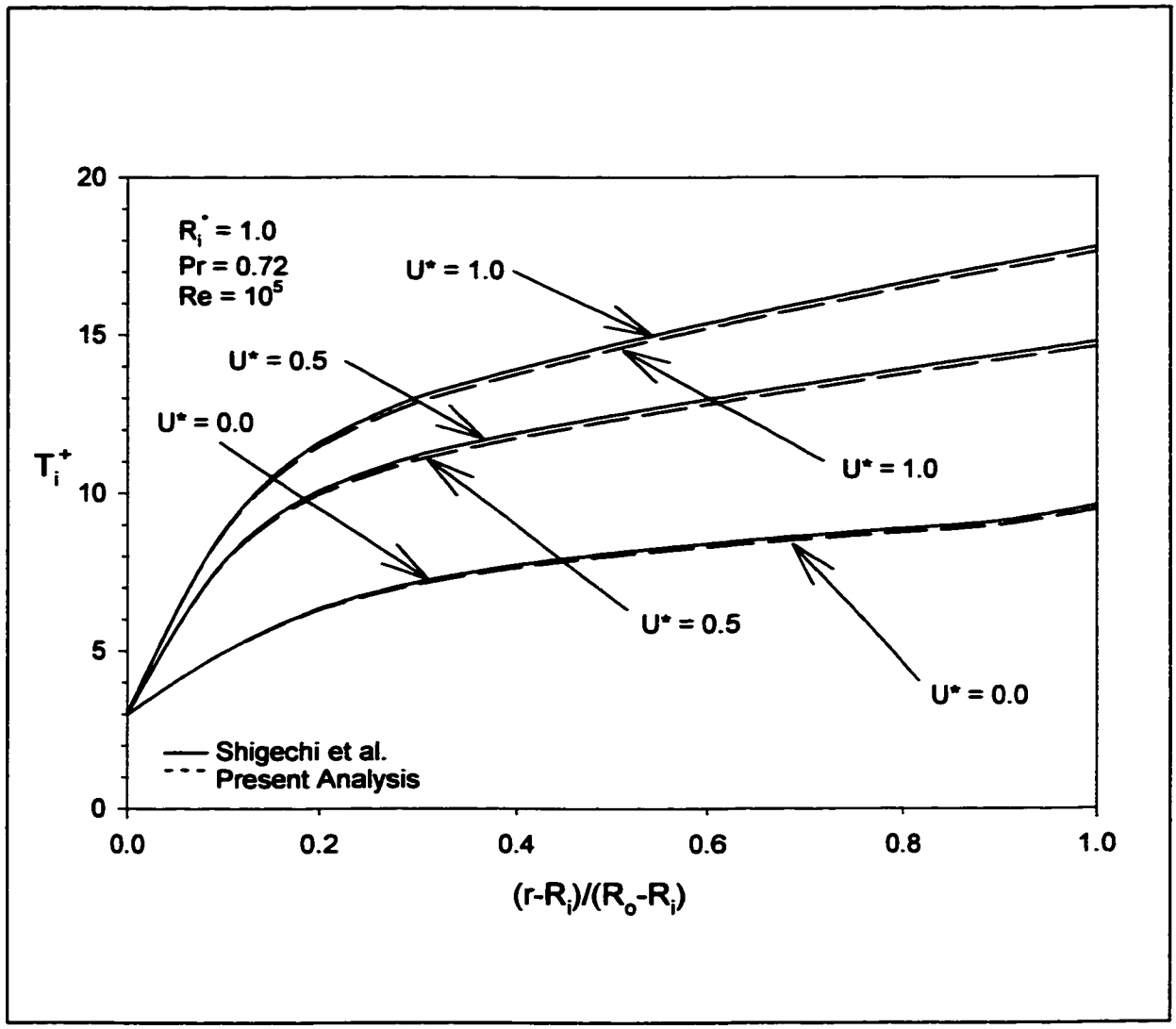

Figure 2.26 Effect of U* on Dimensionless Temperature Distribution; $R_i^* = 1.0$, $\alpha = 0.5$, Pr = 0.72 and U* = 0.0, 0.5 & 1.0

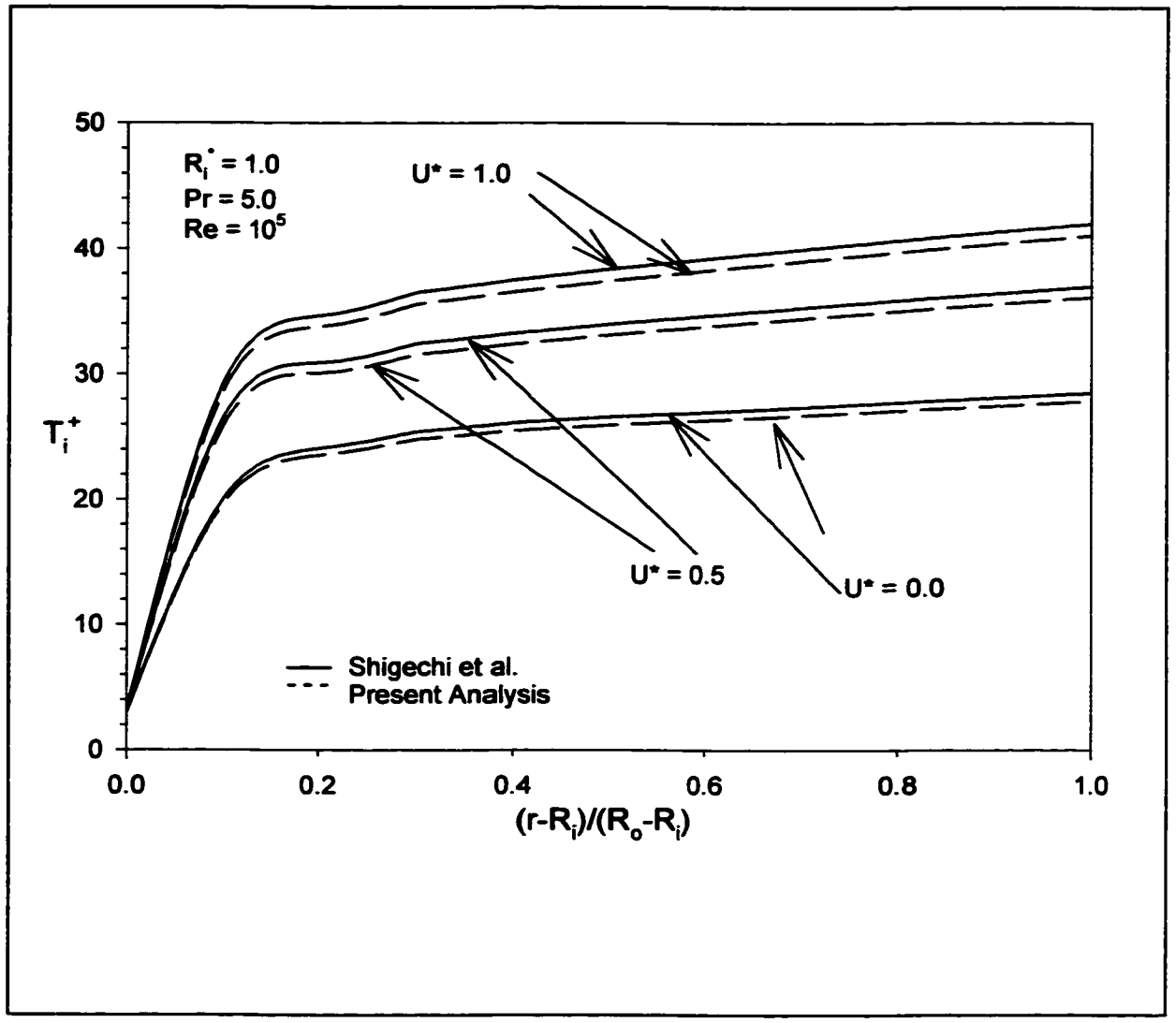

Figure 2.27 Effect of U* on Dimensionless Temperature Distribution; $R_i^* = 1.0$, $\alpha = 0.5$, Pr = 5.0 and U* = 0.0, 0.5 & 1.0

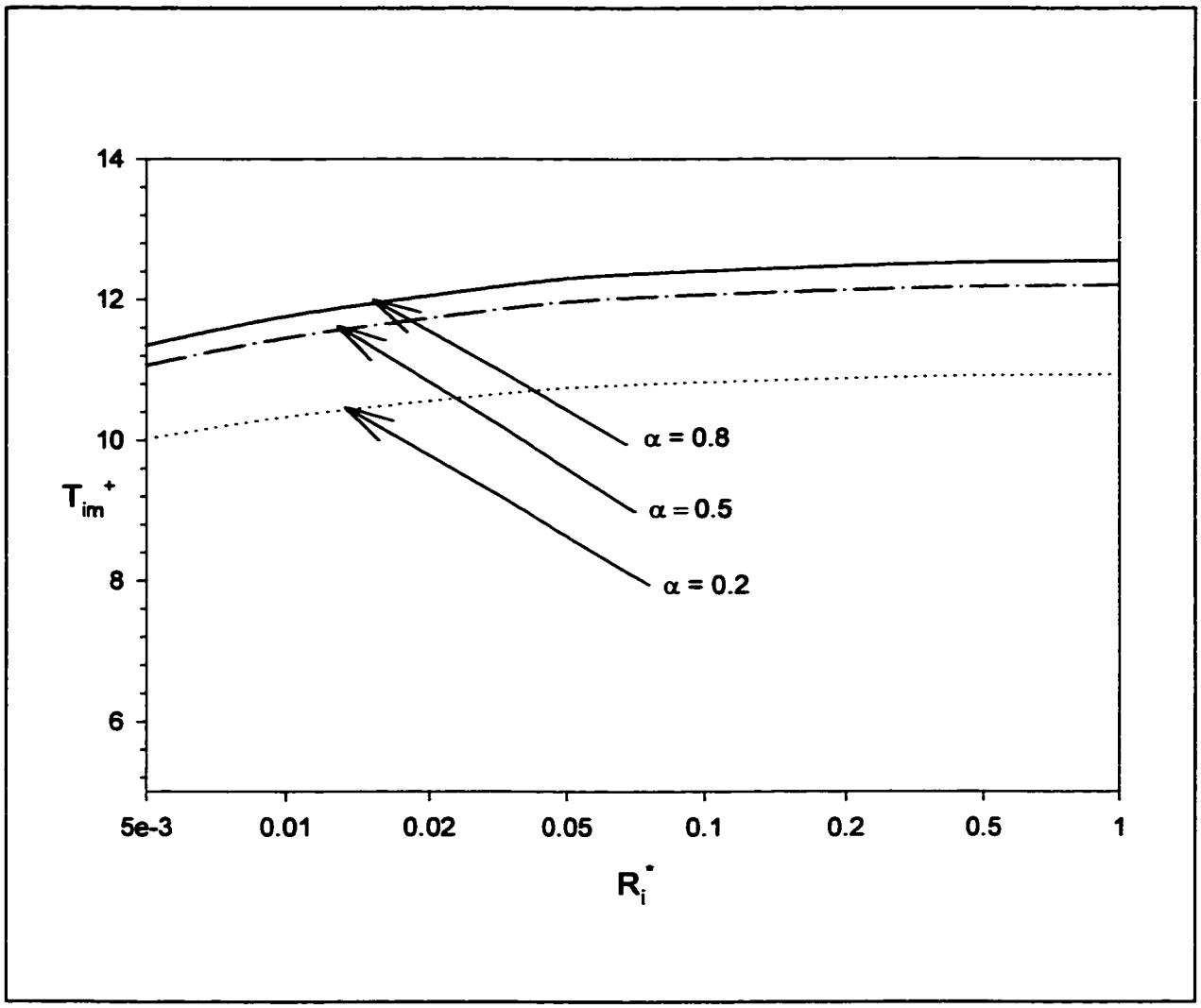

Figure 2.28 Effect of R_i^* on Maximum Dimensionless Temperature; Effect of Radius Ratio, α; Pr = 0.72, Re = 10^5 and U* = 0.4

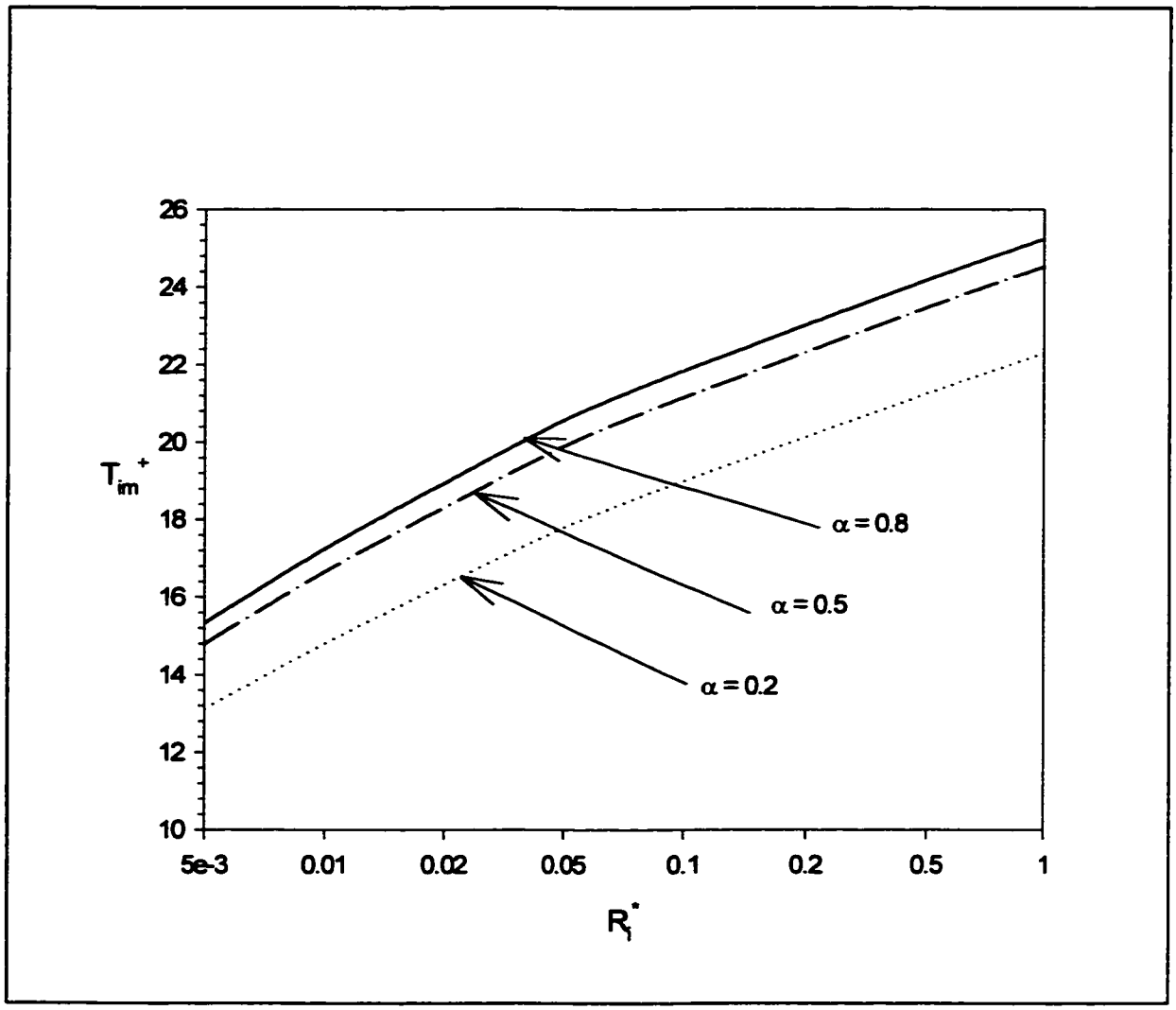

Figure 2.29 Effect of R_i^* on Maximum Dimensionless Temperature; Effect of Radius Ratio, α; Pr = 0.72, Re = 10^5 and U* = 0.8

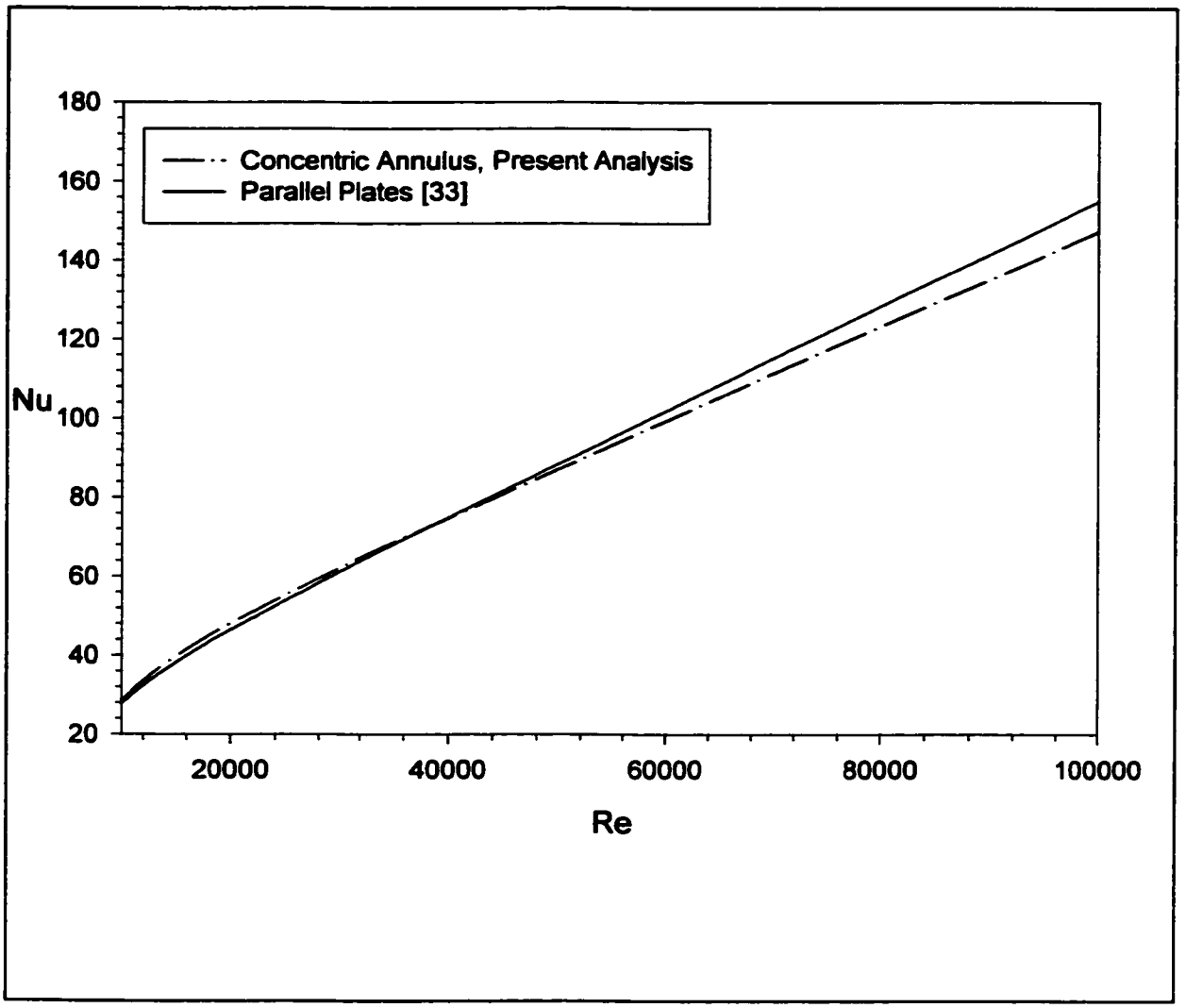

Figure 2.30 Nusselt Number for Fully Developed Turbulent Flow between Parallel Plates and in a Concentric Annulus, $R_i^* = 1.0$, $\alpha = 0.999$; Constant Heat Flux; Pr = 0.7; $\mathrm{Re} = u_b \cdot 2(R_o - R_i)/\nu$

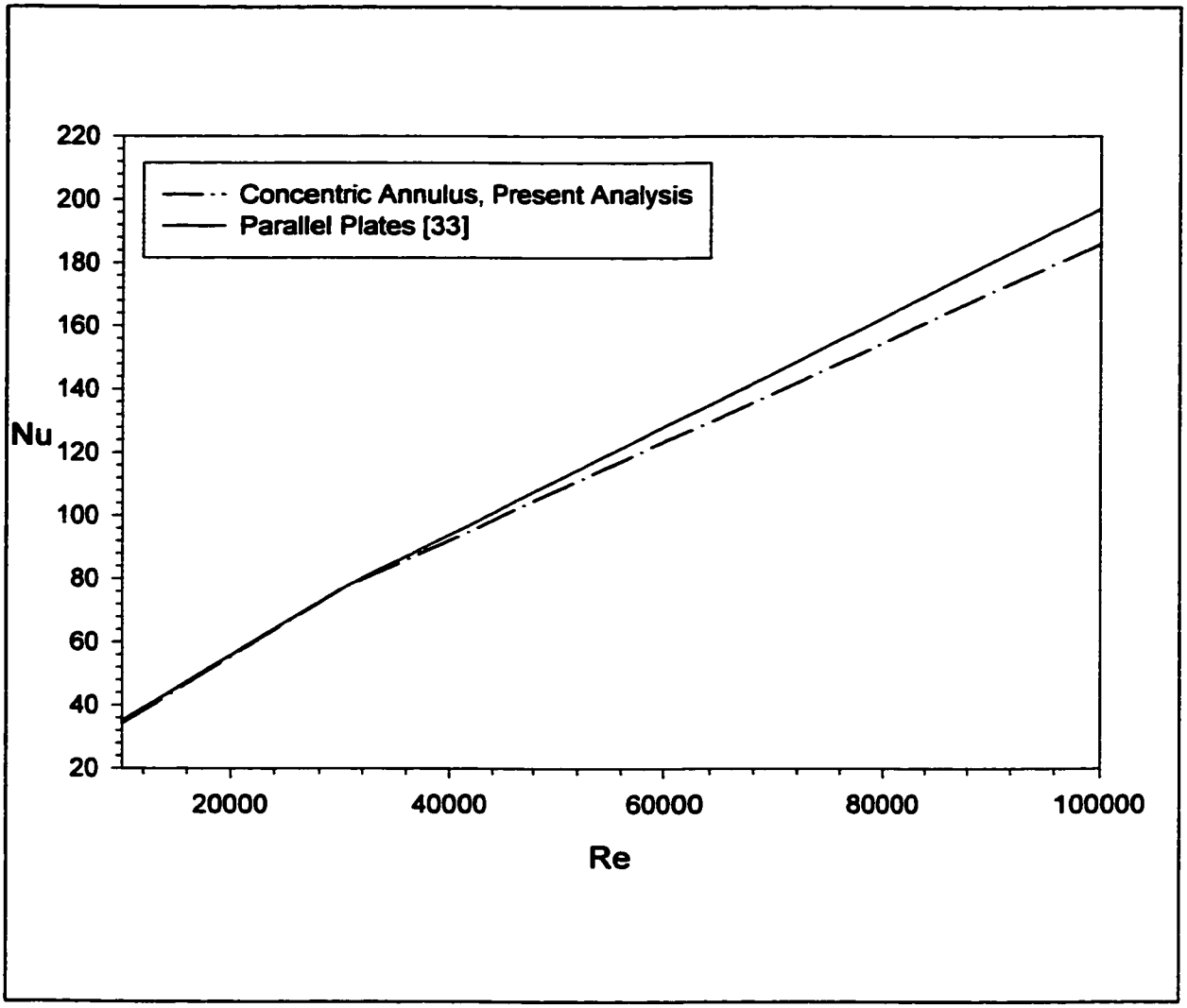

Figure 2.31 Nusselt Number for Fully Developed Turbulent Flow between Parallel Plates and in a Concentric Annulus, $R_i^* = 1.0$, $\alpha = 0.999$; Constant Heat Flux; Pr = 1.0; $\mathrm{Re} = u_b \cdot 2(R_o - R_i)/\nu$

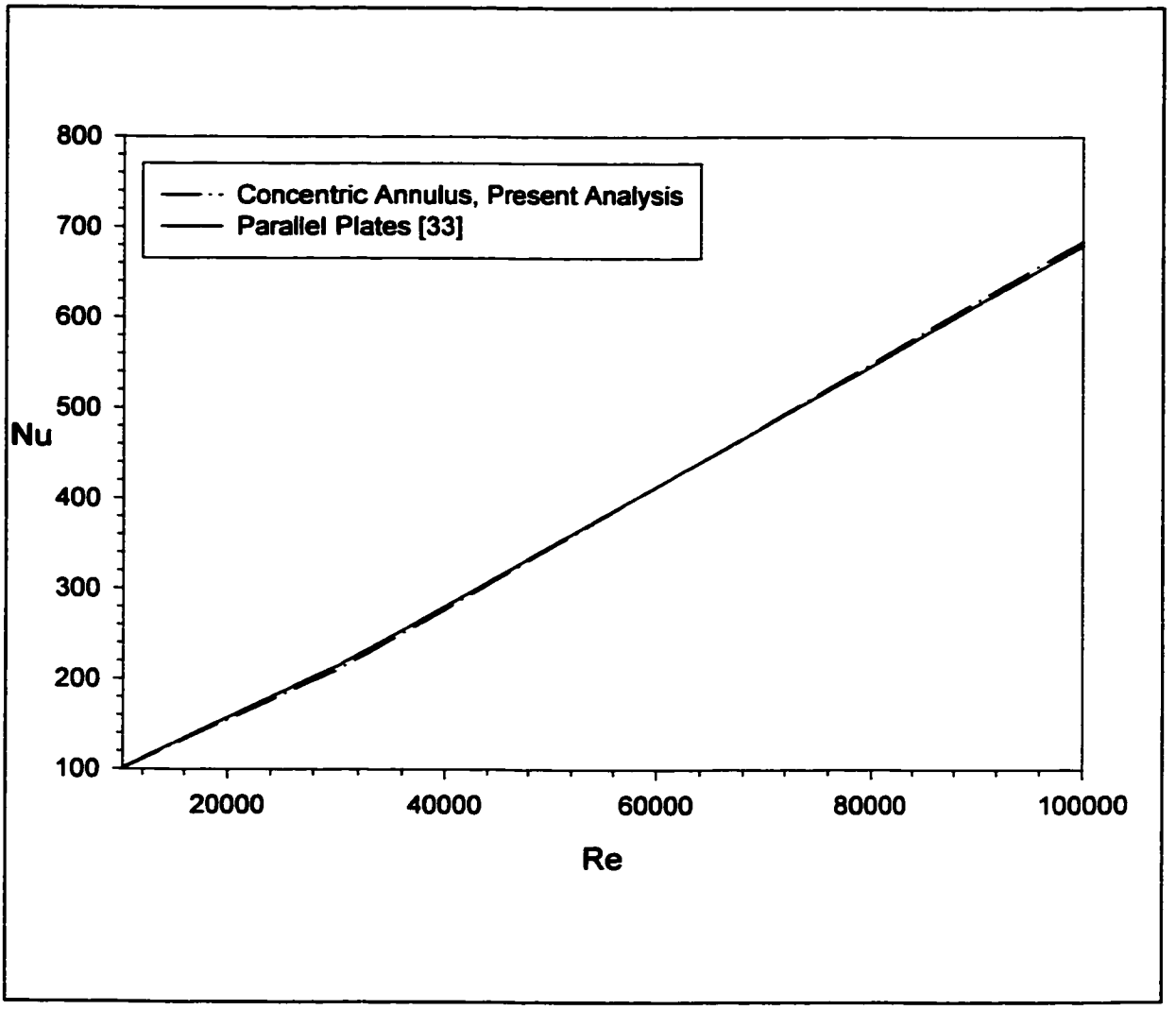

Figure 2.32 Nusselt Number for Fully Developed Turbulent Flow between Parallel Plates and in a Concentric Annulus, $R_i^* = 1.0$, $\alpha = 0.999$; Constant Heat Flux; Pr = 10.0; $\mathrm{Re} = u_b \cdot 2(R_o - R_i)/\nu$

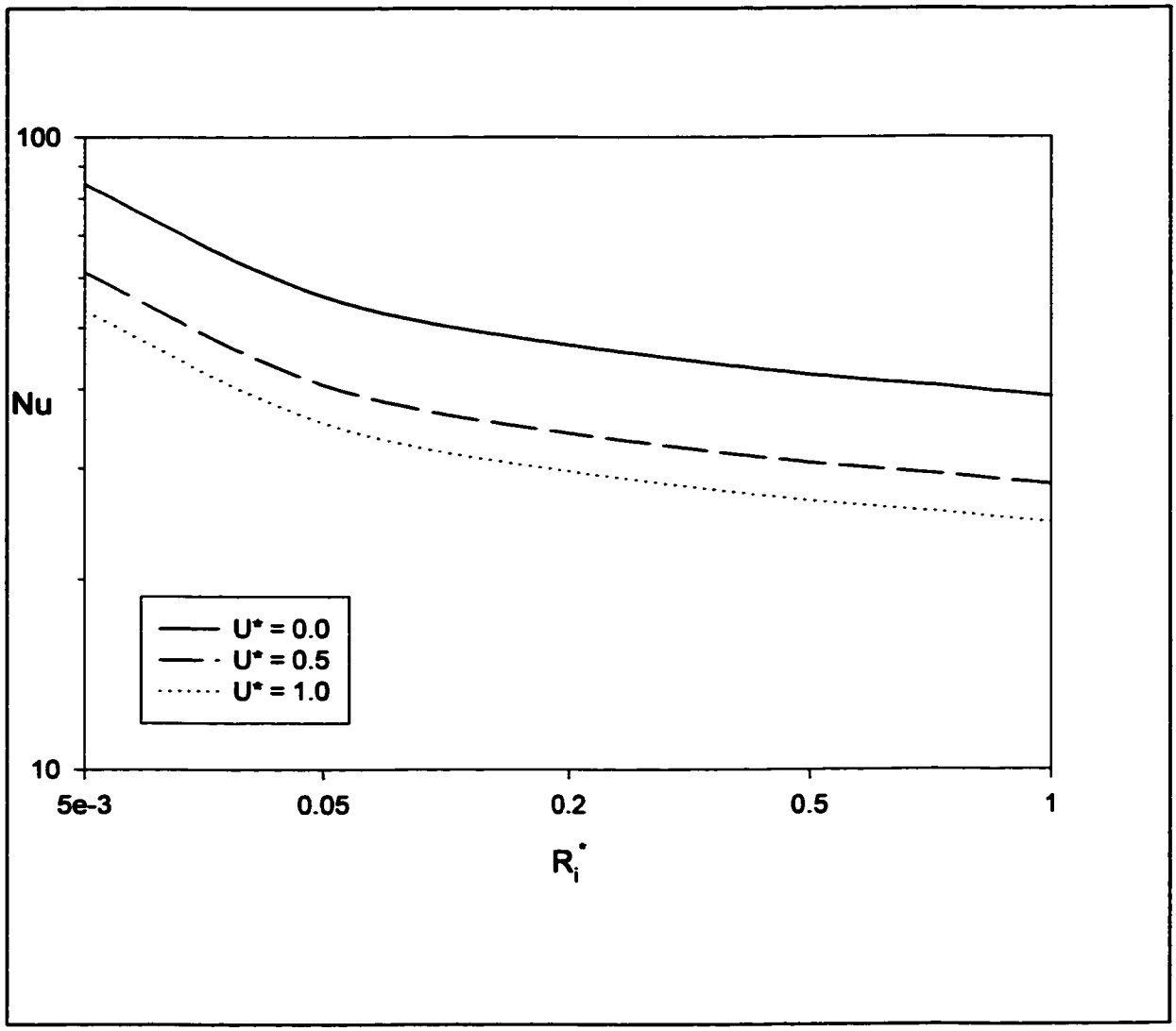

Figure 2.33 Nusselt Number; Effect of Relative Velocity, α = 0.5, Re = 20000 and Pr = 0.72

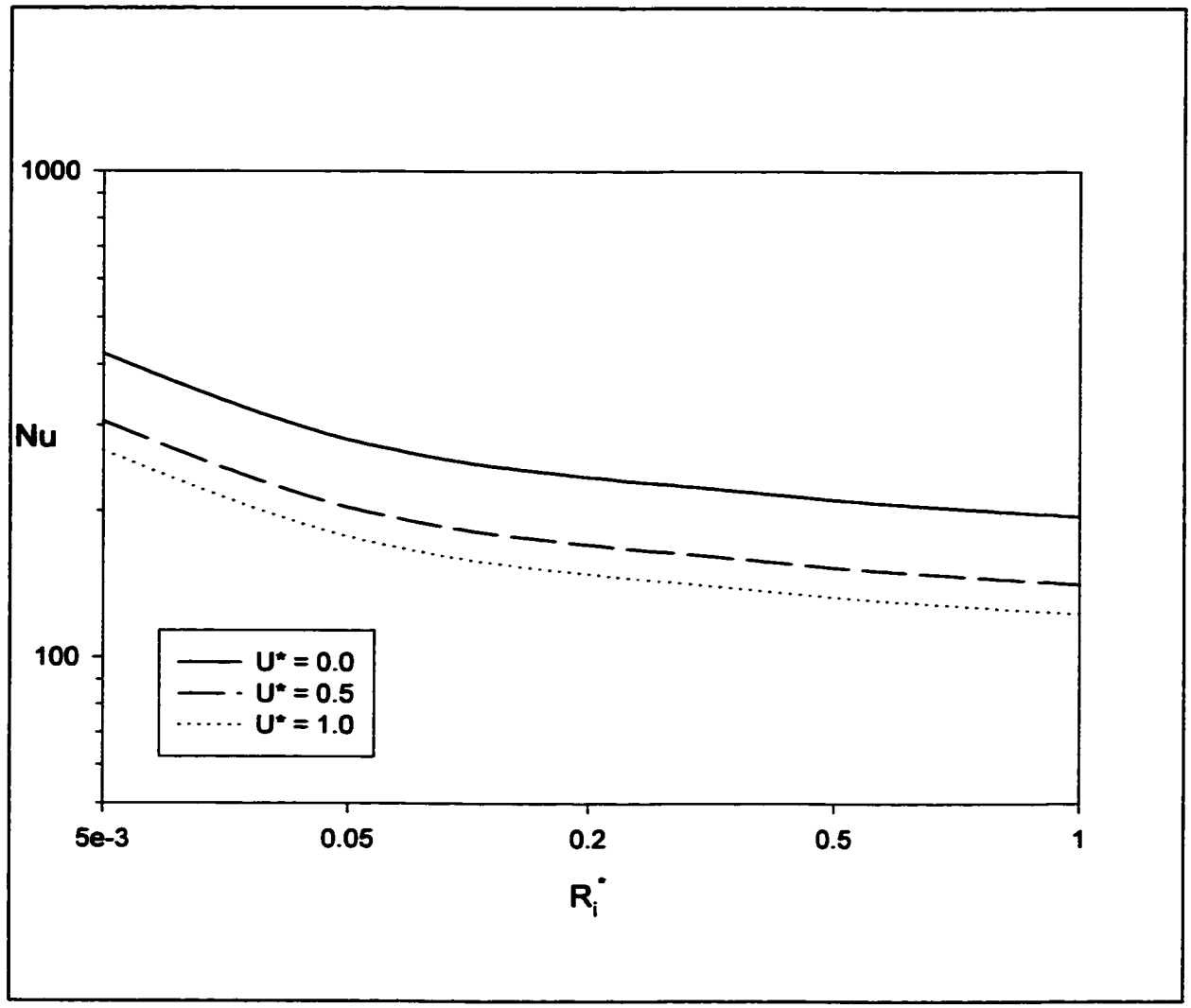

Figure 2.34 Nusselt Number; Effect of Relative Velocity, $\alpha = 0.5$, Re = 10^5 and Pr = 0.72

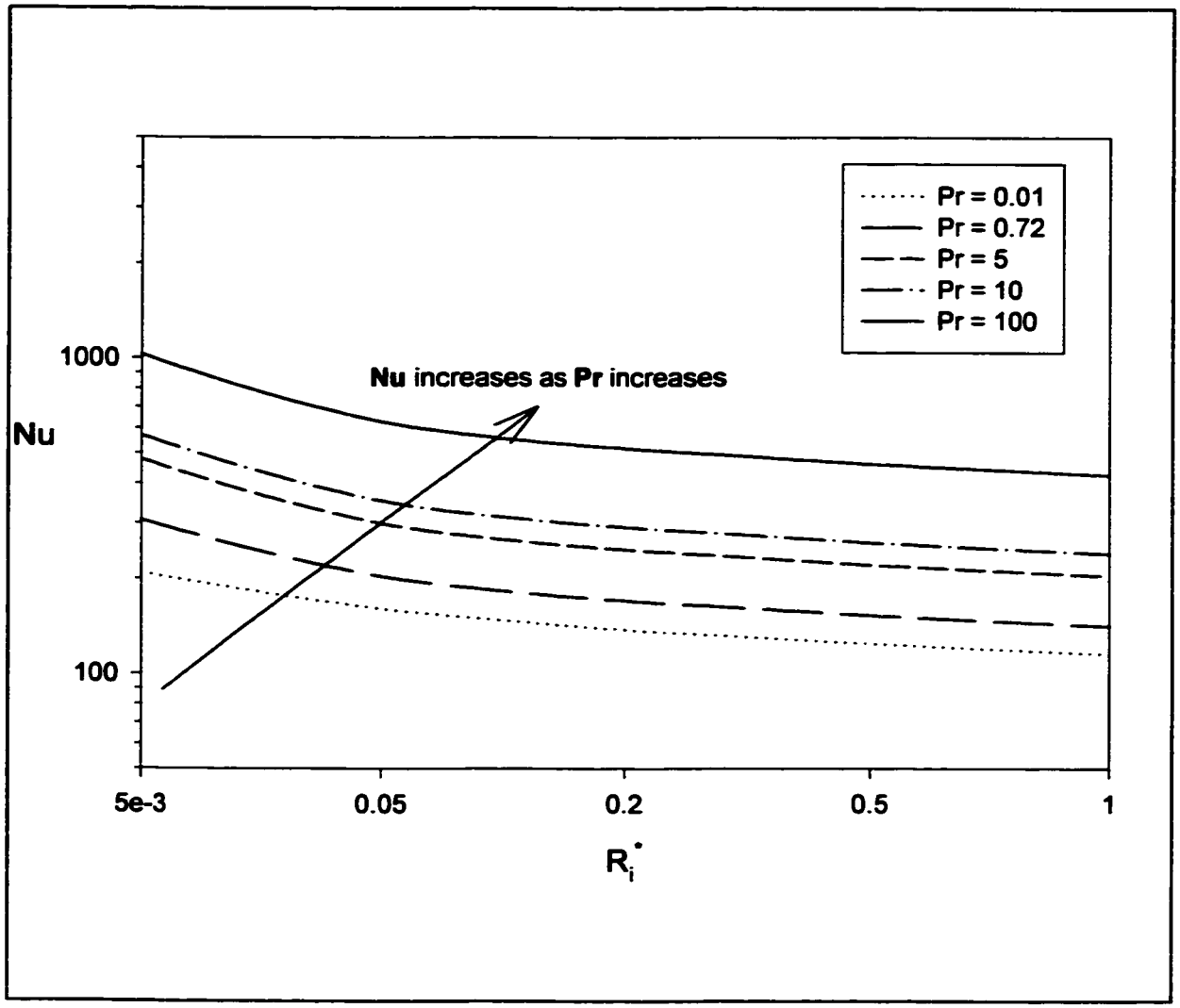

Figure 2.35 Nusselt Number; Effect of Prandtl Numbers, $\alpha = 0.5$, U* = 0.5 and Re = 10^5

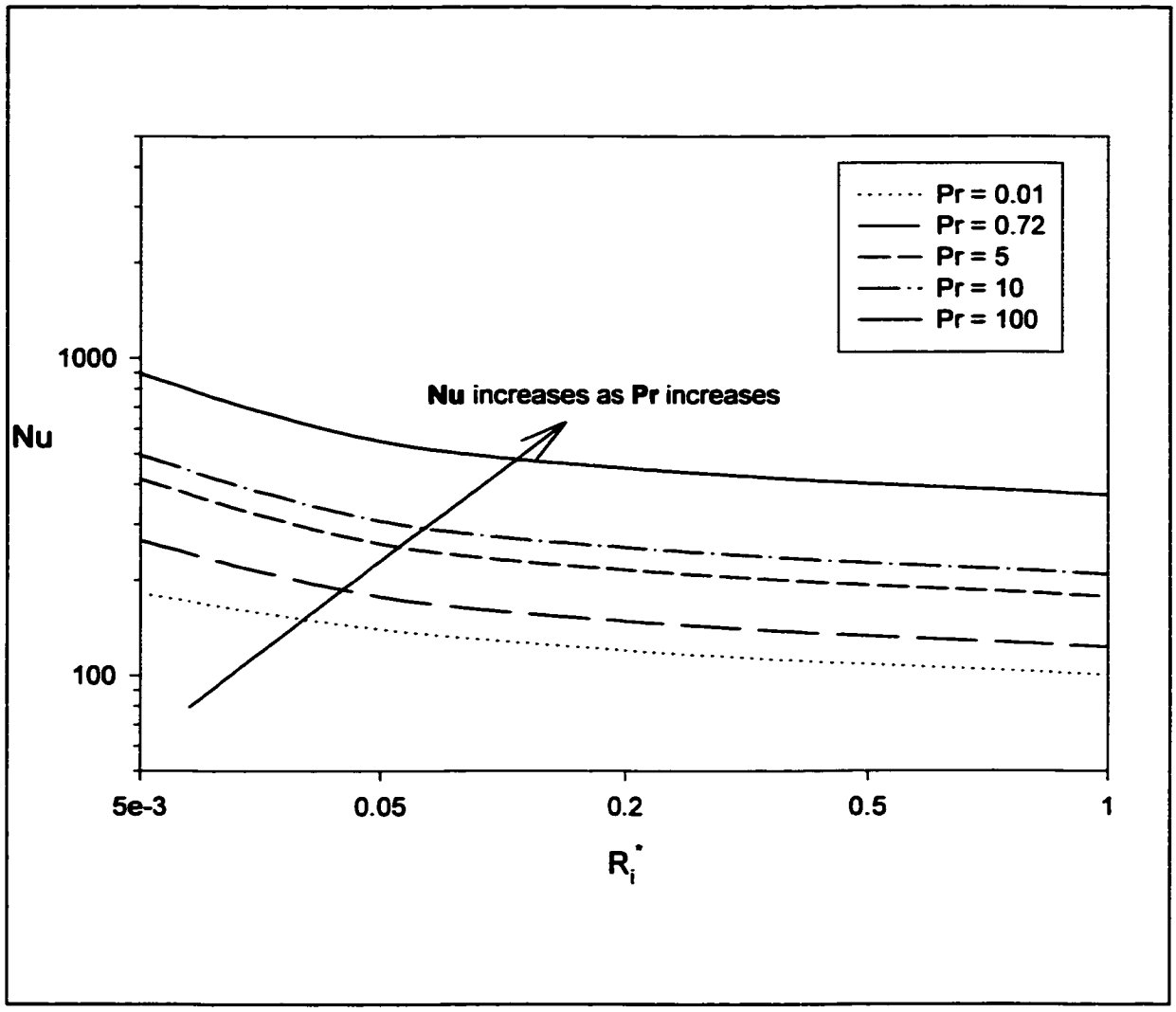

Figure 2.36 Nusselt Number; Effect of Prandtl Numbers, α = 0.5, U* = 1.0 and Re = 10^5

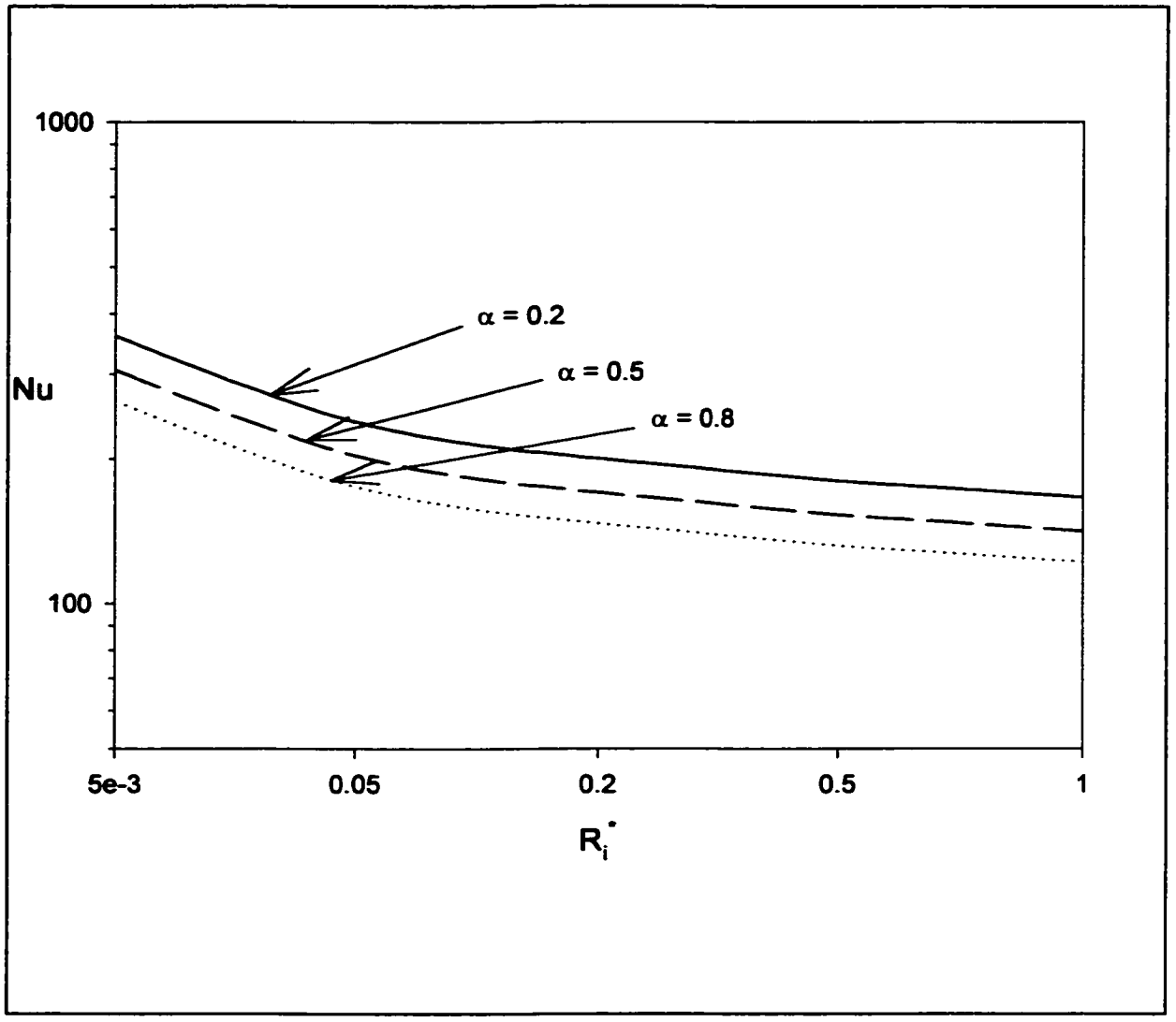

Figure 2.37 Nusselt Number; Effect of Radius Ratio, Pr = 0.72, U* = 0.5 and Re = 10^5

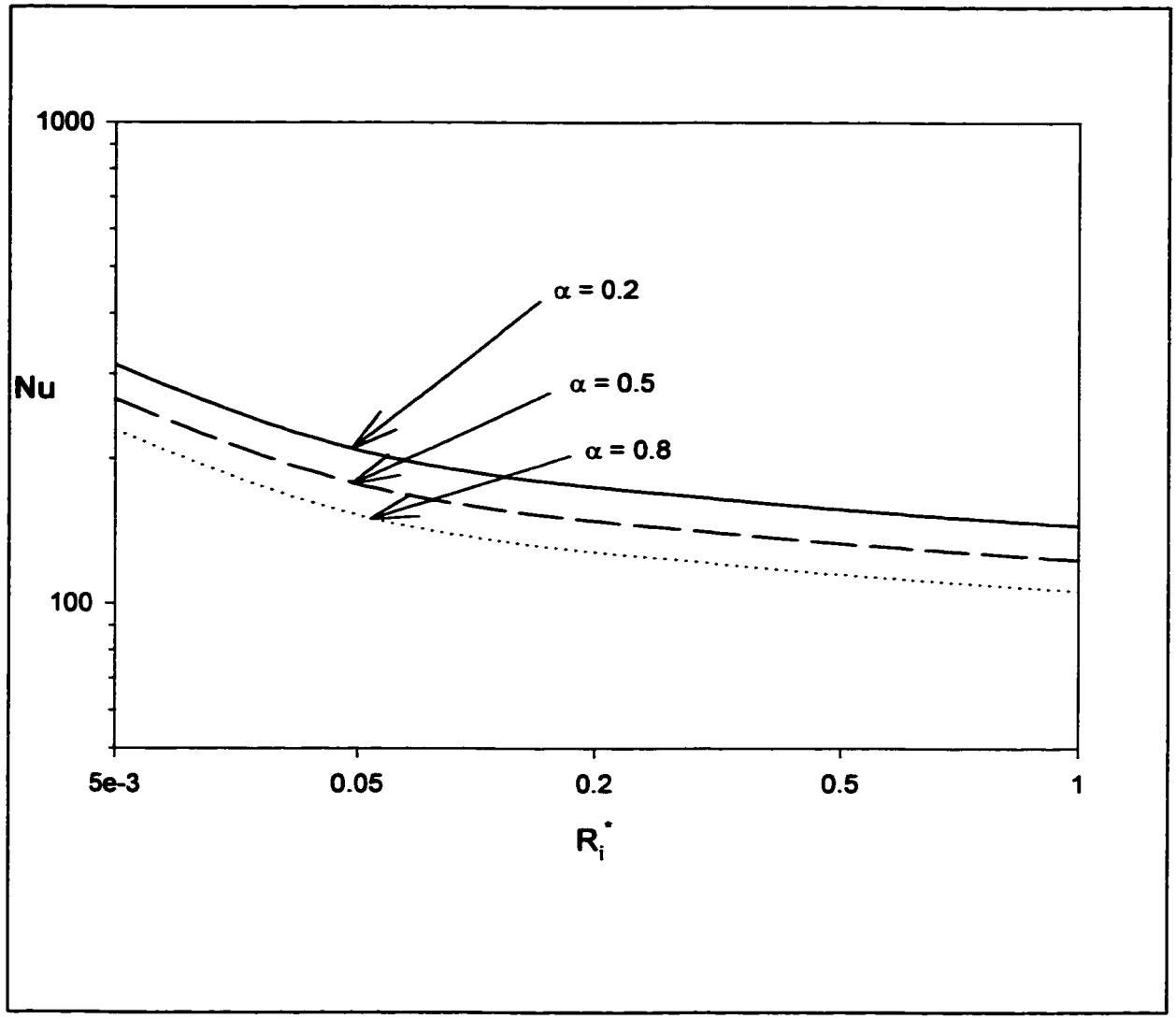

Figure 2.38 Nusselt Number; Effect of Radius Ratio, Pr = 0.72, U* = 1.0 and Re = 10^5

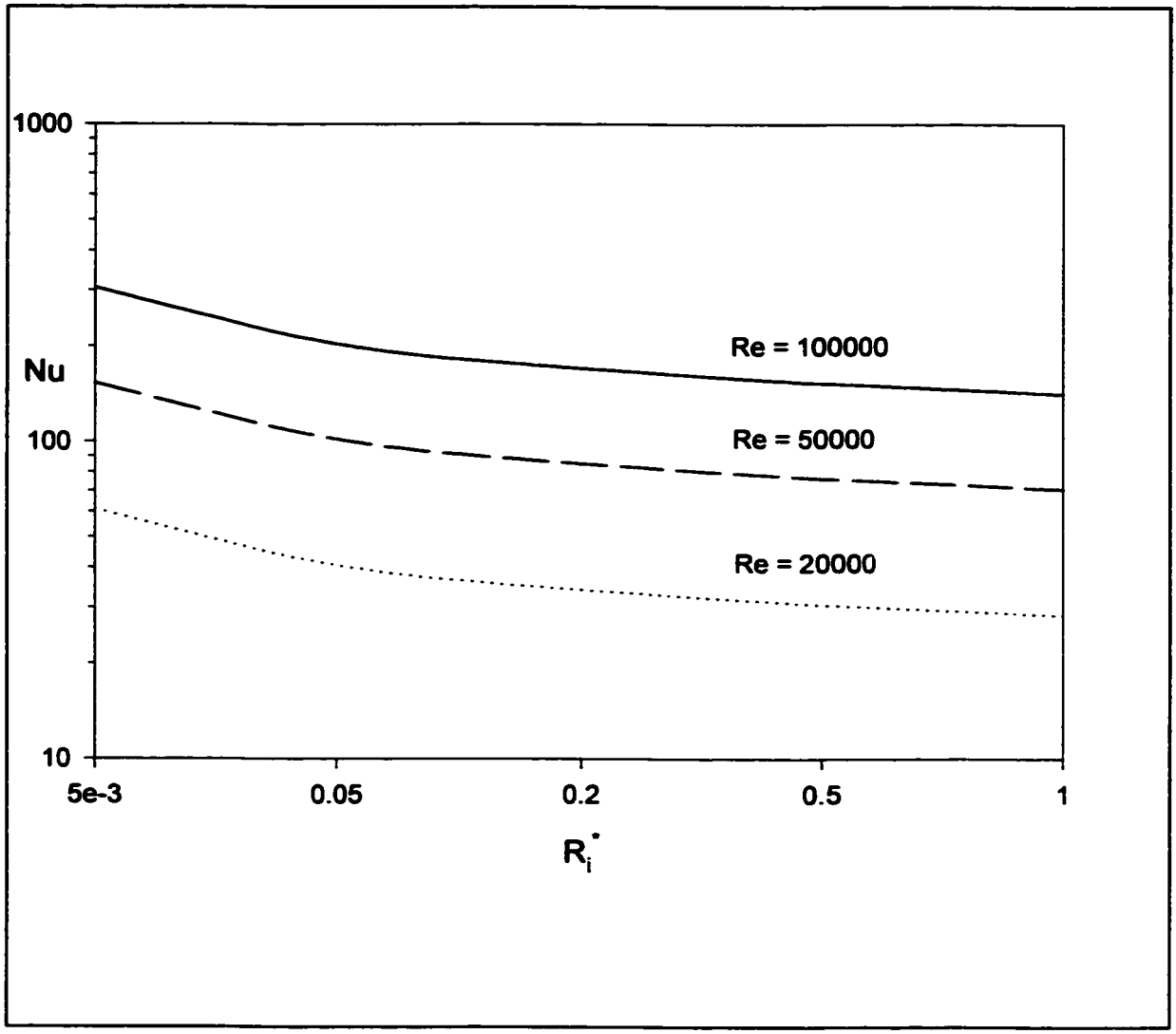

Figure 2.39 Nusselt Number; Effect of Reynolds Numbers, α = 0.5, U* = 0.5 and Pr = 0.72

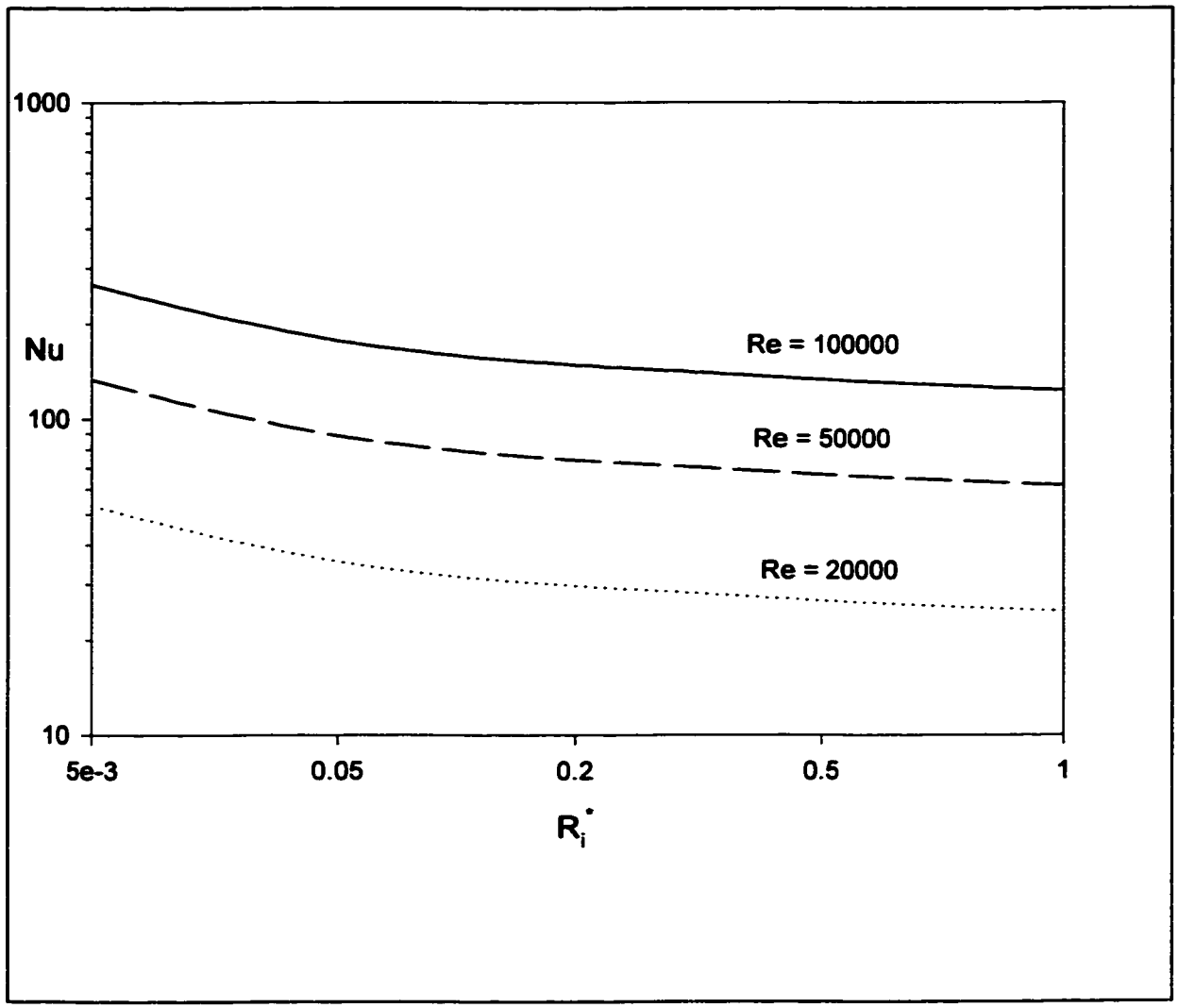

Figure 2.40 Nusselt Number; Effect of Reynolds Numbers, α = 0.5, U* = 1.0 and Pr = 0.72

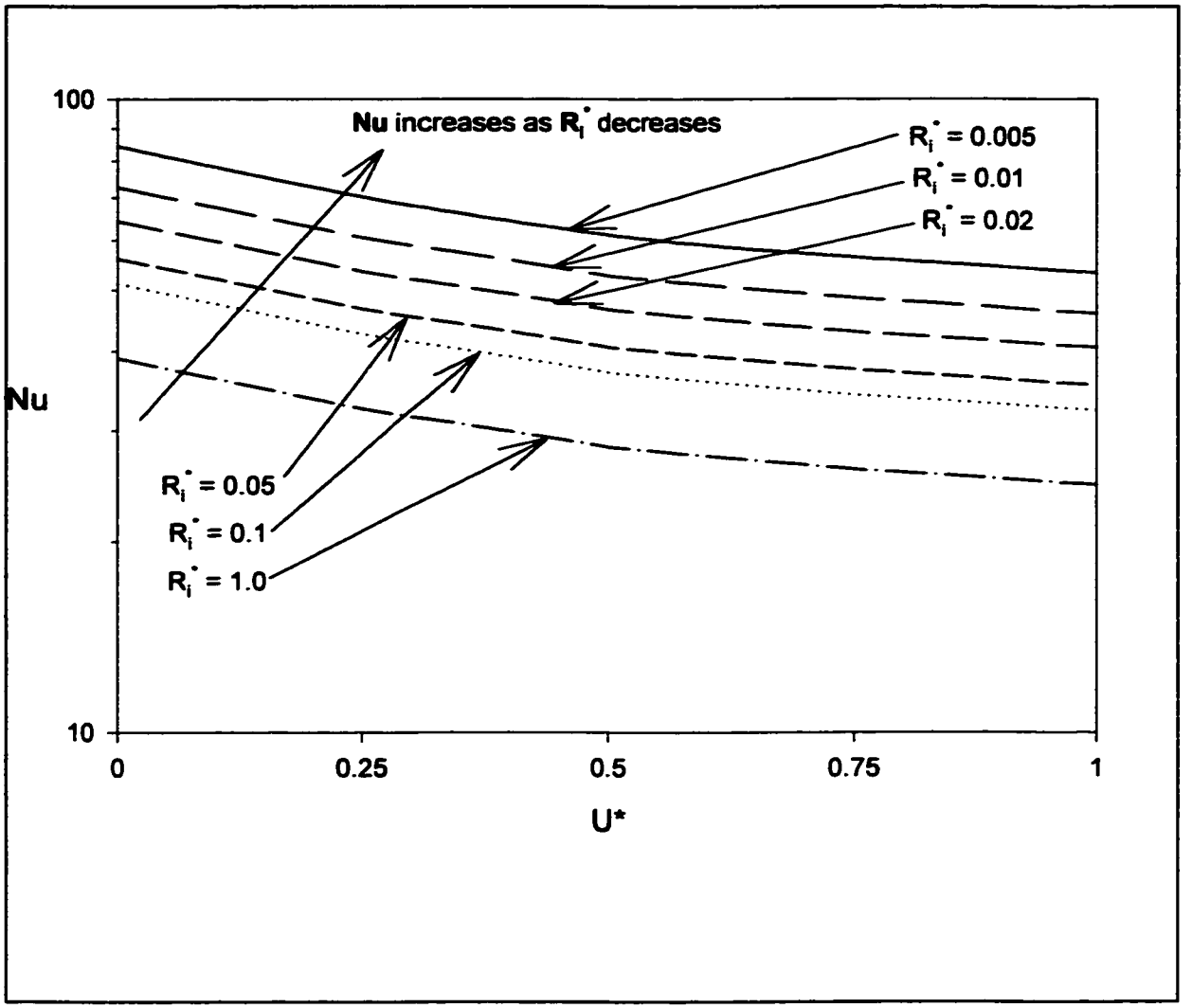

Figure 2.41 Nusselt Number; Effect of Relative Velocity, Pr = 0.72, α = 0.5 and Re = 20,000

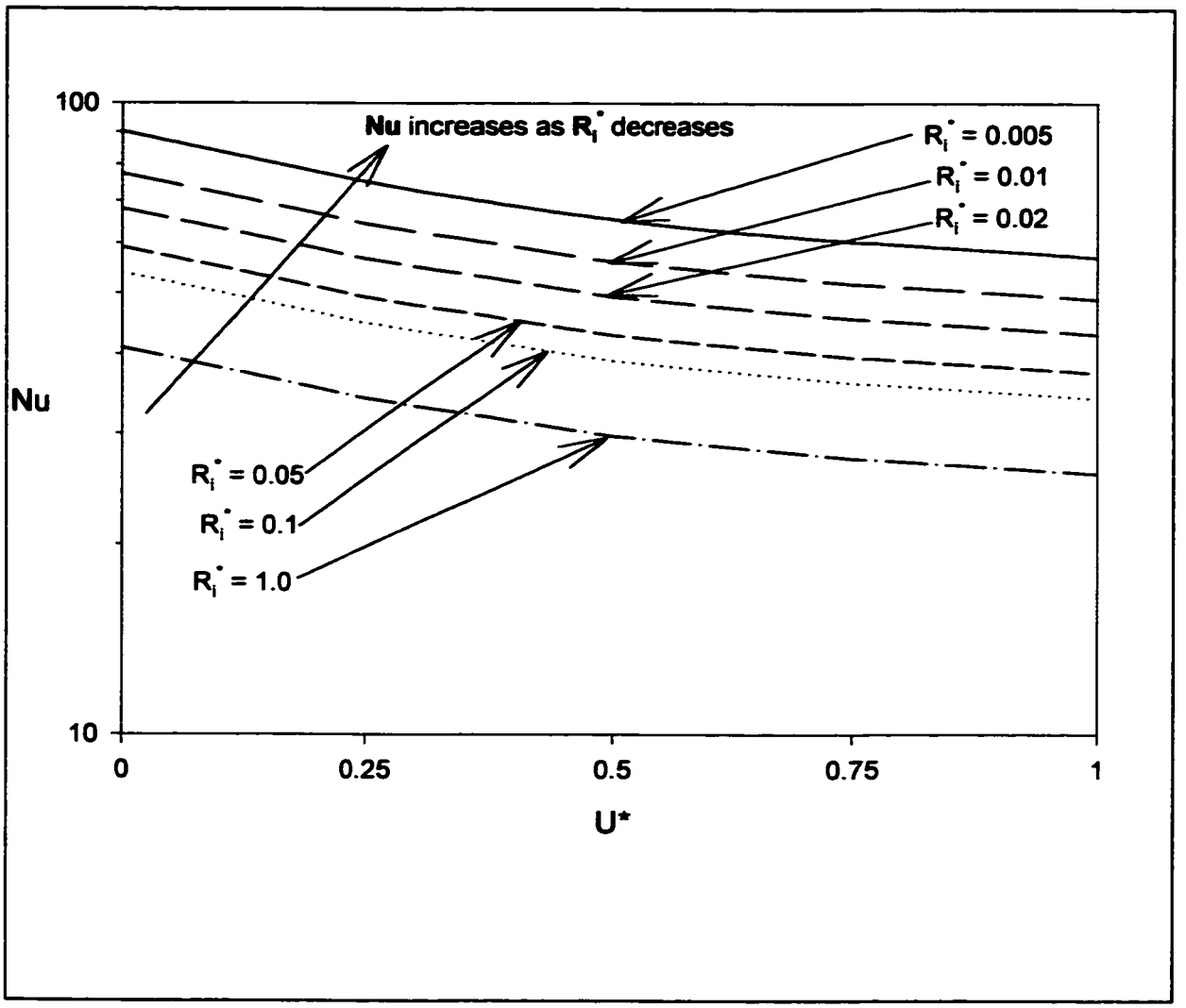

Figure 2.42 Nusselt Number; Effect of Relative Velocity, Pr = 1.0, α = 0.5 and Re = 20,000

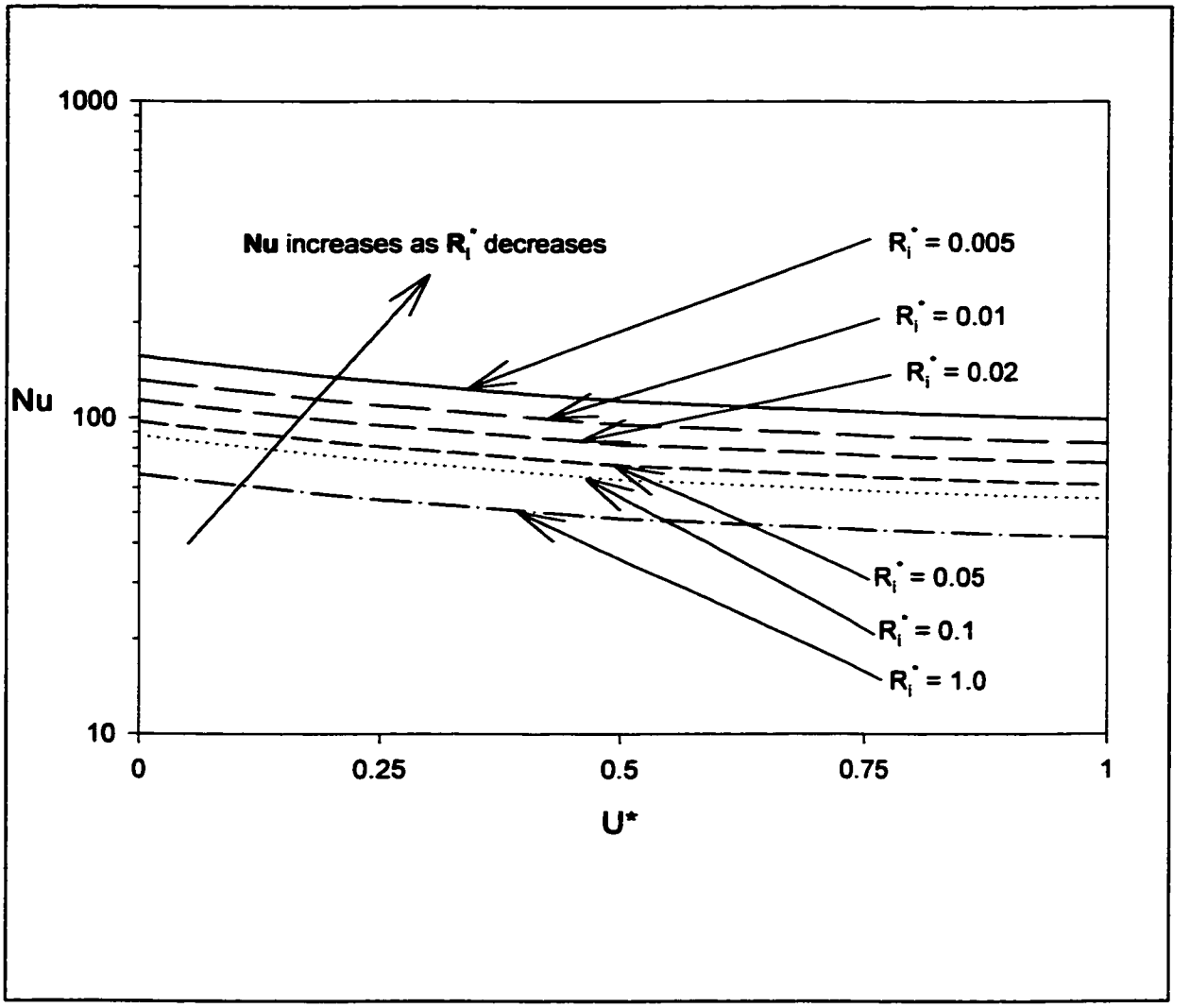

Figure 2.43 Nusselt Number; Effect of Relative Velocity, Pr = 10.0, α = 0.5 and Re = 20,000

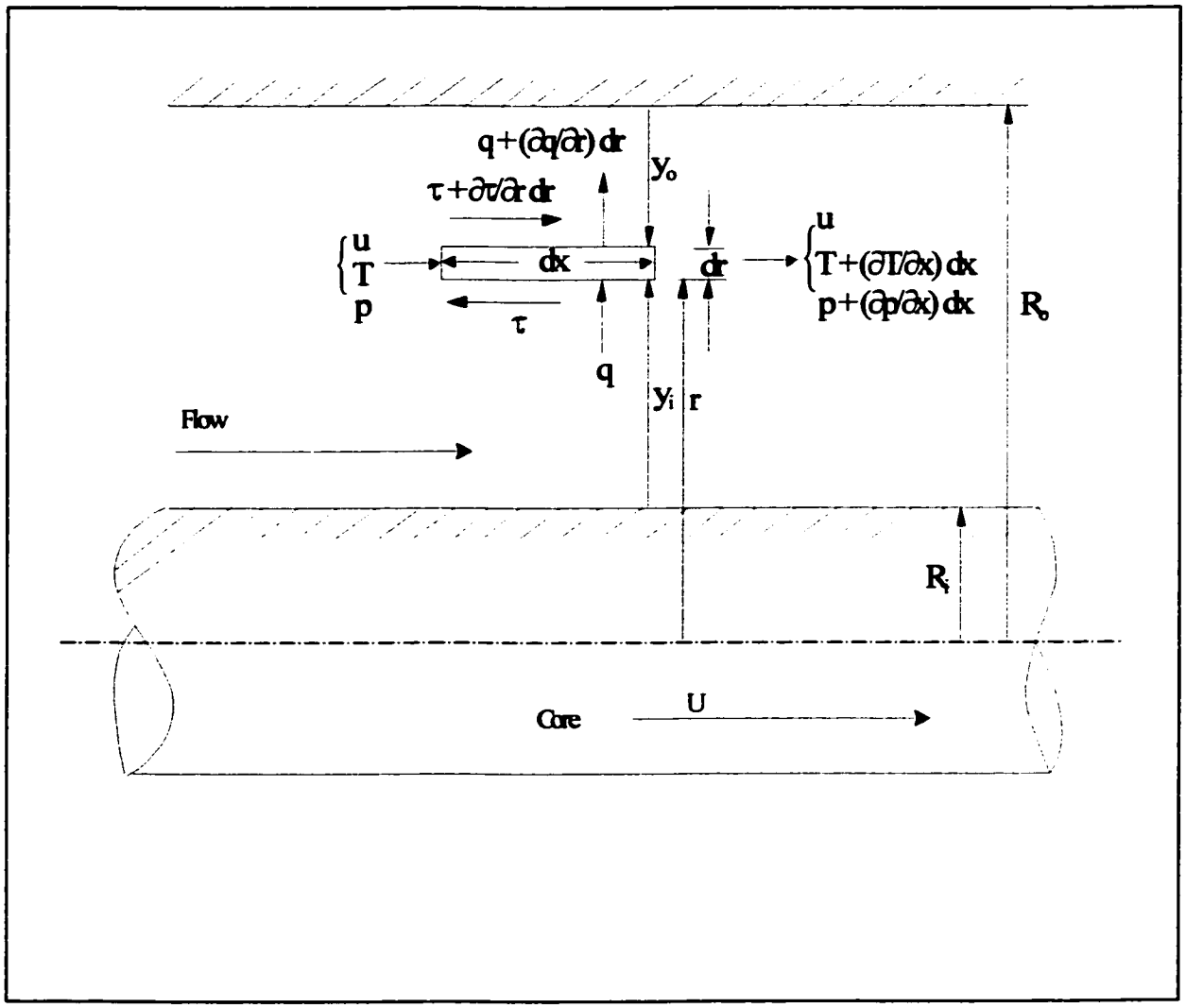

Figure A1.1 Shear Stress and Heat Flux Distribution in a Concentric Annular Flow

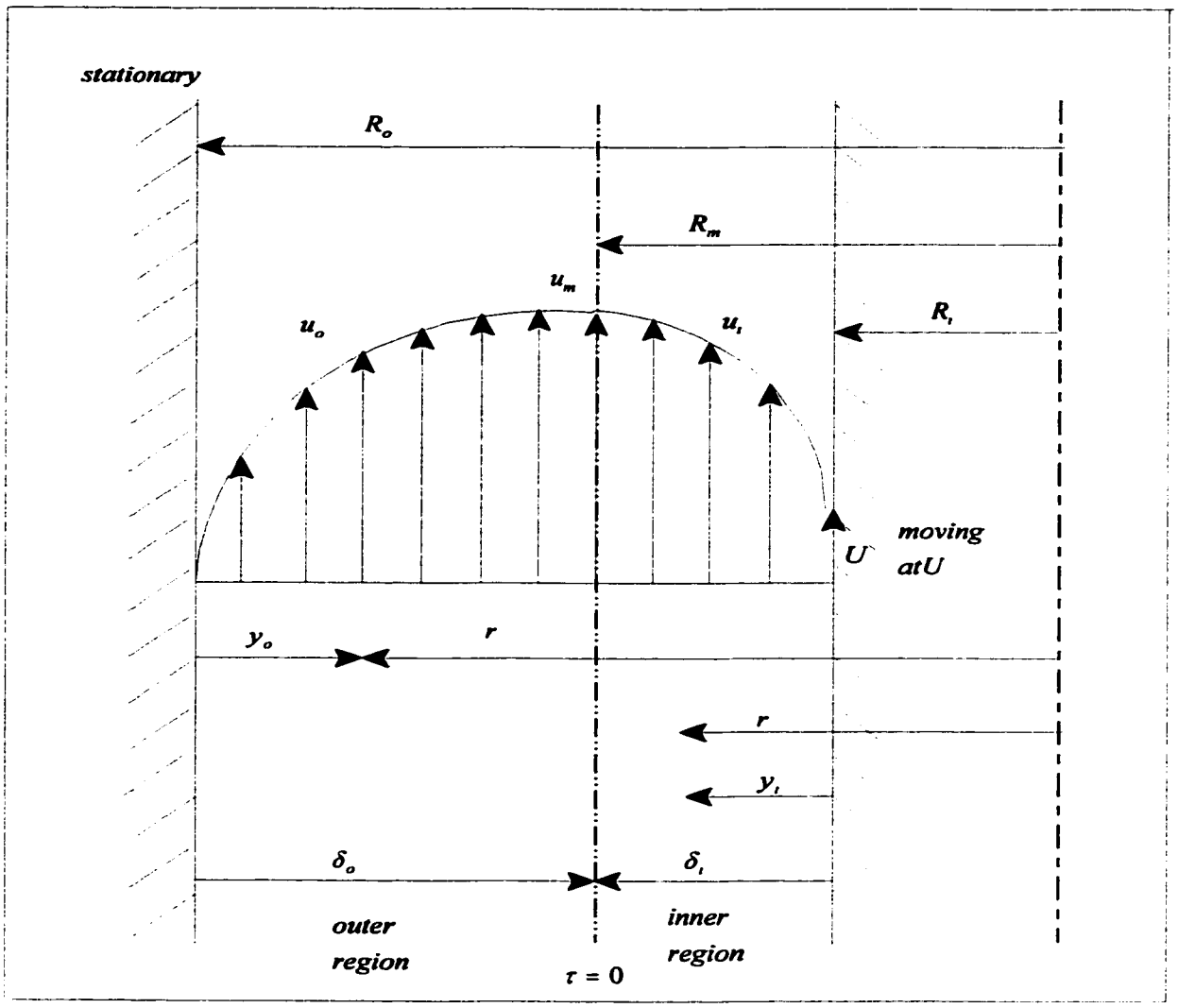

Figure A4.1 Idealized Model: Fully Developed Turbulent Flow in a Concentric Annulus